DEVELOPING MICROFLUIDIC VOLUME SENSORS FOR CELL SORTING AND CELL GROWTH MONITORING

Jason Riordon

Thesis submitted to the
Faculty of Graduate and Postdoctoral Studies
In partial fulfillment of the requirements
For the Doctorate in Philosophy degree in Physics

Department of Physics
Faculty of Science
University of Ottawa

"What I want to talk about is the problem of manipulating and controlling things on a small scale."

-Richard Feynman, 1959, from *"There's plenty of room at the bottom."*[1]

"*Microfluidics has the potential to influence subject areas from chemical synthesis and biological analysis to optics and information technology.*"

-George M. Whitesides, 2006, from "*The origins and the future of microfluidics"*[2]

Summary

Microfluidics has seen an explosion in growth in the past few years, providing researchers with new and exciting lab-on-chip platforms with which to perform a wide variety of biological and biochemical experiments. In this work, a volume quantification tool is developed, demonstrating the ability to measure the volume of individual cells at high resolution and while enabling microfluidic sample manipulations. Care is taken to maximise measurement sensitivity, range and accuracy, though novel use of buoyancy and dynamically tunable microchannels. This first demonstration of a microfluidic tunable volume sensor meant volume sensing over a much wider range, enabling the detection of ~1 μm^3 *E.coli* that would otherwise go undetected. Software was written that enables pressure-driven flow control on the scale of individual cells, which is used to great success in (a) sorting cells based on size measurement and (b) monitoring the growth of cells. While there are a number of macroscopic techniques capable of sorting cells, microscopic lab-on-chip equivalents have only recently started to emerge. In this work, a label-free, volume sensor operating at high resolution is used in conjunction with pressure-driven flow control to actively extract particle/cell subpopulations. Next, a microfluidic growth monitoring device is demonstrated, whereby a cell is flowed back and forth through a volume sensor. The integration of sieve valves allows cell media to be quickly exchanged. The combination of dynamic trapping and rapid media exchange is an important technological contribution to the field, one that opens the door to studies focusing on cell volumetric response to drugs and environmental stimuli. This technology was designed and fabricated in-house using soft lithography techniques readily available in most biotechnology labs. The main thesis body contains four scientific articles that detail this work (Chapters 2-5), all published in

peer-reviewed scientific journals. These are preceded by an introductory chapter which provides an overview to the theory underlying this work, in particular the non-intuitive physics at the microscale and the Coulter principle.

Sommaire

La popularité de la microfluidique a subit une croissance remarquable ces dernières années, offrant aux chercheurs (chercheuses) une variété de nouvelles « laboratoires sur puce » pouvant performer une grande variété de fonctions analytiques et biochimiques. Dans ce travail, un outil capable de mesurer le volume de cellules individuelles à haute résolution est développé en paire avec un système microfluidique pour manipuler les échantillons. La sensibilité, précision et l'étendue de mesure sont optimisées à l'aide d'innovations scientifiques, telles que l'utilisation de flottabilité d'échantillons et de canaux microfluidiques dynamiques à dimensions ajustables. Cette première démonstration d'un senseur microfluidique ajustable a grandement amélioré l'étendue de mesure, permettant la détection de *E.coli* (~1μm^3) qui, autrement, passerait inaperçus. Un logiciel fut créé qui permet un contrôle du flux à l'aide de régulateurs à pression à l'échelle de cellules individuelles; ceci a permis (a) la séparation de cellules selon leur volume et (b) la mesure continue du volume pendant la croissance de cellules. Bien qu'il existe des technologies macroscopiques capables de séparer des cellules, des équivalents sur puce représentent un dévelopement récent. Dans ce travail, un senseur à volume sans étiquette et opérant à haute-résolution est intégré avec un système de contrôle de flux avec pressions, de sorte à extraire des sous-populations de particules/cellules. Ensuite, un système microfluidique capable de mesurer la croissance de cellules est démontré, où une cellule est envoyée périodiquement à travers un senseur à volume. L'intégration de valves de triage permet l'échange rapide de fluides. Cette combinaison de piège à cellule dynamique et de l'échange rapide du milieu de culture représente une contribution scientifique importante, une contribution technologique qui ouvre la porte à de nouvelles expériences portant sur la réponse

volumétrique cellulaire aux stimuli environnementaux et aux drogues. Cette technologie fut conçue et fabriquée dans le laboratoire à l'aide de la lithographie molle, une technique généralement disponible dans les laboratoires biochimiques. Le corps de cette thèse est formé de quatre articles scientifiques qui détaillent ces travaux (Chapitres 2-5), tous publiés dans des journaux scientifiques avec évaluation par les pairs. Ceux-ci sont précédés par un chapitre d'introduction qui présente un aperçu de la théorie de base, particulièrement à la physique non-intuitive à l'échelle micrométrique et au principe de Coulter.

Statement of originality

This work is, to the best of the author's knowledge, wholly original. Research was conducted under the supervision of Professor Michel Godin at the Department of Physics of the University of Ottawa. Chapters 2-5 are comprised of manuscripts published in refereed, peer-reviewed scientific journals:

- **Riordon, J.**, Mirzaei, M. & Godin, M. Microfluidic cell volume sensor with tunable sensitivity. *Lab on a Chip* **12,** 3016 (2012). doi: 10.1039/c2lc40357a.
- **Riordon, J.**, M. -Catafard, N. & Godin, M. Using the fringing electric field in microfluidic volume sensors to enhance sensitivity and accuracy. *Applied Physics Letters* **101,** 154105–154105–4 (2012). doi:10.1063/1.4759033.
- **Riordon, J.**, Nash, M., Calderini, M. & Godin, M. Using active microfluidic flow focusing to sort particles and cells based on high-resolution volume measurements. *Microelectronic Engineering* **118,** 35–40 (2014). doi:10.1016/j.mee.2014.02.003.
- **Riordon, J.**, Nash, M., Jing, W. & Godin, M. Quantifying the volume of single cells continuously using a microfluidic pressure-driven trap with media exchange. *Biomicrofluidics* **8,** 011101 (2014). doi: 10.1063/1.4867035.

Each of these chapters is preceded by a manuscript information sheet, detailing the contribution of other authors. Work has also been presented at poster presentations for Ontario-on-a-chip/MATCH in May 2012 and May 2013. In partial fulfilment of Ph.D. requirements, an oral presentation was given at the Ottawa-Carleton Institute of Physics (OCIP) graduate student symposium in February 2012.

- **Riordon, J.**, M.-Catafard, N., Mirzaei, M. & Godin, M., Enhancing the accuracy and sensitivity of microfluidic volume sensors, Ontario-on-a-Chip/MATCH,Toronto, ON, May 23-24 2013 (Poster)
- **Riordon, J.**, Sensitivity enhancement in microfluidic volume sensors, OCIP Graduate Student Symposium, February 2012 (Talk)
- **Riordon, J.**, Mirzaei, M. & Godin, M., Microfluidic impedance flow cytometer with tuneable sensitivity, Poster presentation at Ontario-on-a-Chip/MATCH, Toronto, ON, May 17-18 2012 (Poster)

Statement of contributions

I, Jason Riordon, contributed the large majority of the work presented in this thesis: this includes computer modelling, device design, microfabrication (photolithography, lift-off, PDMS moulding), electrical setup, software design, pressure control, cell culturing, data acquisition and all analysis presented herein. I completed background research on state of the art technologies, with which I compare my specific technological contributions. I wrote the first drafts of each of the manuscripts presented herein (chapters 2-5), and completed revisions.

Other researchers contributed to this work as well. Individual contributions to manuscripts are outlined in an information sheet at the beginning of each chapter. The quantification of carrier fluid densities in Chapter 3 was conducted by Nicolas M-Catafard, an undergraduate student at the time. Dr. Maryam Mirzaei, Matias Calderini, Dr. Benjamin Watts and Wenyang Jing assisted with some microfabrication aspects; Mike Nash and Lukasz Andrzejewski assisted with LabVIEW© software development. Several undergraduate students assisted with various aspects of preliminary microfabrication and modelling work: Ian Jardine, Dylan Stone, Jeff Salvail, Dominique Laniel and Eric Hoogkamp. Radin Tahvildari, a Ph.D. candidate, provided advice on sample preparation. Hilary Phenix and Professor Mad Kaern provided the initial yeast samples used throughout this work.

Acknowledgements

First and foremost, I thank my supervisor, Prof. Michel Godin, for introducing me to the wonderful and (now somewhat less) mysterious world of microfluidics. Contributing to a new lab has been a fantastic learning experience, and I am grateful to have had this opportunity. For guidance, motivation, patience and enthusiasm throughout, I thank you.

I wish to thank my thesis committee, Prof. Paul G. Charette, Prof. Xiaoyi Bao, Prof. Andrew Pelling and Prof. Robert de Kemp. I also thank Prof. Christophe Py who participated in my Ph.D. progress committee. Your insightful comments and constructive criticism of my manuscript has led to a much improved, polished thesis.

I also thank all the researchers – professors, support staff, graduate and undergraduate students alike- who have provided direct assistance to my thesis work: Michael Nash, Nicolas M-Catafard, Dr. Maryam Mirzaei, Matias Calderini, Wenyang Jing, Lukasz Andrzejewski, Prof. Mads Kaern, Hilary Phenix, Dr. Benjamin Watts, Radin Tahvildari, Ian Jardine, Dylan Stone, Jeff Salvail, Dominique Laniel and Eric Hoogkamp. Your specific contributions, outlined in the *Statement of Contributions*, have directly contributed to this thesis, and I am grateful.

In addition, I wish to thank other Godin lab members whom I've had the pleasure of working with over the years: Eric Beamish, Sophie Chagnon-Lessard, Jeremie Gaudreau, Gabriel Dupras, Andrew Todd, Laurent Gagné-Dumais, Jeremie Harris, Alan Manning, Chloé Promsy and Noam Lightstone. You have all helped shape my journey, and made countless hours in the lab much more pleasant. I also thank Prof. Vincent Tabard-Cossa, Dr. Dominique Tremblay, Dr. Nickolay V. Bukoreshtliev, Daniel Modulevsky, Louise

Guolla and Sebastian Hadjiantoniou for insightful discussions on various aspects of my work, from microelectrode chemistry and microfabrication to cell biology.

Finally, I wish to thank my family: my parents Charles and Mariette Riordon, and my sister Michelle Riordon. You have been forever supportive, and I cannot thank you enough. Love always.

List of abbreviations

General

- µ-Coulter: Microfluidic Coulter counter
- AC: Alternating current
- DC: Direct current
- DEP: Dielectrophoresis
- *E.coli*: *Escherichia coli*
- EF: Electrokinetic Flow
- FACS: Fluorescence-activated cell sorting
- FEM: Finite element method
- Inner Helmholtz Plane (IHP)
- MDCK: Madin-Darby Canine Kidney
- Outer Helmholtz Plane (OHP)
- Pe: Péclet number
- Re: Reynolds number
- *S. cerevisiae*: *Saccharomyces cerevisiae* (yeast)
- SNR: Signal-to-noise ratio
- UV: Ultra-violet

Chemical

- Ag: Silver
- Au: Gold
- BSA: Bovine serum albumin
- DI Water: Deionised water
- EtOH: Ethanol
- HMDS: Hexamethyldisilizane
- IPA: Isopropanol
- KCl : Potassium chloride
- LB: Lysogeny broth
- NaCl: Sodium chloride
- NMP: 1-methyl-2-pyrrolidinone
- PBS: Phosphate buffered saline
- PDMS: Polydimethylsiloxane
- SiOH: Silanol
- TMAH: Tetramethylammonium hydroxide
- YPD: Yeast bacto-peptone

Table of contents

List of figures

List of tables

1 INTRODUCTION

Sizing and manipulating small, *very small*, living organisms: this is what defines this work. How small? *E. coli* cells measure roughly 1 μm^3 (1fL). To put this in perspective, the volume of an *E. coli* cell is to the volume of a male *elephant* what this same *elephant* is to Earth's *Moon*. How does one even go about manipulating and analyzing something so small? In contrast, at the macroscale, if one were to measure the volume of a reasonably sized object/creature, there are a number of options. One could use back-of-envelope calculations, along with some measuring tape and obtain a good approximation. If one were more rigorous, and had a cooperative elephant, one could do as Archimedes once did, and measure displaced volume as the creature is submersed in a body of water. Such a measurement would lead to an accurate measurement of volume.

At the micro-/nano- scale, volume measurements become more challenging. Since its introduction in 1956, the Coulter counter has been the tool of choice for sizing cells in a population.[3] Traditional Coulter counters operate as follows: a current is applied between two chambers separated by a narrow aperture and filled with target microparticles or cells suspended in a conducting electrolyte. In a manner analogous to the previous example, where an object displaces its own volume in liquid by virtue of Archimedes' principle, microfluidic objects flowing through the aperture displace their own volume in ions, causing a current pulse (decrease) proportional to their volume. This simple but powerful technology allows colloidal solutions or populations of cells to be analyzed serially at high-throughput. Unfortunately, these devices are expensive, bulky, and generally confined to hospital or laboratory use.[4,5] The immergence of microfluidics and soft lithography in the mid-90s and 00s has opened the door to lab-on-chip equivalents to such systems, devices

that are low cost and relatively simple to fabricate. Further, microfluidics makes it possible to manipulate cells in new and exciting ways.

This thesis is focused on measuring the volume of individual cells, and exploring microfluidic technologies capable of using this information to (a) sort cells and (b) measure cellular growth rate. Cells are the building blocks of life, the very foundation of living organisms. Of the many fundamental parameters one can measure – mass, dimensions, coloration, etc. – volume stands out as being of particular interest. It can be used to differentiate cell types within a mixed population[6], identify cell cycle stage[7], or study cell response to external stimuli, such as media osmolarity.[8] Of particular importance, volume can be ascertained without requiring any cell modification (label-free), making it particularly attractive to researchers in the field worried about influencing the cell being studied.

In terms of measuring cellular growth, obtaining information on mass, density and volume is essential to obtain a full picture. For example, the mass of budding yeast cells during the cell cycle has been shown to follow linear[9] or exponential[10–13] growth curves. Volume, on the other hand, displays a sigmoidal pattern, with periods of slower volume increase corresponding to a time before daughter bud emergence and at daughter cell maturity.[9,14] The "plateau" in volumetric growth has been attributed to water loss of the mother cell at bud initiation.[15] Thus, volume sensing provides a useful tool with which to quantify such behaviour.

Recently, efforts have been made to miniaturize volume sensing technology, and integrate sensors on lab-on-chip platforms. In the devices developed in this work, two

coplanar electrodes, located at the bottom of a microfluidic channel, are utilised. This microfluidic version of the Coulter counter operates in much the same way (Fig. 1-1). A current is drawn between two neighbouring electrodes by applying an AC potential. Cells flowing through the microfluidic sensing channel will displace ions, causing a current pulse. Microfluidic devices show great promise since they have the advantages of lower cost, less sample required and small form factor. Such a platform also allows for the easy integration of microfluidic PDMS valves, capable of dynamically altering a microfluidic flow channel. The first part of this thesis is focused on developing and improving upon volume sensing technology, based upon the Coulter principle (Chapters 2-3); the second part of this thesis explores direct applications of this technology, in cell sorting (Chapter 4) and cell growth monitoring (Chapter 5).

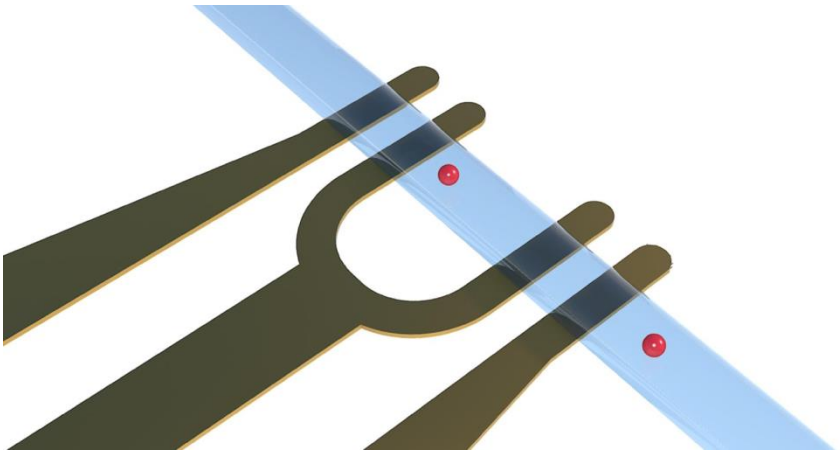

Figure 1-1 Microfluidic volume sensor with embedded, coplanar electrodes. As microtargets traverse the sensing volume, a pulse of amplitude proportional to target volume is measured.

In a publication in *Lab on a Chip*[16], the first fully tunable microfluidic volume sensor is described and characterized. This work will be detailed in Chapter 2. This innovation demonstrated an ability to not only size target cells over a wide range, but also

render a device capable of detecting particles that would otherwise go undetected in sensing channels of large cross-section, such as *E.coli*.

In Chapter 3, the effect of particle trajectory through the sensor is analyzed in the context of further improving device accuracy and sensitivity. This work, featured in Applied Physics Letters,[17] was presented in two parts. First, finite element modelling was performed to quantify the effect of particle trajectory through the sensor. As had been previously postulated, the sensors' innate asymmetry results in a signal dependence on target position.[18] However, rather than decrease signal reproducibility, this work demonstrates how this effect can be utilised to further enhance the signal. By guiding buoyant particles through the sensor by finely adjusting media density, one can precisely control particle trajectories over the sensing electrodes, resulting in improvements in signal strength, accuracy and reproducibility.

In Chapter 4, there is demonstration of a cell sorter developed utilizing the previously described on-chip volume sensor. The manuscript was published in *Microelectronic Engineering* on February 13th 2014.[19] This device was shown fully capable of sorting a population of particles or cells purely based on volume. In addition, integrated PDMS valves were not only used to tune the sensor, but also allowed extracted cells to be visually inspected through sieving. Volume-based sorting at high-resolution was achieved, capable of distinguishing cells at various stage of the cell cycle.

Finally, in Chapter 5, a device capable of trapping and sizing individual cells is demonstrated. The manuscript was published as a Fast Track article in *Biomicrofluidics* on February 28th 2014.[20] An individual cell can be rapidly flown back and forth across a

sensor, confined in a dynamic trap. This technology allowed for continual growth statistics on individual cells, accompanied by real-time optical analysis. Most technologies to date have focused on measuring the behaviour of cell colonies as a whole. For example, cell growth rate can be ascertained by monitoring the optical transmittance of a cell suspension with the Beer-Lambert Law.[21,22] As cells multiply and divide, culture opacity increases. The disadvantage herein is that the behaviour of rare cell events are easily lost in the statistics. In addition, to obtain information on growth rate changes within the cell cycle, cells in a culture need to be synchronized,[23] which is not trivial. In this work, the cell cycle stage of individual cells was visually correlated with cell volume. Further, it is demonstrated that integrated PDMS valves can be used to physically trap a cell within a microfluidic channel, and enable media to be rapidly exchanged. This new functionality opens the door to cytotoxicity assays, where the effects of drugs on volumetric growth rate can be studied.

These four scientific articles represent the heart of this thesis. In these works, each individual innovation is fully motivated as a true step forward with respect to current technology. That being said, the compressed article format is not always amiable to lengthy descriptions of state-of-the-art alternative methods. For this reason, Section 1.4 will provide an overview of recent developments in the field, and highlight the advantages and disadvantages of these technologies. The introductory chapter (Chapter 1) will introduce the key concepts that underline the physics behind these technological achievements and breakthroughs. These include not only the principles behind the volume sensing mechanics, but also physics at the microscale, the sensing physics as well as technical information

underlying device fabrication. Though these topics are briefly mentioned in the aforementioned articles, they are here presented in a comprehensive fashion.

1.1 Microfluidics

1.1.1 Introduction

Microfluidics has seen a surge of interest recently, and holds great potential in revolutionizing both chemistry and biochemistry processes. Lab-on-chip devices, such as the one depicted in Fig. 1-2, hold many advantages over conventional counterparts, including:[2]

- *Less reagents*: Fluid manipulation on the microscale means fewer reagents are required. This is both cost effective, and preferential in terms of rare samples.
- *Multiplexing*: Microfluidic manipulation of fluids means individual sensors can be easily parallelized, multiplying the throughput of such devices.
- *Small form factor*: Lab-on-Chip microfluidic systems are small, often no larger than a small coin. This makes them portable, and ready to use in point-of-care applications.
- *Cost*: Microfluidic chips can be batch-fabricated, substantially reducing the cost compared to conventional systems.

On the other hand, the novelty of these lab-on-chip systems can be a disadvantage from a developmental perspective: many of the devices described in this work and others are at a prototype stage, and work remains to be done before commercialization. Ghallab and Badawy list the following disadvantages:[24]

- *Novelty*: New, yet to be fully developed technology.

- *Signal-to-noise ratio*: Detection capabilities do not always scale-down.
- *Accuracy/Precision*: Engineering features of precise, reproducible geometries can be a challenge.

Scaling systems down to the microscale allows these devices to exploit microscale physics. This often non-intuitive microworld, where diffusion dominates over momentum, and where capillary forces, wetting and adhesion dominate over gravity, will be the focus of this section.

1.1.2 Reynolds Number and laminar flow

A handful of dimensionless numbers help to quantify the dominant effects in microfluidic regimes under different conditions, i.e. different flow rates, particle size, density, channel configurations and so forth. It becomes important to understand and exploit the physics and design your system in consequence. Among these numbers, the Reynolds number *Re* stands out as being of particular importance. It is the ratio of inertial to viscous forces.[25]

$$Re = \frac{\rho U_0 L_0}{\eta} \quad \textbf{1-1}$$

where ρ is the fluid density, U_0 the fluid velocity at the centre of the channel, L_0 a characteristic length scale such as channel width and η the kinematic viscosity. At a low Reynolds numbers (*Re* < 1000), flow is laminar, while at high Reynolds number (Re > 2000), there is turbulent flow. In the pressure-driven flow conditions of this work, the velocity will scale with channel width:

$$U_0 \sim \frac{\Delta P L_0}{\mu} \quad \textbf{1-2}$$

with μ the dynamic viscosity. We thus have:

$$Re \sim L_0 \quad \text{1-3}$$

In all but extreme cases, the flow will always be laminar in microfluidic systems (Fig. 1-2). For example, if microchannel width is on the order of 10 µm, and flow velocity on the order of 1 mm/s, one obtains Re ~ 10^{-2}. In the case of the microfluidic volume sensors developed in this work, this result guarantees flow conditions necessary for controlling cells and particles on the micron scale. In Chapter 3, where buoyancy is used to finely adjust trajectories within a sensor, or in Chapter 5, where a dynamic cell trap uses completely reversible flow, maintaining laminar flow conditions is of utmost importance.

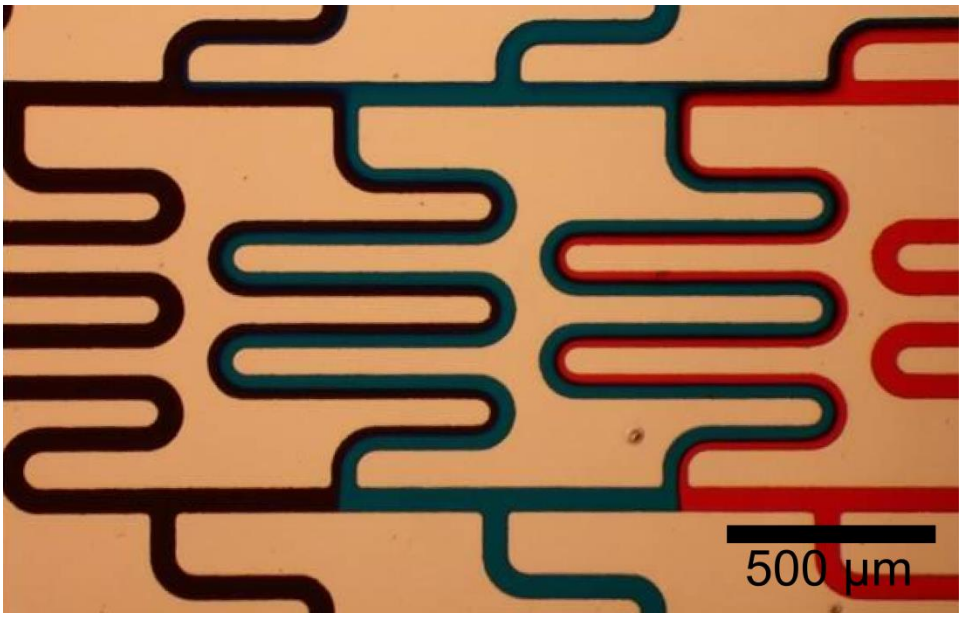

Figure 1-2 PDMS device fabricated to demonstrate the laminar flow conditions at the microscale. Solutions dyed with food coloring flow in parallel with minimal mixing.

1.1.3 Péclet Number and mixing

Another useful number in microfluidic systems, one that quantifies the transport and mixing of fluids, is the Péclet number; it is the ratio of the rate of convection to the rate of diffusion.

$$Pe = \frac{U_0 L_0}{D} \quad \textbf{1-4}$$

where *D* is the diffusion constant. Diffusion can be estimated using the Stokes-Einstein law, where it can be represented by the random walk of small spherical particles immersed in a viscous fluid. Following a procedure described by Tabeling, we first use the Langevin equation to describe the behavior of a particle:[26]

$$\frac{du}{dt} - \beta u = f(t) \quad \textbf{1-5}$$

where *u* is a velocity component (along *x*, *y* or *z*), and β is a friction coefficient. Stokes' law states that the drag force F_D will be:

$$\frac{F_D}{V} = \beta m = 6\pi r\eta \quad \textbf{1-6}$$

with *V* the particle velocity, *r* the radius of the diffusing spherical particle and η the viscosity. Brownian-type motion will have diffusion:

$$D = \frac{\langle u^2 \rangle}{\beta} \quad \textbf{1-7}$$

The energy equipartition theorem states:

$$\frac{1}{2} m \langle u^2 \rangle = \frac{1}{2} k_B T \quad \textbf{1-8}$$

Combining 1.6, 1.7 and 1.8, we obtain the Stokes-Einstein relation:

$$D = \frac{k_B T}{6\pi r\eta} \quad \textbf{1-9}$$

Why is this important? A low diffusion constant allows a user to manipulate cells and microspheres without worrying about them diffusing too far in either direction. These concepts of diffusion and mixing play a large role in the case of the cell growth monitoring

device described in Chapter 5. Such a device operates on the principle of a reversible flow, whereby a living cell is being shuffled back and forth within a microchannel. Every time it passes through a sensor, flow is reversed. While this dynamic trap principle will be further explained in Chapter 5, it is here mentioned as an example of a system where diffusion and mixing plays an important role. Ideally one would want a trapped cell to NOT diffuse, and small molecules (glucose, proteins, nutrients) to diffuse very rapidly, constantly replenishing a cell held in a trap. A steady nutrient supply is essential to maintaining normal growth conditions. For a cell suspended in aqueous solution at 30 ºC, this equates to a very manageable 0.1 μm^2/s. The diffusion of glucose is about 5000 times larger, guaranteeing a steady nutrient supply.

Mixing is further enhanced by Taylor dispersion in situations where Pe >> 1. Taylor dispersion is a microfluidic effect whereby an uneven flow profile, a Poiseuille flow, causes liquid to disperse faster than through diffusion alone. Poiseuille flow is a direct result of the no-slip condition on the edges of a pipe or channel. This effect is described visually in Fig. 1-3. This leads to an effective, axial diffusivity[25]:

$$D_Z \sim \frac{U_0^2 w^2}{D} \sim Pe^2 D \qquad \textbf{1-10}$$

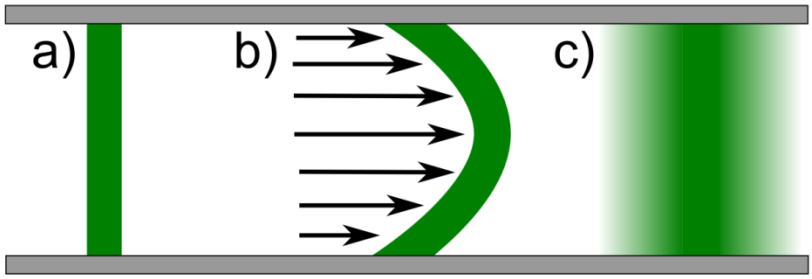

Figure 1-3 (a) Thin liquid plug. (b) Poiseuille flow stretches out the liquid plug through convection. (c) Liquid diffuses within the channel, leading to a Gaussian spreading profile.

Or analytically, in the case of rectangular microchannels:

$$D_Z = \frac{\overline{U}^2 h^2}{210D} \quad \textbf{1-11}$$

where h is the channel height and $\overline{U}$ the average velocity. As pointed out by Squires and Quake[25], it should be noted that this is only valid for a time scale:

$$t \gg \frac{w^2}{D} \quad \textbf{1-12}$$

since it is necessary for diffusion along the width of the channel to occur. Mixing of fluids occurs on shorter time scales purely from convection.

To provide an idea as to how fluids behave in the compressed channels discussed in Chapter 2 (specifically, Fig. 2-1), FEM modeling (numerical simulations) was performed using Comsol software (Fig. 1-4). Poiseuille flow is observed in all configurations.

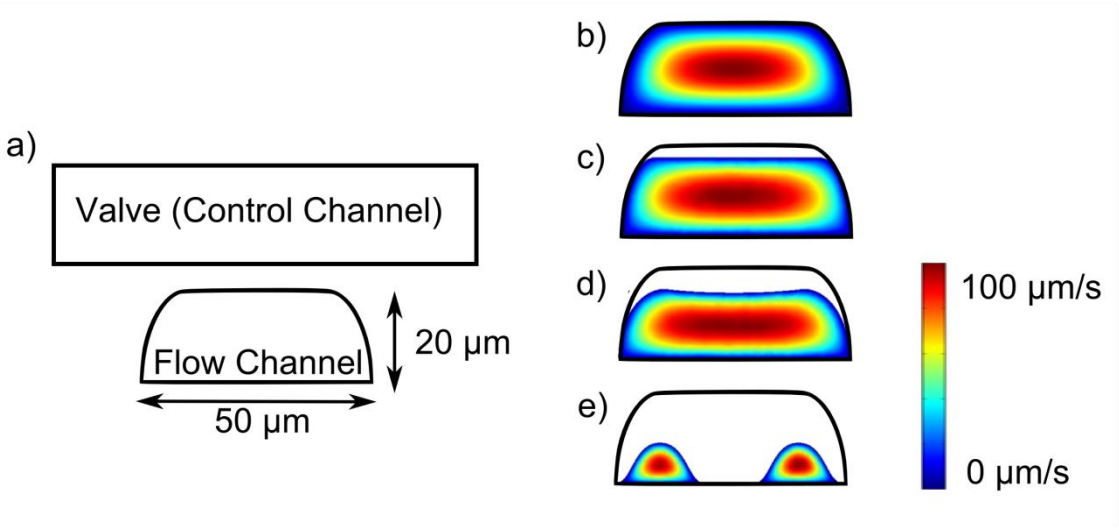

Figure 1-4: a) Typical valve and flow channel configuration in a multilayered PDMS system. b-e) A 20 μm tall x 50 μm wide flow channel is compressed as the valve is pressurized. Pressures can be

set to obtain a flow rate of approximately 100 µm/s in each case. Although the valve/flow channel mechanism is highlighted in Chapter 2, it is here included to highlight Poiseuille flow behavior.

1.1.4 Buoyancy

While momentum's role in a microfluidic system is greatly reduced due to a low Reynolds number, it nonetheless has an impact at longer time scales. This was put to the test in Chapter 3, where particle buoyancy was used to guide microparticles along different flow trajectories. Gravity will act upon a microparticle/cell with a force:

$$F_g = \frac{4}{3}\pi \mathrm{r}^3(\rho_s - \rho_f)g \qquad \textbf{1-13}$$

where ρ_s and ρ_f are the densities of the solid particle/cell and fluid, respectively. Combining (1-13) with Stokes' equation (1-6), one obtains a terminal velocity:

$$v_s = \frac{2}{9}\frac{r^2(\rho_s - \rho_f)}{\mu}g \qquad \textbf{1-14}$$

Thus, if one wants particles to settle either at the top or the bottom of a microchannel using buoyancy, Equation 1-14 allows for an estimate of terminal velocity and settling times. For the channels described in Chapter 3, this equation lead to a vertical velocity of 0.3 µm/s, and provided an upper flow limit of 240 µm/s on channel flow velocity. This permitted particles to reach their final position within the channel prior to reaching the sensor.

1.1.5 Studying cells using microfluidics

1.1.5.1 Types of cells

Microfluidics lends itself well to studying a large variety of cells, including red blood cells[27], Madin-Darby Canine Kidney (MDCK) cells[8], *Saccharomyces cerevisiae* (yeast)[14] and *Escherichia coli*.[27,28] In terms of test organisms for a growth sensor, *E.coli* and yeast

are particularly interesting because of their short cell cycle (rapid growth). These organisms have doubling times of 15-20 min and 1.5-2 hrs, respectively. Yeast is also of ideal size (diameter ~ 5 μm) to be easily measured by the microfluidic volume sensors developed in this work. For these reasons, yeast is featured in Chapters 4-5, whereas *E.coli* is used to demonstrate the limits of a tunable sensor in Chapter 2.

1.1.5.2 Tailoring cellular microenvironment

The use of microfluidics allows researchers to tailor every part of a cell's microenvironment. Laminar flow can be used to create finely adjustable gradients, at subcellular resolution.[29,30] The chemical microenvironment can be adjusted to mimic what a cell would encounter in-vivo: pH, temperature, osmolality and oxygen content can all be controlled.[31] In addition, temperatures can be changed much more quickly than for macroscopic systems.

The cell itself should also be a major consideration when designing a microfluidic environment. Not all cells will grow properly in suspension; certain cells, such as 3T3 fibroblasts, HeLa (transformed epithelial) and primary human umbilical artery endothelial cells (HUAECs) require surfaces with which to adhere in order to thrive.[32] For such adherent cells, surface properties should be taken into consideration.

The act of restricting a cell to a physically confined environment can also affect cellular behaviour. This has been documented in several studies, where micro- and nano-environments directly influenced cellular growth. In one experiment performed by Arneborg *et al.*, individual yeast cells were grown in environments with either zero or multiple yeast cell neighbours using optical traps.[33] It was found that a cell that was heavily

confined had a 15% longer growth cycle. Huang *et al.* created transparent microtubes to function as 2D culture scaffolds, some of diameter as small as 5 μm.[34] In wider tubes, yeast cells cultured within this confining environment rotated as they grew. For the smallest tubes, cells became elongated, stretching out along the length of the tube. In another work, Minc *et al.* created femtoliter chambers and forced rod-shaped fission yeast cells inside[35]. They then observed how this confinement affected factors, specifically those affecting microtubules. In each of these cases, cells were confined so tightly that they were in direct contact with channel walls. In the growth measurements detailed in Chapter 5, this is not the case; cells are suspended in solution in channels several times larger than their dimensions. Geometrical considerations should always be taken into account when designing microfluidic systems.

1.1.5.3 PDMS

A number of materials can be used to create this microenvironment, but none have gained as much widespread use as Polydimethylsiloxane (PDMS). PDMS is an organic polymer that holds many advantages when dealing with live cells (Fig. 1-5). PDMS is transparent, which allows for simple optical monitoring of cells. It is also non-toxic and air permeable, allowing cells to breathe while confined within microchannels.[36] PDMS has a low autofluorescence,[37] providing an ideal background for fluorescence measurements. PDMS is autoclavable, an added benefit when dealing with biological materials. The easy integration of multiple layers opens the door to PDMS being used for more than a simple cell cultivation tool; it can also be used to measure mechanical forces on cells. PDMS pillar deflection has been used to monitor traction forces on epithelial cells.[38]

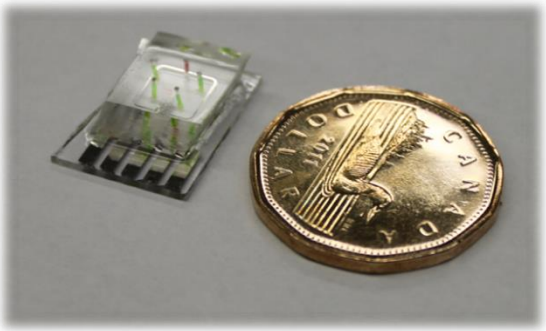

Figure 1-5 Typical dimensions of a microfluidic lab-on-chip device. Left: tunable volume sensor detailed in Chapter 2, fabricated through PDMS moulding (soft lithography).

However, PDMS is not without its flaws. In fact, some of its greatest assets can become a liability. The air permeability may help cells breathe, but it can also allow water vapors to escape, causing concentration and osmolarity changes in the cell media. This not only affects the cell, but also the baseline conductivity in impedance-based volume sensors. Given enough time, these channels can completely dry up, killing the cell culture. PDMS has also demonstrated an affinity for small hydrophobic molecules, such as proteins and drugs.[39] The reverse effect can also be a challenge: uncrosslinked oligomers can leach out and bind to cells.[31] These effects should be considered when using PDMS to construct microfluidic systems. Despite these challenges, PDMS remains widely used in microfluidic systems.

1.1.5.4 Shear stress

Another aspect of cell detection and manipulation is making sure a cell is not subjected to excessive shear stress. The cells used in this work, *E. coli* and *S. cerevisiae*, are both studied in suspension, where they can freely rotate. In cases where cells are held in place, such as in Chapter 5, shear stress is worth considering. The microchannels in this work are rectangular, with some rounded features depending on the choice of photoresist mould (see

Section 1.3). When valves are used to compress a channel, the shape changes considerably (Figure 2-2, 1-4). This makes it difficult to ascertain flow profiles in this region, without the help of numerical techniques. However, the shear stress τ of a cylindrical microchannel can be expressed through the Poiseuille formula:[40]

$$\tau = \frac{4\mu Q}{\pi r^3} \qquad \textbf{1-15}$$

with μ the viscosity, *Q* the flow rate and *r* the channel radius. A cell stuck in place at the entrance to a compressed channel region (see Chapter 5), where flow is~2 mm/s through a channel section of cross section diameter 3 μm, will be subject to a shear stress on the order of $\tau = O(10)$ Pa. How substantial is this? Yeast cells are generally considered to be quite resilient; in tests with a shear stress of 17 kPa, no ill-effects were observed.[41] In the work performed in Chapter 5, growth appeared unperturbed by the short-term exposure to the elevated shear stresses during cell media exchange.

1.1.5.5 Manipulating and analyzing cells

In the works presented herein, a number of techniques are adopted to manipulate and analyze cells within microfluidic environments. Control techniques include buoyancy, pressure-driven flow focusing and redirection and dynamic tuning of microchannel height. In each case, these techniques are paired with a microfluidic volume sensor (Chapters 2-5). In section 1.4, state of the art biosensing platforms are described, and compared to the work developed in this thesis.

1.2 Sensing physics

1.2.1 Coulter principle

The Coulter principle lies at the very heart of the microfluidic volume sensor. Simply stated, a particle or cell passing through a small aperture in an electrolytic solution through which a current is drawn shall produce an impedance change proportional to its volume. This effect is due to electrolyte being displaced by nonconductive objects. This concept was first developed by Wallace H. Coulter in the 1940s and 50s, as a means of counting red blood cells.[3,42] At the time, technologies capable of performing complete blood counts (CBCs) were based on optical detection. Today, lab-on-chip equivalents of such systems function in the same fashion, with a microfluidic channel playing the role of the aperture. A number of designs have been studied, including external electrodes[43] (wires) and embedded thin film electrodes, of either coplanar[44] or parallel[28] configurations. As discussed by Cheung *et. al.* in a recent review article,[45] there are three key parameters one can use to improve sensitivity: cell volume fraction, cell positioning in the flow and the electrical double layer.

1.2.1.1 Cell volume fraction

Sensitivity is directly proportional to cell volume fraction, as defined by Sun *et al.*:[46]

$$S = \frac{\left|\Delta\tilde{Z}\right|}{\left|\tilde{Z}_m\right|} \qquad \textbf{1-16}$$

with $\Delta\tilde{Z}$ the impedance change in the channel due to the presence of a single particle/cell, and $\tilde{Z}_m$ the impedance of the sensing volume. Further, at low frequencies where the cell membrane capacitance renders the cell nonconductive, the conductivity of the detection volume k_0 can be written:[45,47]

$$k_0 = k_s \frac{(1-p)}{\left(1+\frac{p}{2}\right)} \quad \text{1-17}$$

with k_s the media conductivity and p the ratio of particle volume to detection volume. Thus, a number of recent innovations have targeted sensitivity improvements by simply altering the size of this sensing volume. Recently, this has been accomplished by using side streams of nonconductive fluid to squeeze a central conductive stream of liquid containing target microparticles.[4,44,48] Thus, the effective sensing volume is decreased, improving sensitivity. In Chapter 2, a dynamic, mechanical means of reducing sensing volume will be discussed.

1.2.1.2 Cell Positioning

Another method to enhance sensitivity is through adjusting the trajectories of particles traversing the sensor. This has generally been performed by flow focusing, but without using nonconductive fluids. In positioning particles nearest to sensing electrodes, the current pulse signal is enhanced dramatically[18,46]. Planar electrodes, commonly used in microfluidic volume sensors for their simplicity of fabrication, create an asymmetric fringing electric field. A method describing an alternative, buoyancy-based technique is presented in Chapter 3, along with finite element method (FEM) modeling of the electric field.

1.2.2 Electrical Double Layer

The third method used to increase sensitivity has been to minimize the effect of the electrical double layer (EDL) on the electrode surface. This layer, depicted in Fig. 1-6, is formed at the interface between a metal and an aqueous solution.[49] A first layer (Inner Helmholtz plane, IHP) is formed by anions, chemically adsorbed to the metallic surface. A second layer (Outer Helmholtz plane, OHP) consists of solvated cations. Per Stern's

modification to EDL theory, these are hydrated, and thus separated by the first layer by a distance δ[49,50]. These ions are drawn by Coulomb forces, and electrostatically screen the inner Helmholtz layer. Beyond that lies the diffuse layer, which in turn screens the remainder of the charge. It is these two layers, the Stern layer (OHP) and the diffuse layer, that act in series to create an EDL capacitance:[51,52]

$$\frac{1}{C_d} = \frac{1}{C_H} + \frac{1}{C_D} \qquad \textbf{1-16}$$

The EDL capacitance makes it difficult to make accurate measurements at DC and low frequencies. In the works described in Chapters 2-5, a 50 kHz probing signal was chosen, since it lies in a frequency range that is high enough to be only minimally affected by the EDL, and low enough that the biological cell membrane remains fully nonconductive.[44] At higher frequencies (MHz), the cell membrane can be probed, where measurement of cell internal cytoplasm conductance is performed.[18]

1.2.3 Cellular response to the electric field

Keeping cells alive during the measurement process is a major concern in microfluidic volume sensors. A number of factors come into play that can have an impact on cell viability. The nature of the Coulter-based detection mechanism is such that a cell will be exposed to an electric field; this exposure can directly affect the cell. In addition, the power dissipated by the electric field will heat up the media and the cell (Joule heating). Finally, the confinement process itself, whereby a cell is exposed to a confined, microfluidic environment can also have an impact. These will be discussed in the following sections.

1.2.3.1 Electric field effect on cell viability

Electric fields can have a direct impact on cell viability; the most probable way through which this takes place is the cell membrane,[53] where electric fields can affect proteins and ion channels. The transmembrane voltage applied by an external electric field can be written:[54]

$$|V| = \frac{1.5|E|r}{\sqrt{1 + (\omega\tau)^2}} \qquad \textbf{1-17}$$

with ω the frequency of the applied field (rad/s), r the cell radius and τ a time constant:

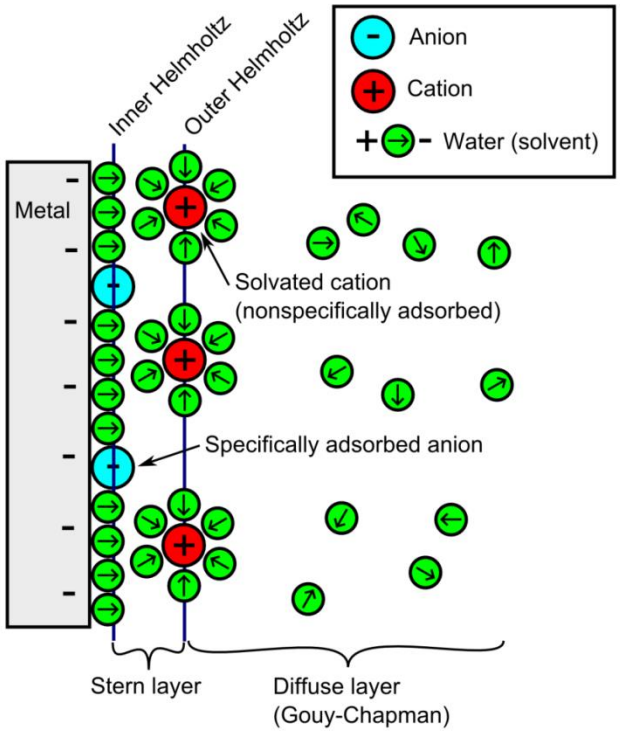

Figure 1-6 Electrical double layer according to the Gouy-Chapman-Stern model, which exists at the interface between a metal and an aqueous solution. The inner Helmholtz layer contains adsorbed anions along with water molecules. The outer Helmholtz plane contains non-specifically adsorbed solvated cations. Beyond these planes lies the diffuse layer.

$$\tau = \frac{rc_{m(\rho_{cyto}+0.5\rho_{med})}}{1 + rg_{m(\rho_{cyto}+0.5\rho_{med})}} \quad \textbf{1-2018}$$

with ρ_{cyto} and ρ_{med} the resistivity of the cytoplasm and medium, c_m the specific capacitance (F/m^2) and g_m the conductance (S/m^2). In combining these known parameters[55–57] with values consistent with experiments performed in this work, for example a d = 5 µm yeast cell suspended in 0.2 M KCl being probed with a V = 210 mV potential at 50 kHz, we have that $\tau \approx 5x10^{-8}$s and $|V| \approx 30$ mV. In the growth measurement experiments described in Chapter 5, cell exposure is limited to 200 ms per cycle, with 30 cycles per minute. This is much less than the breakdown voltage (500 mV-1V)[58], and significantly less than the endogenous transmembrane potential of plants and fungi, between -120 and -250 mV.[43,59] In general, for electric fields producing drops in potential across the cell less than these critical values, there appears to be little effect on cellular growth.[53] For example, fibroblasts can tolerate exposure to double the endogenous trans-membrane potential over several days.[58] As will be discussed in Chapter 5, trapped yeast cells demonstrated a growth cycle comparable to that found under normal incubation conditions.

1.2.3.2 Joule heating

Another concern in microfluidic devices operating electric fields is that of Joule heating. Power is dissipated within the channel, causing a rise in temperature. This is an important concern since even small temperature shifts can reduce cell viability,[60,61] particularly in mammalian cells. Temperature shifts above the mean of >4º C quickly kill mammalian cells.[53] Bacteria are far more robust, but temperature remains nonetheless a concern. Joule heating is a major challenge in microfluidic systems that use dielectrophoresis[43] or

electrokinesis[62] to drive particle flow, since applied voltages can reach as high as 1 kV. However, in devices that use embedded electrodes, where electric fields are highly localized and used uniquely as a probing mechanism, dissipated power is low. In the growth sensor in Chapter 5, the dissipated power can be estimated at 0.4 µW, based on the potential drop between the electrodes (0.22V RMS), where an AC current of 1.8 µA is drawn. This is easily dealt with through a combination of constant flushing with fresh media, and external temperature control.

1.3 Microfabrication

1.3.1 Introduction

Over the course of this work, a number of different microfabrication techniques have been developed and fine-tuned to create the devices described in this work. Detailed protocols are presented in the Appendix and are also available online through the Godin lab wiki. These processes are summarized along with a description of how these processes evolved over the course of this work, and how designs were adapted to each of the individual manuscripts presented in Chapters 2-5. First, there is a primer on photolithography and multilayer soft lithography.

1.3.2 Photolithography

Photolithography is a patterning technique whereby UV light is illuminated through a photomask, and used to transfer a pattern onto a substrate coated with light-sensitive photoresist. In positive photoresists, exposed regions become soluble to the chemical developer; for negative photoresists, exposed regions become insoluble in the chemical developer. Both types of resists are used for this work. SU-8 10 and SU-8 2050, negative photoresists, are used in situations where high-resolution (5 µm) features are required. AZ

P4620, a positive photoresist, was used as part of an alternate fabrication process, whereby the photoresist is reflowed through an additional heating step to create rounded channels (Fig. 1-7). These rounded channels make it simpler to fully compress channels with a control layer.[63]

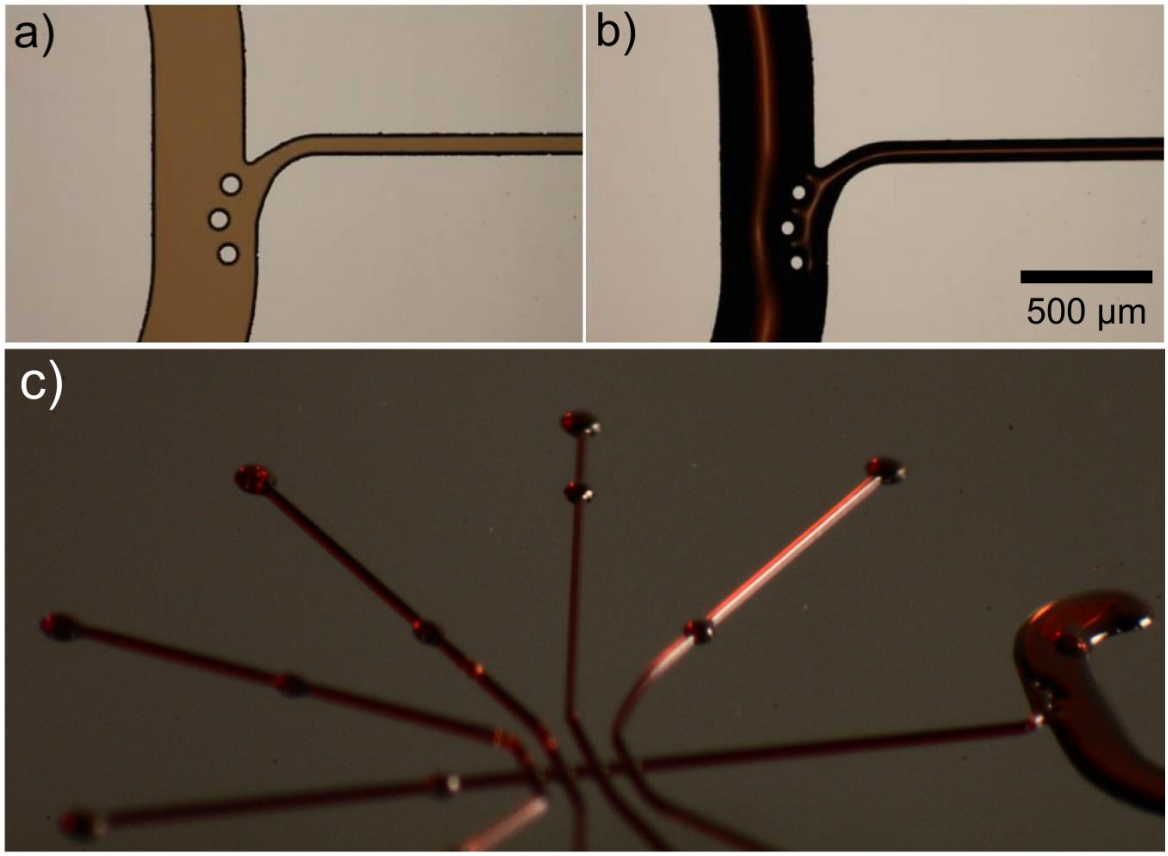

Figure 1-7 Demonstration of the photoresist reflow process for AZ P4620. (a) Rectangular channels of untreated photoresist. (b) Reflowed photoresist. (c) Angled view with rounded features visible.

1.3.3 Soft lithography

1.3.3.1 Summary

In soft lithography, these patterned substrates are used to transfer patterns onto a "soft" silicone elastomer, such as PDMS.[64] Its mechanical viscoelastic properties can be altered during fabrication by modifying the base to curing agent ratio. In this work, ratios of 7:1 (stiff), 10:1, and 20:1 (soft) are used. In fact, multiple layers of this soft material can be

deposited on top of one another,[63] creating structures of increasing complexity. These layers are bonded to each other through an oxygen plasma treatment and additional polymer crosslinking. The plasma treatment is used to create polar functional groups, in particular silanol (SiOH).[65,66] The surface, originally hydrophobic, becomes hydrophilic. When two PDMS layers are brought together (or a PDMS layer with glass), these layers form a covalent siloxane bond (Si-O-Si).[67,68]

1.3.3.2 Designs

Over the course of this work, many designs were used for different purposes, and with varying degrees of success. Most devices consist of two PDMS layers, a flexible "flow channel" layer made out of 20:1 PDMS, and a stiff 7:1 PDMS valve layer. The idea is to use a valve layer to mechanically alter the flow channels directly adjacent. By pressurizing the valve layer, the flexible PDMS surrounding the flow channel is compressed, drastically altering the channel geometry. This was used to great effect in Chapter 2, to create a tunable volume sensor, and again in Chapters 4 and 5 to create sieve valves capable of holding cells in place. Photomasks are comprehensively listed in section 9.1.2 and 9.1.3, for flow channels and control valves, respectively. Not all of these patterns lead to successful devices; others were used to fabricate prototypes and explore microfluidic capabilities in prototypes.

1.3.4 Electrode Fabrication

The electrodes used throughout this work were all fabricated using a lift-off process detailed in section 9.2.1.2 of the appendix. As shown in Fig. 1-8, electrodes lie at the base of the volume sensing devices, adhered to microscope slides and tightly bonded to PDMS. In summary, Shipley *S1813* photoresist is coated onto glass microscope slides, and then

patterned using a positive photomask. This leaves photoresist everywhere on the slide, except for areas to be occupied by the electrodes. These slides are then coated with a thin metallic film, through either thermal deposition or e-beam evaporation. The photoresist is then removed chemically with an etchant, leaving only metallic electrodes.

1.3.4.1 Material

For the devices featured in Chapter 2, Ag electrodes were used; all other chapters feature Au electrodes. The advantage of Au is that it in addition to being highly conductive and simple to deposit, it is also chemically inert. For this reason, Au quickly became a favourite.

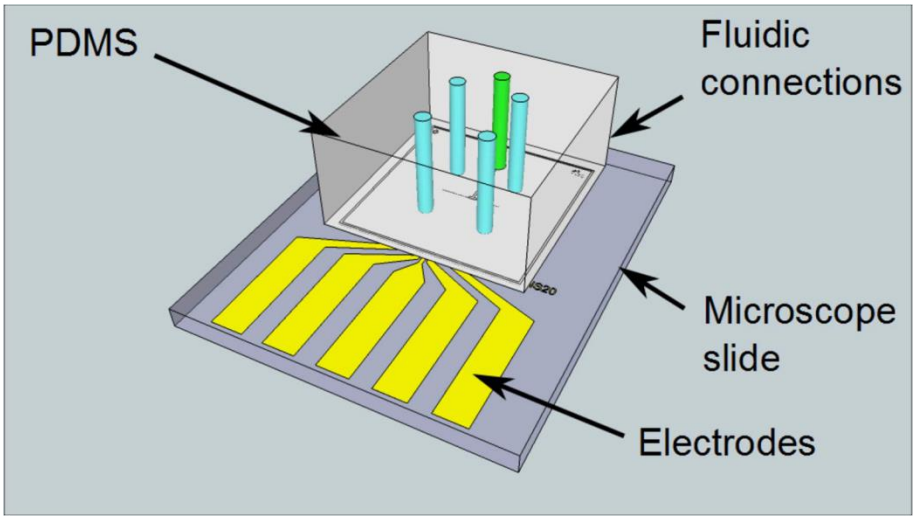

Figure 1-8 Microfluidic chip with PDMS and electrodes on a glass microscope slide.

1.3.4.2 Designs

In terms of designs, these were adjusted in response to the demands of the particular project. Section 9.1.1 lists the various photomasks used for electrode fabrication. The design *E2* was the first configuration tested, and was used in Chapters 2-4. It featured

designs with multiple contact points within the sensing channel. This redundancy proved useful, since devices with a few damaged tips could still be used. However, the large number of contact points with the fluid also lead to leaking. The minimalist *E5* pattern was thus designed, and was featured in the cell trapping device of Chapter 5. The other listed designs *E1*, *E3* and *E4* were developed for PDMS devices that were not pursued, but are listed nonetheless for completeness.

1.4 State of the Art

1.4.1 Introduction

It is important to highlight the importance of the contributions described in this thesis (Chapters 2-5) in the context of state of the art developments in the field, as well as commercially available systems. This section will review the pros and cons of some of the technologies being developed for volume sensing, cell sorting and growth monitoring.

1.4.2 Volume sensing

1.4.2.1 Commercial systems

1.4.2.1.1 Flow Cytometers

Flow cytometers are instruments that can interrogate particle/cell samples by optical means, often in conjunction with fluorescent probes. Scattered and emitted light is collected and analyzed, at rates up to 25,000 cells s^{-1}.[69] Flow cytometers provide an indirect means of measuring volume, since light scattering does not always correlate with volume.[70]

1.4.2.1.2 Coulter Counters

As discussed in Section 1.2.1, Coulter counters provide powerful means of ascertaining the volume distribution of particles/cells in suspension. There are a few companies that sell

Coulter-based particle sizing and counting systems, including Beckman Coulter and EMD Millipore. Coulter counters are produced for a variety of uses, such as examining the size distribution of particles in paint or obtaining complete blood cell counts.[71] For example, Beckman Coulter states its Multisizer™ 4 Coulter Counter® is capable of sizing particles/cells in an overall range of 400 nm to 1.6 mm diameter, at a rate of 10,000 particles per second. Apertures are changed depending on the size of the particles being sized, reducing the measurement range to, for example, 400 nm - 16 µm diameter particles. Accuracy on volume is about 3%. As discussed previously, the high cost and shear size of this instrument mean that it's generally found in clinical or research environments.[4,5] The EMD Millipore Scepter is a handheld device available at a lower price point, but lacks the accuracy and precision of the Multisizer™ 4 Coulter Counter®.

1.4.2.2 Microfluidic volume sensing

The Coulter principle can also be applied to microfluidic systems, where it can be combined to a host of cell/particle manipulation tools as a lab-on-chip. For example, Cheung *et al.* used an impedance spectroscopy flow cytometer to size red blood cells at 1,000 cells/min. In designing these devices, consideration must be given to particle trajectories as they traverse the sensing volume.[18,46] A number of innovative approaches have been explored with the aim of regulating target paths.

1.4.2.2.1 Hydrodynamic flow focusing (multiple streams)

Hydrodynamic flow focusing is a process whereby a central, conductive stream containing particles/cells is focused between multiple nonconductive streams. Bernabini *et al.* showed how in a parallel electrode device, flow in a 200 µm wide channel can be confined to~10

μm, leading to the detection of *E.coli*.[28] Nieuwenhuis *et al.* demonstrated a device capable of focusing a flow stream on three sides using a 2-dimensional liquid aperture control.[44] They found that flow velocity had to be precisely controlled: at flow rates below 0.5 μL/s, diffusion becomes problematic whereas at flow rates above 10 μL/s, flow becomes unstable. Scott *et al.* developed a three-dimensional focusing system, and found that sensitivity was improved by a factor of 2.5 compared to two-dimensional focusing.[4] Hydrodynamic flow focusing is a versatile tool capable of greatly enhancing sensitivity, but care must be taken in manipulating flow conditions.

1.4.2.2.2 Dielectrophoresis (DEP)

Dielectrophoresis is a technique whereby a non-uniform electric field exerts a force on a dielectric particle/cell. Such a force can be used to direct particles towards the center of a channel. Zhu *et al.* demonstrated how applying a DC potential between both ends of a serpentine channel could be used to focus particles.[72] The cross-stream DEP force housed inside each of the turns, made particles drift towards the central stream. However, this process required fields up to 500 kV/m, which is rarely used in microfluidic systems.[72] Joule heating, as well as the direct impact of the high electric field on the cell, become a concern (see 1.2.2). Lagally *et al.* fabricated a system that used AC DEP to concentrate a stream of *E.coli* by a factor of 160.[73] Interdigitated electrodes were used to apply the field. As discussed by Cheung *et al.* in a recent review article, a disadvantage of DEP is that the applied force decays rather rapidly with distance from the electrodes.[45]

1.4.2.2.3 Flow effects

Various microfluidic flow phenomena can be harnessed to focus particles within microchannels. These techniques often make use of the microscale physics discussed in

Section 1.1, in new and innovative ways. For example, Lee *et al.* constructed a microchannel that would expand and contract, effectively building a contraction-expansion array: at each contraction region, centrifugal forces act to envelop the sample flow on all sides.[74] They demonstrate three-dimensional focusing of RBCs using an easy to fabricate, single-layered PDMS structure. Golden *et al.* were able to integrate chevron structures within a microfluidic channel that converted a two-dimensional focused sample stream into a stream surrounded in three-dimensions.[75] The chevrons effectively transfer fluid from the side streams above and below the central core, surrounding it with a tight focus. Such passive techniques are elegant and simple. However, they generally only function properly within a defined flow speed range, which may not be suitable for all applications.

Method	**Advantages**	**Disadvantages**
Multiple streams	● Simultaneous particle focus and sensor volume reduction ● Prevents channel blocking	● Requires steady flow ● Diffusion-limited
DEP	● Force can be adjusted ● Tolerance in flow velocity	● High E-Field ● Joule heating
Flow effects	● Low cost ● Simple fabrication	● Requires steady flow ● Flow velocity restrictions

Table 1-1 Advantages and disadvantages of particle focusing methods in microfluidic volume sensors

1.4.2.3 Microfluidic Tunable volume sensor + Using Buoyancy

As will be discussed in Chapters 2-3, this thesis explores two different approaches to improving cell volume ***sensitivity***, ***accuracy*** and volume ***resolution***. Chapter 2 outlines the fabrication and analysis of the ***very first*** microfluidic ***tunable volume sensor***, where a valve

positioned directly above the sensing electrodes can be adjusted, dynamically altering the sensing volume and thus ***dynamic range***. This not only helps guide the particles along controlled flow lines, but also reduces the overall volume of the channel, increasing sensitivity.[16] It is a method that is simple to implement, requiring no flow constraints like there are for hydrodynamic techniques, or high electric fields as there are to induce DEP (Table 1-1). In addition, the dynamic nature of this valve-based approach makes it simple to release obstructions in the channel by depressurizing the valve. In Chapter 3, a buoyancy-based approach is outlined, where particles are flowed near planar electrodes, vertically confined by gravity, demonstrating improvements in volume measurement ***sensitivity*** and ***accuracy***.

1.4.3 Sorting cells by volume

1.4.3.1 Commercial systems

1.4.3.1.1 Fluorescence-activated cell sorting (FACS)

Fluorescence-activated cell sorting (FACS) was invented in the 1960s, and continues to this day to play a vital role in cell sorting applications.[76] Light scattering and/or fluorescence is used to identify cells, and then deflect electrostatically, at rates between 10,000-20,000 cells /s.[77] FACS remains in many ways the gold standard in cell sorting, and is the instrument with which microfluidic equivalents are compared. FACS is commonly used in medical diagnostics,[78] cell purification[79] and cell therapy.[80] However, as with other flow cytometers based on optical methods, it does not measure volume, at least not directly.

1.4.3.2 Microfluidic cell sorting

1.4.3.2.1 Microfluidic FACS

Microfluidic equivalents to FACS, aiming to combine sorting with other lab-on-chip functionalities have been proposed.[81–83] Studer *et al.* developed a microfluidic cell sorter out of multi-layered PDMS, with valves capable of sealing off a detection chamber, and cycling liquid through peristaltic action.[84] Other designs have reached commercialization: Owl Biomedical claims to have developed a microfluidic system capable of sorting cells based on FACS readings, using a valve operating at an astounding 30 µs/cycle. Again, FACS-based systems do not separate based on volume.

1.4.3.2.2 Optical tweezers

Optical tweezers can be used to manipulate dielectric particles and cells using a focused laser beam. A microscope is used to tightly focus a laser beam within a microfluidic channel, causing an optical trap: particles are drawn toward the region of strongest electric field.[85,86] Applegate *et al.* demonstrated a version of this mechanism that utilises a much wider trapping zone, capable of deflecting suspended colloids or red blood cells flowing in a microchannel into one of several outlet ports.[87] Optical methods offer unparalleled precision in manipulating individual cells, but these require external expensive optics, not always suitable for lab-on-chip applications.

1.4.3.2.3 Acoustics

Acoustic forces can be used to separate particles in a flow.[88] Petersson *et al.* used a free flow acoustophoresis technique to separate platelets, red blood cells and leukocytes in a continuous flow.[89] A piezo ceramic actuator creates an ultrasonic standing wave, forcing cells to migrate laterally across the channel width, into one of three outlets. This acoustic

force is proportional to the volume of the particle/cell, but also to its density and compressibility compared to that of the medium.[90] These targets, denser than the medium, will be displaced toward a wave node. Particles need to be tightly focused, since the parabolic flow profile causes cells at different positions to experience different levels of exposure to the wave.

1.4.3.2.4 Passive separation

There exists a wealth of techniques available that use passive methods to sort particles, including methods based on lateral displacement,[91] pinched flow fractionation,[92,93] and both hydrophoretic[94] and diffusive filtering [95]. Field flow fractionation techniques in general rely on a transverse force, usually gravity, across a channel.[96] The competition between thermal energy and the potential energy drop through the field cause a concentration gradient to form. Yamada *et al.* demonstrated pinched flow fractionation, where particles are flowed through a "pinched" (narrow) microchannel which opens into a much wider channel.[92] As the particles emerge, the broadening flow profile will cause particles of different sizes to follow different trajectories, enabling size-based lateral separation. These can then be collected into any of multiple outlet channels. Through improvements in outlet channel dimensions, Takagi *et al.* developed an asymmetric version of pinched flow fractionation, where the separation of microspheres 1.0, 2.1, 3.0 and 5.0 μm in diameter were separated.[93] Hydrophoresis is a separation method that relies on the pressure field induced by microstructures within a microchannel.[97] Song and Choi show that microspheres can be deflected based on size, allowing the separation of particles with diameter 12 μm, 15 μm and 20 μm.[98] Diffusive filtering techniques use obstacles to prevent the passage of larger cells, and achieve sorting of a blood sample. Sethu *et al.* designed such a microfluidic

system, where sieves allow erythrocytes to pass, while physically blocking larger leukocytes.[95] Huang *et al.* demonstrated a lateral displacement technique, whereby microspheres of 0.8 µm, 0.9 µm and 1.03 µm diameter were separated as they were flowed through an array of obstacles.[91] Rectangular obstacles separated by a gap distance are positioned in an array, each row shifted from the previous. Unlike the previous diffusive filtering technique, this lateral displacement method does not physically block the passage of particles, thus preventing clogging issues. Particles of different size will flow with varying degrees of ease laterally, causing each to follow a very distinct path and subsequent separation. The above examples are but a sampling of the vast amount of passive techniques being researched. Of particular appeal, these techniques do not require active manipulation of fields, thus making them simple to implement at lower cost. The disadvantage lies in the fact that these techniques often sort based on multiple parameters at once, often being dependent on cell shape as well as size.[95] In addition, these devices generally require precise flow controls, and volume calibration by external methods, such as commercial Coulter counters.[99]

1.4.3.2.5 Dielectrophoresis (DEP)

DEP has been used effectively in a number of microfluidic systems.[63,100] DEP makes use of a non-uniform electric field to push/pull on cells, enabling cell sorting based on size[6] or internal properties.[101] The nonuniform electric field induces a dipole in polarisable particles, causing them to migrate.[102] It is of note that DEP is just as well suited to manipulate neutral particles as they are charged particles. Green *et al*. used an interdigitated electrode design to separate colloidal particles of diameter 2 µm, 1 µm and 0.5 µm at 99.9% efficiency.[102] Sun *et al.* demonstrated how 4T1 tumour cells and murine bone

marrow cells could be separated through DEP.[103] However, in their approach, they integrated two microfluidic volume sensors as a means of verifying sorting efficiency in each of the collection branches.

1.4.3.2.6 Combining volume sensing with electrokinetic flow sorting

As discussed previously, microfluidic volume sensors provide high resolution volume measurements. Combining these powerful systems with a means of manipulating particles after detection becomes particularly attractive. Song *et al.* demonstrated such a device, where particles were actively sorted after a volume measurement was performed.[104] In this case, a single channel with a sensor branched off into two outlet channels, and particles could be deflected into either through electrokinetic flow (EF) through feedback with the measurement. Particles suspended in a charged solution are driven by an external field. This phenomenon requires a charged double-layer at the channel walls (see 1.2.1.3), as is almost always the case.[105] At a rate of 30-40 cells/min, 5 μm diameter particles were sorted from 4 μm diameter particles at near-100% efficiency. As with DEP methods, driving the flow of particles with EF requires relatively high voltages (~ 50V).

1.4.3.3 Microfluidic flow focusing based on volume sensing

In Chapter 4, ***high-resolution*** microfluidic volume sensing (~3 μm^3) is combined with hydrodynamic flow focusing. This ***label-free***, purely ***volume-based*** separation method demonstrates a 100% efficiency, successfully isolating a subpopulation of yeast. Multilayered soft lithography is used to integrate valves, used for both the ***collection of extracted sample***, as well as ***sensor tuning***. Unlike DEP or EF methods which require voltages to drive particles/flow (Table 1-2), sorting is controlled through cell-friendly pressure-driven flow manipulation.

1.4.4 Measuring cell growth

1.4.4.1 Culture methods

1.4.4.1.1 Optical density and cell synchronization

In general, the optical density (OD) of bacterial cultures is proportional to bacterial density.[106] The simplicity of simply shining a laser through a cell suspension and measuring transmittance make this technique particularly appealing. Through the Beer-Lambert Law, the attenuation over a path length L is obtained:[107]

$$\mu = -\frac{1}{L}\log_e \frac{I}{I_0} = \epsilon[C] \qquad \textbf{1-22}$$

With μ the absorption coefficient, I and I_0 the detected and incident light intensity, C the concentration of the bacteria and ε the extinction coefficient. The downside of this technique is that it averaging can hide the behaviour of rare individual cells. To study the cell division cycle, cells must be synchronized. In a 1999 review paper, Walker discusses the synchronization techniques available, which include induction methods (physical, chemical stress) and elutriation (separation by size) techniques.[23] Centrifugal elutriation is a widely-used method, where cells are separated based on size and sedimentation rate. These cells are then used as a new, synchronous culture. However, culture synchronicity decays over 2-3 cycles, and elutriation requires highly trained personnel.[23]

1.4.4.2 Cell-by-cell methods

1.4.4.2.1 Microscopy

When asked how to measure the volume of an individual cell, perhaps the first method that comes to mind is simply looking at it. Such techniques are among the first to study cell

growth , and began in the 1930s.[108] Woldringh *et al.* used an image cytometry technique to study the volume growth of *S.Cerevisiae*.[109] They measured the volume of emerging buds, and compared them to mother cells. They were also able to estimate how many daughter cells a mother had produced by counting scars on the cell surface. Interestingly, they found that mother cells grow~10% during budding, and second and third generation mother cells display a lower volume growth rate, and faster budding than first generation cells. However, as with all optical methods, certain geometric assumptions must be made to measure volume.

1.4.4.2.2 Suspended microchannel resonator (SMR)

This technique uses a hollow cantilever to weigh cells at high resolution.[13,110] Godin *et al.* developed a suspended microchannel resonator (SMR), a cantilever with an embedded fluidic microchannel.[13] In this work, the instantaneous growth rates of individual cells, such as *S. cerevisiae* was measured. Cell trapping was accomplished dynamically, by periodically cycling a cell back and forth through the sensor. A computer-controlled pressure regulator operated on feedback, enabling this periodic redirection of flow through the sensor. They found a size dependence on growth rate, where larger cells grew faster than smaller ones. This device is capable of high-resolution mass measurements, 0.1% for yeast.[111] This technology is also used to obtain density information on carrier solutions in Chapter 3.

1.4.4.2.3 Continuous volume sensing – static trap

Two works in particular have recently examined long-term volume measurements using a volume sensor. The first method, developed by Hua and Pennell., establishes a static trap, whereby a cell is caught in a microstructure within a sensor, and volume measured over

extended periods.[8] This method was used to measure the cellular response of MDCK cells to osmotic stress. The cellular media could be quickly and easily exchanged. However, channel impedance changes with time, due to effects such as electrochemical reactions at electrodes and evaporation. This causes a baseline shift, which can obscure cell volume changes.

1.4.4.2.4 Continuous volume sensing – dynamic trap

A volumetric approach proposed by Sun *et al.* uses a dynamic trap[43], where cells are cycled back and forth across the sensor, similar to the trapping scheme for the SMR (Section 1.4.4.2.2). In this work, an applied electric bias is reversed every 15 min, enabling periodic measurement of volume of *S.cerevisiae.* This relatively long delay between measurements was chosen to prevent electric field effects on the cell and Joule heating. This technique inherently corrects for baseline drift, by continuously acquiring a new baseline.

1.4.4.3 Continuous volume sensing with a dynamic trap and media exchange

In Chapter 5, a method that combines the best attributes of the abovementioned techniques (Table 2-2) is described, enabling ***dynamic trapping*** with ***media exchange***. The device operates through pressure-driven flow manipulation, where a cell is kept in a dynamic trap. Multilayered PDMS is used to integrate microfluidic sieve valves, which act as physical barriers during media exchange, keeping a cell firmly in place. The volume of *S. cerevisiae* can be monitored for ***entire growth cycles***, and ***cellular response*** to media exchange measured.

Type		Method	Advantages	Disadvantages
Cell sorting	**Commercial**	FACS	● High throughput ● Commercially available	● Not a volume measurement ● Cell labeling ● No microfluidic integration
	Microfluidic	Microfluidic FACS	● High throughput	● Not a volume measurement ● Cell labeling
		Optical tweezers	● High-precision cell manipulation	● Expensive optics ● Alignment
		Acoustics	● Adjustable force ● Non-contact	● Force also dependent on other parameters
		Passive separation	● Ease of fabrication ● Requires no ext. fields	● Measures volume and other parameters ● Requires steady flows
		DEP	● Adjustable force	● High E-Field ● Joule heating
		Volume sensing + EF sorting	● High resolution	● High voltage
Growth Monitoring	**Culture**	OD + cell synchronicity	● Ease of measurement	● Obscures individual cell information ● Synchronicity a challenge
	Cell-by-cell	Microscopy	● Simple observation ● Combined with fluorescence, visual clues	● Volume requires geometric assumptions
		SMR	● High-precision buoyant mass measurement	● No information on volume
		Cont. volume sensing – static trap	● Cell media easily exchanged while trapping	● Baseline drift
		Cont. volume sensing – dynamic trap	● Baseline correction	● Cell media cannot be exchanged while trapping

Table 1-2 Advantages and disadvantages of cell sorting and growth monitoring methods

Manuscript: Microfluidic cell volume sensor with tunable sensitivity

- This work was submitted April 13th 2012, and accepted June 6th 2012 as a *Lab on a Chip Communication*.
- I, Jason Riordon, contributed the large majority of the work presented in this scientific article: this includes device design, microfabrication (photolithography, lift-off, PDMS moulding), electrical setup, software design, pressure control, cell culturing, data acquisition and all analysis presented herein. I wrote the first draft, and completed revisions thereafter.
- Dr. Maryam Mirzaei, a postdoctoral researcher, contributed to the microchannel design and aided in microfabrication.
- Ian Jardine, Jeff Salvail, Dominique Laniel and Eric Hoogkamp made minor contributions with preliminary work in modelling and microfabrication.
- This manuscript has been modified from the original, in order to match the formatting style of this thesis. Section titles were added to guide the reader through the work. References are consolidated at the end of the thesis.
- The supplementary material presented in section 2.7 was published with this work.

2 Microfluidic cell volume sensor with tunable sensitivity

Reproduced by permission of The Royal Society of Chemistry from:

Riordon, J., Mirzaei, M. & Godin, M. Microfluidic cell volume sensor with tunable sensitivity. *Lab on a Chip* **12,** 3016 (2012). doi: 10.1039/c2lc40357a.

2.1 Abstract

We report the fabrication and validation of a microfluidic cell volume sensor integrated on a multi-layered polydimethylsiloxane (PDMS) microchip with a tunable detection volume for dynamic control of sensitivity, enabling the detection of individual Escherichia coli and microparticles.

2.2 Introduction

The development of microfluidic cell volume sensors has been fuelled by a need for biological detection capabilities in a low-cost, portable and energy efficient format. Impedance-based volume sensors[27] and micro-Coulter counters[3,112] monitor the variation in ionic current through a narrow sensing region as individual micro-sized particles transit through. Prototypes have been developed to measure the size of a number of biological targets including individual red blood cells[27], yeast[43] and *Escherichia coli.*[28] Maximum sensitivity is attained by fabricating a sensing channel similar to the dimensions of the target particle. Unfortunately, this both limits the device to targets of a narrow size range, and increases the chance of clogging.

In an effort to increase the dynamic range, some have used hydrodynamic focusing[4,28,44,113] to accommodate a broader range in target sizes. By flowing a conductive sheath of liquid between parallel nonconductive sheaths in a low-Reynolds number microfluidic

environment, the electrolytic volume is reduced and sensitivity increased. Thus, effective sensing volume can be optimised, without risk of obstruction. However, diffusion between sheaths could pose issues during experiments requiring much reduced or stopped flows, or in long-term trapping experiments requiring the introduction of various drugs.[13,43]

Another approach to increasing dynamic range while mitigating these issues is to integrate a tunable valve above the sensing channel. Multilayer soft lithography allows for the integration of valves and pumps into PDMS-based microfluidic devices.[63,114] Pressurizing a valve chamber above a microfluidic channel enables dynamic control of the channel height (Fig. 2-1a). By measuring electrical conductance in electrolytic media, channel volume is accurately characterized.[115] The sensing volume becomes tunable over a wide range (0.5pL to 23pL in the following examples), and can not only heighten sensitivity, but allow the detection of smaller diameter microspheres (~1μm) that would otherwise pass undetected. The molded PDMS is bonded to a glass slide patterned with 80nm thick Ag electrodes (deposited by electron beam physical vapor deposition with a 5nm Cr adhesion layer). By pressurizing the valve, the PDMS membrane separating the fluidic and the pneumatic valve layers is adjusted to alter the volume of electrolytic solution separating the electrodes (Fig.2-1c,d). The resistance of the sensing volume is that of a conductor of uniform cross section A and length l (electrode separation): $R=\alpha\rho l/A$, where ρ is the resistivity the electrolyte and α is a geometrical factor due to the use of planar electrodes.[48] A micro-sized target in transit through the detection volume will cause a momentary increase in resistance as the electrolyte is displaced.

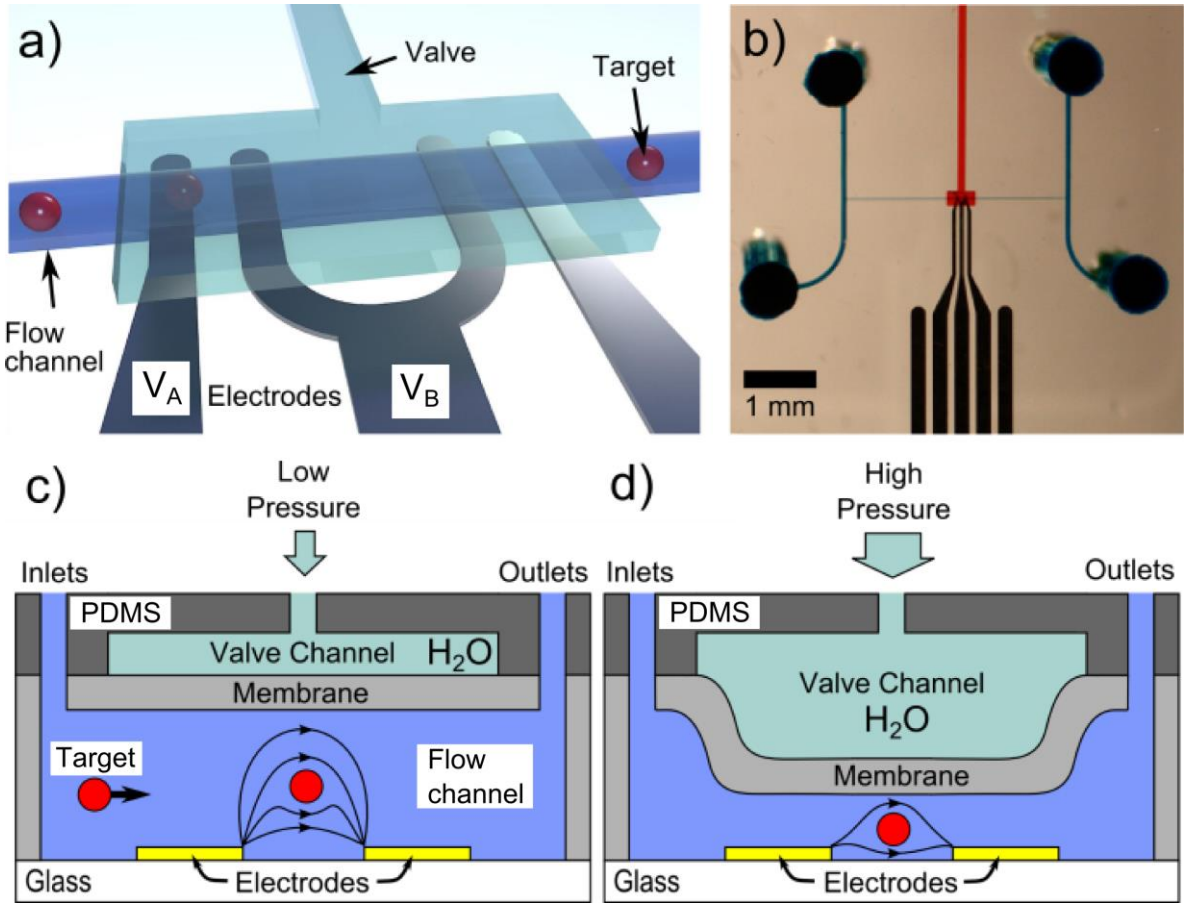

Figure 2-1 (a) Device schematic illustrating the valve, flow channel, electrodes, and targets. Only the two leftmost electrodes are utilized, labelled V_A and V_B. (b) Volume sensor with flow channels (blue), valve (red) and electrodes (black). A central sensing channel links two wider channels, which serve as inlet and outlet. (c) Cross-section of device illustrating the PDMS channel layer (light grey) and valve layer (dark grey). As targets flow between sensing electrodes, electrolytes are displaced resulting in a drop in conductance proportional to target volume. (d) In pressurizing the valve, sensing volume is reduced and sensitivity increased.

2.3 Materials and Methods

The device consists of two parallel 80 µm wide bypass microchannels connected by a narrow sensing channel, as depicted in Fig. 2-1b. Multiple designs were evaluated, with sensing channel widths ranging from 10 µm to 50 µm, and having 10 µm to 20 µm heights. Electrode width/separation varied between 15 µm and 25 µm. Two photoresists were tested as moulds for PDMS channels, SU-8 10 (MicroChem) and P4620 (AZ Electronic Materials). SU-8 was used to create channels of 10µm and 20µm width, whereas P4620

was used to make 30μm and 50μm flow channels. The fabrication protocol for P4620 lead to channels with rounded features, meant to facilitate channel compression during valve pressurization.[63] Complete fabrication details are presented as supplementary material (2.8.1).

The volume sensor operates by applying an AC potential between a pair of sensing electrodes and monitoring changes in current as transiting target microspheres disrupt ionic current. A function generator (Stanford Research Systems DS345) provides a 50 kHz, 30mV signal to a low-noise preamplifier operating at unity gain (Stanford Research Systems SR560). The output voltage is applied to a first electrode V_A with respect to ground. The current collected by the other electrode is sent to a current amplifier (Keithley 428) which converts the ~5μA signal to 0-10V, which is monitored by a lock-in amplifier (Stanford Research Systems SR830 DSP). The lock-in signal is acquired at 200 kHz with a 16-bit DAQ card (NI USB-6353) and monitored via a LabView script. Each data set is subjected to a filtering algorithm using a combination of point-by-point averaging, Savitzky-Golay and lowpass filtering. Briefly, the Savitzky-Golay filter fits a polynomial (linear least squares approach) to a subset of data, and evaluates it at a single point. It does this in succession over the entire data set. The attractiveness of such a filter is that it does a good job of preserving peak shape, which is of primary importance in this work.[116] Flow through the flow channel was controlled using pressure regulators (Bellofram Type 10). The pneumatic valve was also controlled by a pressure regulator (SMC IR2010-N02-R), and filled with deionized water to prevent air bubble formation in the flow channel during pressurization. A flow control diagram is presented in Supplementary Material (2.8.2).

2.4 Results and Discussion

The channel cross-section was calibrated during valve activation by fluorescence imaging;[63] intensity counts were converted to a channel height by combining them with profilometer measurements of the corresponding master mould. Fig.2-2a and 2-2b show typical cross sections of two channels of different height and width. Channel cross-section is altered symmetrically as valve pressure is ramped up. The shape of the channel prior to valve activation determines how the collapse will progress: a square channel will show increased depression at the center, where it is structurally weakest, whereas round channels display a more uniform compression. In the case of a square channel, high valve pressure (>15psi) causes the sensing channel to split axially into two parallel channels. Fig. 2-2c and 2-2d show optical microscope images of the sensing volume with an uncompressed and fully compressed valve, respectively. At a valve pressure of 28 psi, the channel is reduced to 2% of its original volume.

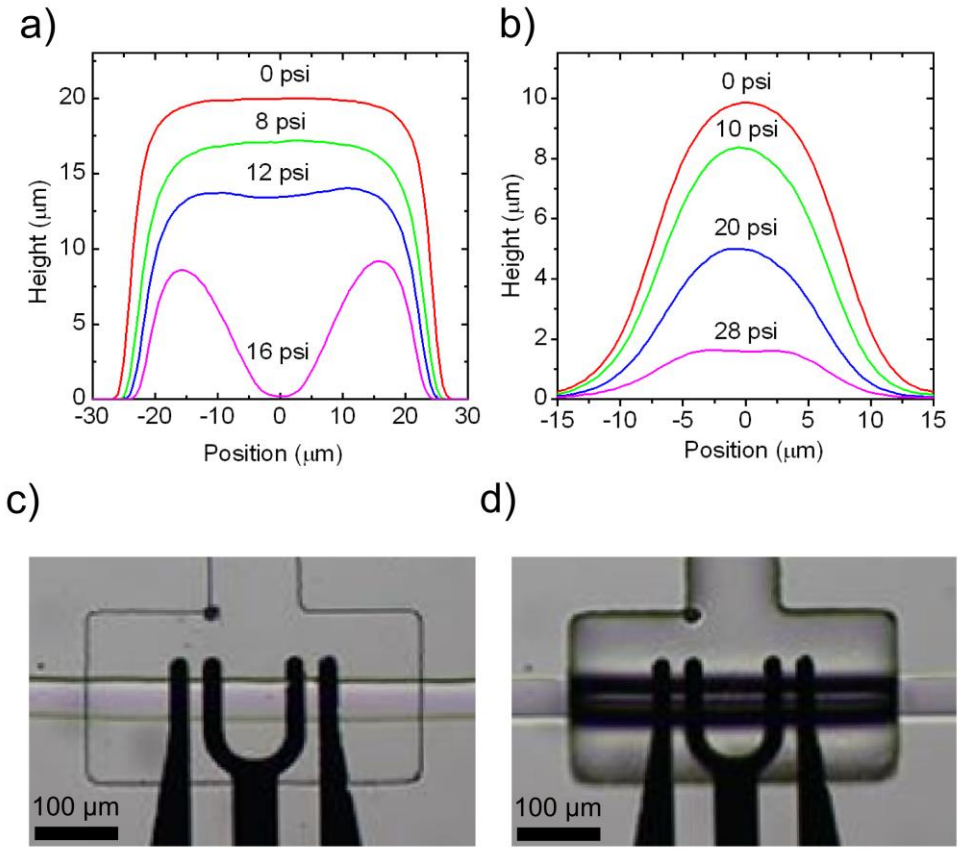

Figure 2-2 Cross-section profile for different valve pressures obtained through fluorescence imaging and profilometer measurement of the P4620 mould for (a) 20 μm high by 50 μm wide channel and (b) 10 μm high by 30 μm wide channel. c) and d) are optical microscope images of an uncompressed and compressed valve, respectively, operating on the 20 μm high by 50 μm wide channel. Channel pressure is 3 psi; valve pressure switches from 0 to 28 psi.

Polystyrene microspheres of different sizes were used to evaluate device performance over its entire range: d = 1.51 ± 0.05μm, 3.9 ± 0.3 μm, 6.0 ± 0.4 μm and 7.3 ± 0.5μm (Bangs Labs). Microsphere solutions were stripped of their buffer through multiple centrifugation/dilution steps, and then resuspended in an aqueous solution containing 0.1M KCl, 1 % bovine serum albumin (BSA) and 13% glycerol to a concentration between 105 and 107 particles/mL; BSA helps prevent microsphere agglomeration and glycerol ensures neutral buoyancy. A 0.1M KCl solution was chosen to mimic conditions necessary to sustain living cells. Fig. 2-3a illustrates a typical current change observed during the

transit of d = 7.3 μm microspheres through the sensing region at different valve pressures for a 20μm high by 50 μm wide channel (P4620 mould). Relative changes in current become stronger as channel is compressed. Fig. 2-3b illustrates histograms obtained at four valve pressures for the d = 1.51μm microspheres for a 20μm high by 10μm wide channel (SU-8 mould). Current drops corresponding to microbead pairs were removed for clarity.

These small microspheres were not detected until a 22.5 psi pressure was applied to the valve. Gaussian fits were taken for each data set, and show a clear widening effect associated with smaller detection volumes. Since the measurement is limited by sample polydispersity, Gaussian width will increase for smaller detection volumes.

Fig.2-3c illustrates a compilation of current variations for various microspheres and valve configurations for the same device as for Fig. 2-3a. The valve was pressurized to 0 psi, 4 psi and 8 psi. Linearity is demonstrated for each valve setting, with slopes of 2.31 ± 0.06, 3.40 ± 0.04 and 5.6 ± 0.2 (%/aL) for the d = 3.9 μm, d = 6.0 μm and d = 7.3 μm targets, respectively. The slope represents the sensitivity of the device operating at a given valve pressure, which reflects the geometry of the system as well as the preferred path taken by the target through the sensor. A sharper slope at increased valve pressure signifies a heightened sensitivity. Moreover, in collapsing the channel, microspheres are forced to follow an alternate route through the sensing region. Finite element method (FEM) modeling with a FEMLAB toolkit (Comsol Ltd) shows a high dependence on vertical positioning: targets flowing near the electrodes alter electric field lines more significantly, thus further enhancing sensitivity. This impedance sensitivity height dependence has been previously reported.[117,118] Standard deviations obtained from current change histograms were converted to standard deviations on volume, and compared to that provided by the

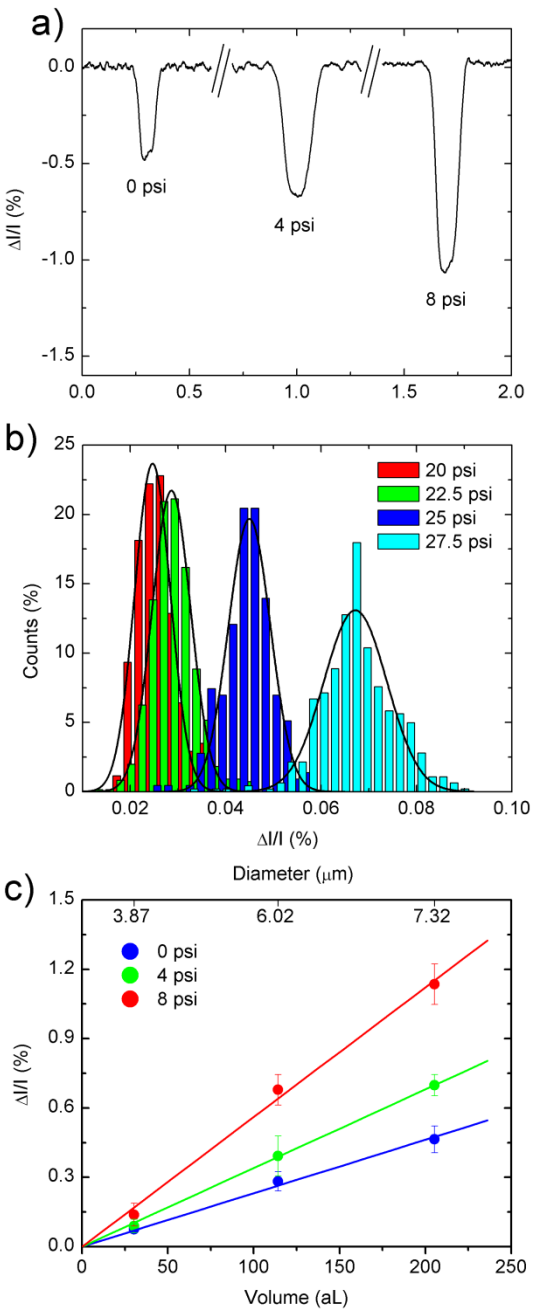

Figure 2-3 (a) Typical signal obtained by monitoring current as a d = 7.3μm microsphere traverses the sensing region in a 20 μm high by 50 μm wide channel. Shown is the change in current ΔI relative to baseline current I_0. (b) Histograms depicting relative change in current obtained from 2046 counts for *d* = 1.51 μm microspheres at variable valve height for a 20μm high by 10μm wide channel. (c) Current change as a function of microsphere volume for *d*=3.9, 6.0 and 7.3μm microspheres on 20 μm high by 50 μm wide channel. A linear relation is observed at all configurations, showing increased sensitivity for a compressed channel. Flow channel pressure is kept constant at ~3 psi, with bypass channels at slightly offset pressures to induce a net flow through the sensor.

manufacturer. For most datasets, these matched quite well. However, for the d = 7.3 µm microbeads it was found to be about half of that indicated by the manufacturer through a commercial Coulter counter. A reduced standard deviation was also reported by Sridhar *et al.*[112] for d = 9.8µm microsphere population (Bangs Labs), and remains puzzling. Table 2-1 lists the signal-to-noise ratio (SNR) measured for various microspheres under different valve configuration on this same device. While valve pressurization leads to improved SNR, the ratio of standard deviation to mean value in population measurements is not always improved. In effect, microspheres become easier to detect, but also show greater population variability. This could be improved by using an alternate electrode geometry, which would produce a more uniform electric field through the sensing volume.

		Valve Pressure (psi)				
		0	**4**	**8**	**12**	**16**
Diameter (µm)	**1.51**	a	a	a	1.7	4.1
	3.9	10	11	16	40	b
	6.0	56	85	130	b	b
	7.3	69	110	190	b	b

a) SNR at sub-detection threshold. b) Microspheres obstructed.

Table 2-1 Signal-to-Noise Ratio (SNR)

To demonstrate the device's functionality for biological samples, a population of wild-type *E. coli* K12 was analyzed with a 20 µm high by 50 µm wide sensing channel (Fig. 2-4). Cells were suspended in LB broth at 10^8 cells/mL, and flowed through the sensor at a valve pressure of 20 psi (4psi channel pressure). The valve pressure was chosen so as to be at the threshold where targets can pass, but only just. The size distribution is log-normal.[119]

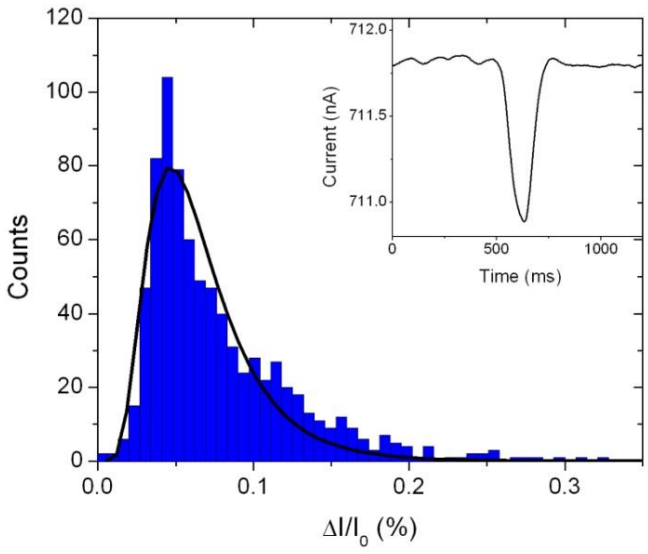

Figure 2-4 Histogram depicting relative change in current for a population of K12 Wild-type *E. coli*, fitted to a log-normal function. Calibration with d = 1.51µm microspheres indicates an *E. coli* cell volume of 1.3 ± 0.3µm^3. Inset graph shows current variation during a typical detection event.

In addition to heightened sensitivity, a volume sensor with a compressible sensing region provides the user with a means to easily dislodge a clog in the sensing volume. If there is a clog, a reduction in valve pressure quickly liberates the device. This flexibility allows the device to be used to study large particles that run the risk of damaging a static device. It is believed that cell volume sensor sensitivity could be further increased by improved electrical shielding through use of a Faraday cage. Long-term signal drift, while not crucial to transient current shift measurements, could be limited through the use of a temperature controller, since electrolytic conductivity is temperature dependent.

2.5 Conclusions

The microfluidic cell volume sensor enhanced with a pneumatic valve provides heightened sensitivity and dynamic range, allowing for the detection of live *E. coli* and smaller diameter microspheres (~1 µm) that would otherwise go undetected. Future work will focus

on trapping cells for growth measurement, and automating valve compression to dynamically adjust channel height based on target volume.

2.6 Acknowledgements

The authors thank Ian Jardine, Jeff Salvail, Dominique Laniel and Eric Hoogkamp for preliminary modelling and microfabrication. This work is supported by the Natural Sciences and Engineering Research Council of Canada (NSERC) and the Canadian Foundation for Innovation (CFI).

2.7 Supplementary Material

2.7.1 Fabrication Details

2.7.1.1 Ag Electrodes

Ag electrodes were fabricated on glass using a common lift-off process. Electrodes were fabricated so as to have multiple independent leads into the fluidic channel, with a width and separation chosen to be similar to channel diameter (15-25 μm). While only two are required for current measurement, the others allow flexibility in measurement technique (4 point measurement), as well as backups in the case of damage. A separate grounding electrode provides electromagnetic shielding along the edges of the device. 1" x 3" x 1mm glass microscope slides were thoroughly rinsed with acetone, isopropanol and ethanol, then heated to 110°C for 10min and cooled for 2 min. They were then spin-coated with Shipley S1813 photoresist for 30s at 4000 rpm, for a final thickness of 1.4 μm. Slides were prebaked 60s at 90°C, UV exposed 60s, toluene soaked 60s, and postbaked at 90°C for 15s. Development was done in tetramethylammonium hydroxide (TMAH). 5nm Cr / 80nm Ag was deposited by sputter deposition, and lift-off was completed in 1-methyl-2-pyrrolidinone (NMP). Electrodes were rinsed with acetone, isopropanol and ethanol prior to bonding to PDMS (Sylgard 184 silicone elastomer kit).

2.7.1.2 Photoresist Moulds

For the flow channel mould, two protocols were followed, one for rounded channels (P4620 photoresist – AZ Electronic Materials), a second for straight-walled rectangular channels (SU8-10 - MicroChem). A silicon wafer was cleaned using piranha etch, then baked at 200°C for 30 min, and let cool for 5 min. For the rounded P4620 channel mould, an adhesion layer of hexamethyldisilizane (HMDS) is first spin-coated. Two P4620 layers

are deposited in turn. Spin speed and time were chosen depending on final thickness requirements. For example, a 20μm layer required the following spin settings (Table 2-2):

Layer 1	Layer 2
4s@500rpm	4s@500rpm
5s @ 0rpm	5s @ 0rpm
5s @ 500rpm	5s @ 500rpm
40s @ 1800rpm	40s @ 1150rpm
40s @ 400rpm	40s @ 400rpm
10s @ 900rpm	10s @ 900rpm

Table 2-2 Spin settings P4620

After each spin-coated layer, the wafer is prebaked at 90°C for 1 min, then 115°C for 1.5 min. The wafer is then exposed to UV for 60s, and immersed in AZ400K developer as required. The wafer is postbaked at 75 °C, 95 °C, 115 °C and 200 °C for 5 min each. For the SU-8 mould, photoresist is spin coated to required thickness. The wafer is then prebaked at 65°C for 2 min, then 95°C for 6 min, and exposed to UV for 45s. The wafer is postbaked at 65°C for 1 min, and 95°C for 3 min. SU-8 developer is then used to remove the photoresist. For the valve layer, a similar protocol is used.

2.7.1.3 PDMS multilayer

All wafers are then coated with aminosilane to facilitate PDMS removal. PDMS for the flow layer was prepared with 7:1 base to curing agent ratio, and baked at 80 °C for 24 min. Devices were cut out, inlet holes were punched, and devices were rinsed with soapy water, deionised water, ethanol and isopropanol, in that order. Fluidic layer PDMS was mixed at a 20:1 base to curing agent ratio. Using two PDMS ratios, one with a higher percentage of base, one with a higher percentage of curing agent, allows for cross-linking of both layers, and thus helps strengthen the bond. Further, a 20:1 ratio leads to more flexible PDMS to

make the channel layer more elastic. The mixture was degassed, spin coated to required thickness, and baked for 20 min at 80°C. PDMS thickness was chosen to be above the height of the channel. For example, for a 20 μm channel, a thickness of 25μm was desired, requiring the following spin settings (Table 2-3):

Layer 1
10s@1000rpm
30s@3000rpm

Table 2-3 Spin settings PDMS

Both PDMS pieces were exposed to oxygen plasma (Glow Research AutoGlow) at 30W for 30s, bonded using a mask aligner, and baked at 80°C for >12hrs. Devices are cut out, and flow channel inlets are punched. Devices were again cleaned using soap and water, deionised water, methanol and isopropanol. Electrodes and PDMS devices were exposed to oxygen plasma (30 W, 30s), and aligned using a mask aligner. Devices were then baked at 80°C for 12 hrs. Completed devices are then glued to PCB boards, where leads are connected with a wire-bonder to bonding pads leading to external electronics.

2.7.2 Flow Control

Fig. 2-5 illustrates our pressure control scheme, used for most measurements featured in this work.

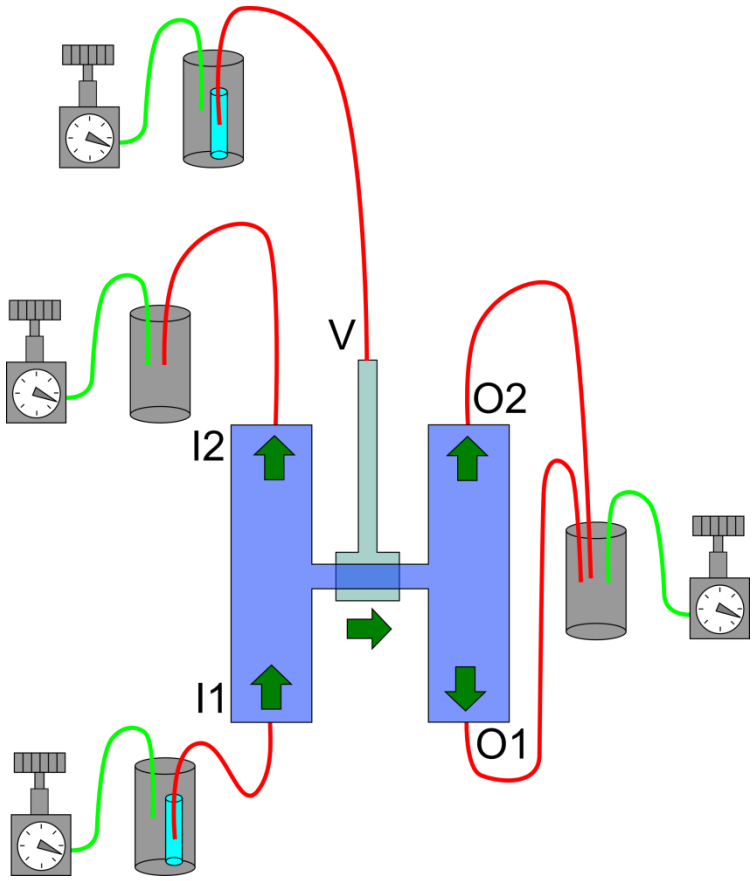

Figure 2-5 Flow control diagram. Pressures at I1, I2, O1 and O2 are set to about 3 psi, with I1 slightly higher. This drives a flow from I1 to I2, and from left to right through the sensor. Solution is driven through the device by pressurizing the corresponding vial with a regulator. The valve is filled with water, and controlled via a separate regulator. Green: Air Tube. Red: Flow Tube.

Manuscript: Using the fringing electric field in microfluidic volume sensors to enhance sensitivity and accuracy

- This work was submitted August 20th 2012, and published October 10th 2012 in Applied Physics Letters.
- I, Jason Riordon, contributed the large majority of the work presented in this scientific article: this includes all computer modelling, device design, microfabrication (photolithography, lift-off, PDMS moulding), electrical setup, software design, pressure control, data acquisition and all analysis presented herein. I wrote the first draft, and completed revisions thereafter.
- Nicolas M-Catafard, then an undergraduate student, performed calibration of carrier fluid densities.
- Dylan Stone, an undergraduate student, assisted with electrode fabrication.
- Radin Tahvildari, a doctoral student, provided useful advice on sample preparation.
- This manuscript has been modified from the original, in order to match the formatting style of this thesis. Section titles were added to guide the reader through the work. References are consolidated at the end of the thesis.

3 Using the fringing electric field in microfluidic volume sensors to enhance sensitivity and accuracy

Reproduced with permission from:

Riordon, J., M. -Catafard, N. & Godin, M. Using the fringing electric field in microfluidic volume sensors to enhance sensitivity and accuracy. *Applied Physics Letters* **101,** 154105–154105–4 (2012). doi:10.1063/1.4759033.

3.1 Abstract

The particle trajectory above impedance-monitoring coplanar electrodes in a microfluidic channel dramatically influences the measured electric current change. We use finite element modeling to predict changes in ionic current for microspheres flowing in highly fringing fields, and validate these results by introducing a buoyancy-based particle focusing technique. Using 6 μm polystyrene particles in solutions of varying density, we control the height of the particle trajectories near the sensing electrodes and show that sensitivity can be increased by up to 3.5× when particles flow close to the electrodes compared to particles flowing further away, while simultaneously improving accuracy.

3.2 Introduction

The use of microfluidic impedance-based flow cytometers has seen a great deal of growth in the past decade, providing an inexpensive means for detection of micron-sized particles with low sample consumption. Impedance-based volume sensors and micro-Coulter counters measure the change in ionic current as individual microtargets transit through a narrow sensing channel[3]. Sensors have been developed to measure the volume of synthetic particles as well as a number of biotargets, such as red blood cells[18], yeast[43], kidney cells[8] and *Escherichia coli*.[28] Multiple electrode configurations have been demonstrated,

including parallel[28] and planar[44] electrode designs. While the latter is advantageous for ease of fabrication, it suffers from sensitivity to particle height, due to the electric field gradient.[46] Consequently, microparticles that flow through the sensor along a path far from the electrodes induce a smaller change in resistance than those flowing nearest to the electrodes.[18] This adds uncertainty to the determination of particle volume, limiting the usefulness of coplanar electrode geometries in comparison with parallel electrodes. In this Letter, we use finite element method (FEM) modelling to study the current response of microspheres flowing along trajectories at different heights within the sensor, and obtain a volume-dependent enhancement factor. To validate results experimentally, we introduce a buoyancy-based technique capable of focusing particles along trajectories at different vertical distances from the coplanar electrodes.

3.3 Materials and Methods

FEM modelling was performed using the COMSOL MULTIPHYSICS *Conductive Media DC* module. A 20 μm microchannel of square cross section was modelled, with a pair of 20 μm wide coplanar electrodes separated by a 20 μm gap located on the top surface of the microchannel. A 30 mV DC potential was simulated between both electrodes, drawing a 420 nA current through conductive media (σ=1.3 $\Omega^{-1}m^{-1}$). Current change was computed by positioning a nonconductive microsphere at fixed coordinates within the channel, and iterating over multiple configurations (Fig. 3-1). Every iteration required a separate FEM calculation using 169 000 mesh elements. Electric current was obtained by integrating the normal electric field over the entire channel cross-section at a given position between the electrodes. To provide an estimate on uncertainty, four such cross sections were integrated. Error bars were smaller than the symbols in Fig.3-1 and thus were omitted.

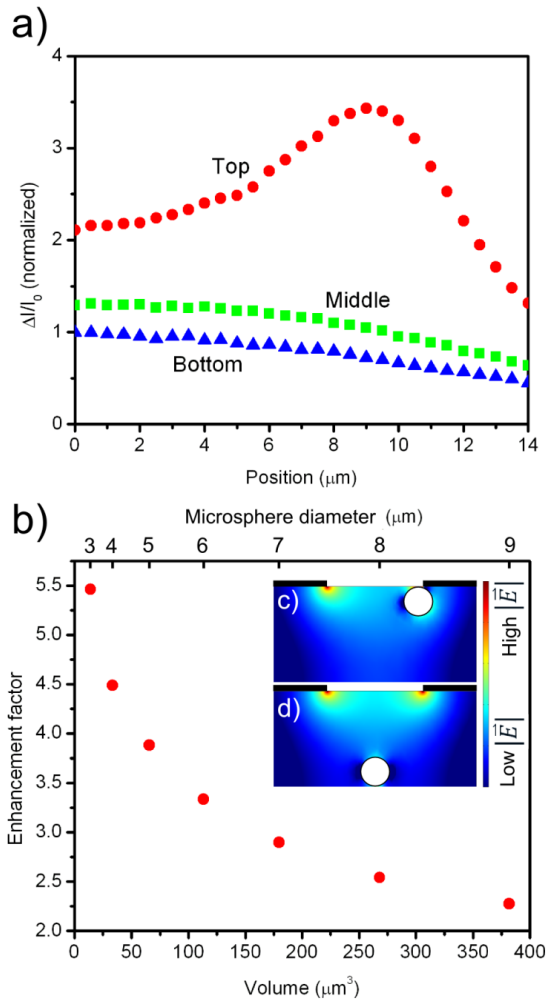

Figure 3-1(a) Current change for d = 6 μm microspheres transiting a 20 μm by 20 μm sensing channel at different heights: Bottom z = 3.1 μm, Middle z = 10 μm and Top z = 16.815 μm, each measured from the channel floor to the center of the microsphere. These positions were chosen so as to be at no more than 100 nm from the electrodes, which are positioned at the very top of the channel. The x-axis represents the position of the bead along the length of the channel, starting from the mid-point between the electrodes. For microspheres passing closest to the electrodes, the maximum current change occurs near the inner electrode edges (x = ± 10 μm). (b) Enhancement factor between Top and Bottom configurations for different microsphere volumes. (c) and (d) illustrate the electric field density in a 2D slice of the device (log plot) for a 6 μm diameter microsphere in Top and Bottom configurations, respectively. The horizontal black bars illustrate electrode positioning.

Fig. 3-1a illustrates how the current pulse differs for microspheres flowing at different heights. The x-axis shows the position with respect to the center of the electrode pair. For a microsphere flowing near the electrodes (*Top*), the maximum current change occurs as it

goes by the electrode edge; for microspheres in the middle or at the bottom of the channel, maximum current change occurs at the center of the electrode pair. Fig. 3-1b maps the enhancement factor between the *Bottom* and *Top* configurations as a function of target volume (diameter on top axis). As shown in Fig. 3-1a, this position of maximum change is different for each trajectory. The enhancement factor is greater for smaller microtargets than for larger ones: in the case of 6 μm diameter microspheres, this corresponds to a 3.3× enhancement in signal.

A target's effect on the fringing electric field can be better visualised in Figs. 3-1c and 3.1d, where a logarithmic plot of the electric field density is shown for a 2D slice of the system in the *Top* and *Bottom* configurations. As the nonconductive microsphere nears the inner corners of the electrodes (Fig. 3-1c), electric field perturbation is maximized leading to a larger change in current. A similar electric field fringing effect was also described in FEM simulations done by Gawad *et al.* with respect to parallel facing electrodes.[117]

To validate these simulations experimentally, 6 μm diameter microspheres were flowed through a microfluidic volume sensor at different heights. This particle size was chosen so as to be small enough to see a significant enhancement between flow paths, and large enough to produce a large current change pulse. Flow height control was accomplished by altering glycerol concentration in the carrier buffer to control density, and thus generate a negative or positive buoyant force on the microparticles. The microfluidic volume sensor chip was fabricated by polydimethylsiloxane (PDMS) molding using photolithography.[16] SU-8 10 photoresist (Microchem) was patterned on a silicon wafer to create a 20 μm wide sensing channel of square cross-section. PDMS of 10:1 base:curing agent ratio was then molded, and bonded to a glass substrate with Au/Ti electrodes (80 nm /

5 nm). The electrodes were fabricated using a lift-off technique described elsewhere.[16] The device is positioned under an upright microscope with the electrodes on glass at the top. The sensing channel connects two parallel bypass channels (Fig. 3-2a), and is designed to be of sufficient length to allow for targets to settle before transiting the sensor (~12 mm from inlet to sensor). From Stoke's Law, the terminal velocity, v_s, of suspended microspheres is proportional to the difference between the particle mass density ρ_p and fluidic mass density ρ_f:

$$v_s = \frac{2}{9}\frac{(\rho_p - \rho_f)}{\mu} gR^2 \qquad (3.1)$$

where μ is the dynamic viscosity, g the gravitational acceleration and R the microsphere radius. For 6 μm diameter polystyrene microspheres (Bangs Labs) in a solution of glycerol of concentration up to 42%, this leads to an upward velocity of $v \approx 0.3$μm/s. For the device depicted in Fig. 3-2, this means maintaining a flow rate below 240 μm/s to insure complete microsphere migration to the electrodes. This serves as an upper estimate, since settling time is slightly increased due to wall effects.

Ionic current was monitored by applying a 50 kHz signal (V_{pp} = 620 mV) between the pair of sensing electrodes, and measuring current in series via a current amplifier (Keithley 428) and lock-in amplifier (Stanford Research Systems SR830 DSP). The probe signal is applied via a function generator (Stanford Research Systems DS345) and a low-noise preamplifier (Stanford Research Systems SR560) operating at unity gain. Lock-in amplitude is measured through a 200 kHz 16-bit DAQ card (NI-USB 6353) using a LabView script. Data is filtered using a combination of point-by-point averaging and low pass filtering. Flow through the channels was controlled by using pressure regulators (SMC

IR2000-N02-R and SMC IR2010-N02-R) to establish the flow pattern in Fig.3-2 (a) as previously described.[16] Three solutions with suspended 6 μm polystyrene microspheres were prepared at an approximate concentration between 1×10^5 and 1×10^6 microspheres/ml. Solution densities were chosen to affect particle buoyancy, such as to draw microspheres up towards the sensing electrodes or down away from the electrodes. The difference in densities between that of the particle and of the carrier fluid was varied to control gravitational settling times. Each buffer contained 0.1% bovine serum albumin (BSA), 0.1M KCl and varying concentrations of glycerol (0%, 21% or 42%). Carrier fluid densities were quantified with a suspended microchannel resonator (SMR):[13] 1.004 ± 0.001 g/cm^3 , 1.065 ± 0.001 g/cm^3 and 1.121 ± 0.001 g/cm^3 for 0%, 21% and 42% glycerol solutions, respectively. To prevent beads from non-specifically interacting with microchannel surfaces, 0.1% g/ml of detergent (Contrex, Decon Labs Inc.) was added prior to experimentation to both the water and glycerol heavy solutions.

3.4 Results and Discussion

For each solution, microspheres were flowed through the volume sensor at ~100 μm/s, and current changes were recorded. This speed was chosen to insure that transiting particles have enough time to settle by gravity as dictated by equation (1). Typical events are presented in Fig. 3-3a. Microspheres flowing near the bottom of the channel (A – away from the sensing electrodes) cause a much lower change in current than those flowing at the top (D – near the sensing electrodes). Events shown in B and C are for particles suspended in a 21% glycerol solution, making them practically neutrally buoyant. The 21% glycerol solution has a density of 1.065 g/ cm^3, which only slightly differs from that of the microspheres (1.062 g/ cm^3). This small difference in densities is sufficient to cause a slight

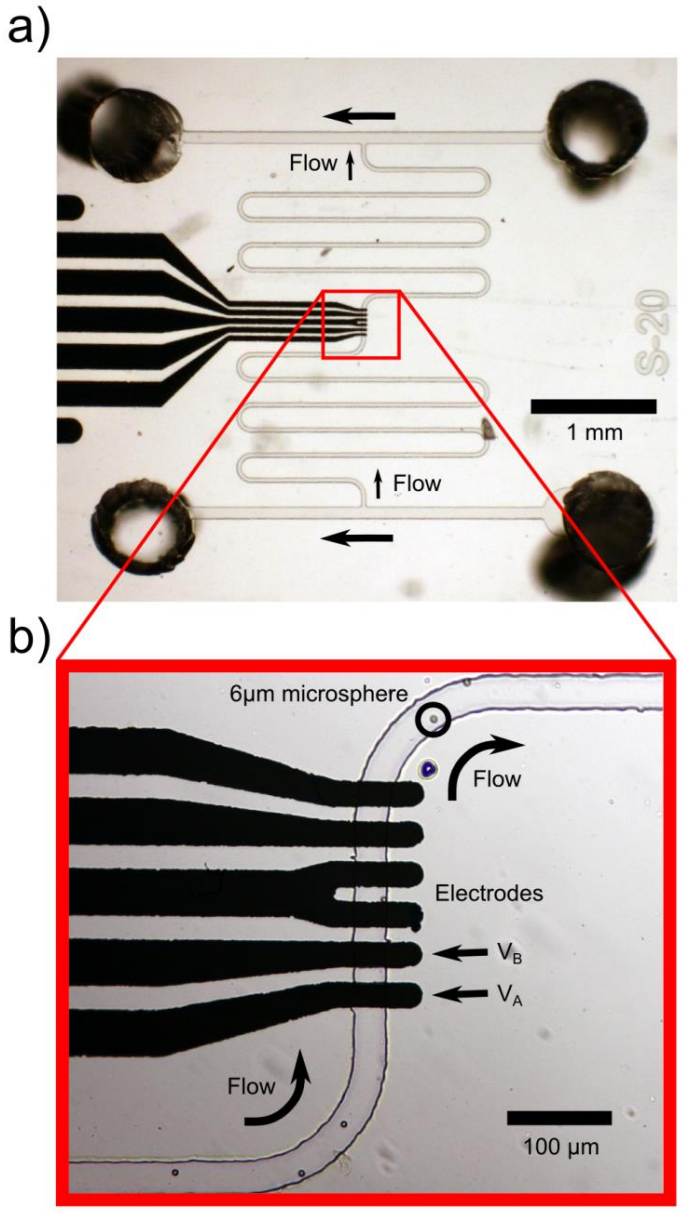

Figure 3-2 (a) Microfluidic volume sensor with meandering channel connecting two parallel bypass channels. Au electrodes are positioned at the top of the channel. Arrows denote flow direction. (b) Enlarged view of sensing volume framed by two electrodes, where an AC potential is applied at VA and VB is grounded. Only the lower two electrodes are utilized in the experiments described here.

settling along the vertical axis in the timeframe of the experiment. In turning the device upside down, this shift is reversed (experiment B in Fig. 3-3a). Population histograms for respective samples are presented in Fig. 3-3b. Current changes of 0.16 ± 0.01%, 0.26 ± 0.01%, 0.35 ± 0.03% and 0.55 ± 0.05% were measured for experiments A, B, C and D,

respectively. There is a nearly 3.5-fold increase in sensitivity when the particles assume a trajectory near the electrodes compared to when they flow near the bottom of the microchannel, as predicted from Fig. 3-1b. One would expect beads flowing in a near-neutrally buoyant solution to follow a Poiseuille distribution, creating a histogram that would span the entire region between histograms A and D (from $\Delta I/I_0 = 0.16$ to 0.55). This is not the case, as the B and C distributions in Fig. 3-3b are too narrow. This suggests that targets are predisposed to follow a certain trajectory, likely due to the geometry of the device, and how microtargets are flowed into the sensor. Though experiments B and C produced a mean current change of similar uncertainty to experiments A and D, their accuracy differs greatly.

The current profile for individual transit events also reveals striking differences depending on particle trajectory. For particles suspended in the 42% glycerol solution (buoyant) the current profiles show a clear M-shaped peak, similar to that observed in Fig. 3-1a. This effect is present in most events for this data set, and can be postulated a direct result of increased proximity to electrodes. As particles flow over the inner corners of the electrodes, the fringing electric field causes an even greater current change than at the center. These M-shaped pulses are similar to those observed in traditional Coulter counters, present when targets flow too close to the edges of the sensing aperture.[120]

To date, there have been several demonstrations of microfluidic focusing techniques[72,75,121,122] aimed at centering particles within microchannels. In the case of impedance-based volume sensors with coplanar electrodes, the idea is to focus them next to the electrodes. Some examples use focusing techniques to improve sensitivity by reducing the sensing volume. One approach is to use sheath flow focusing with an adjustable

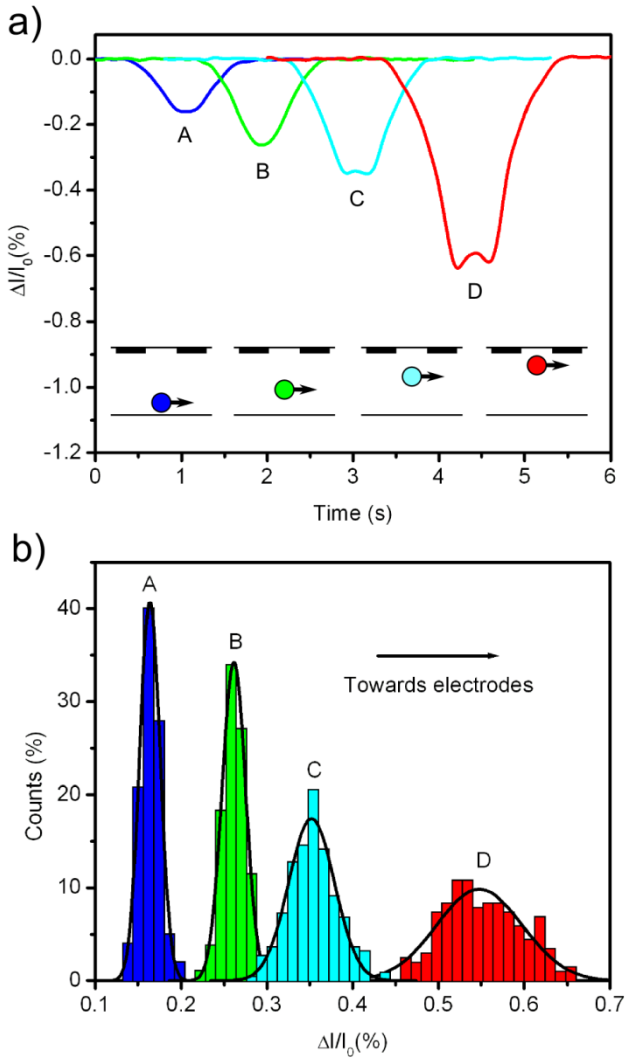

Figure 3-3 (a) Typical current change for a 6 µm diameter polystyrene microsphere flowing through a 20 µm wide square channel for 4 experiments with three different solutions of varying density: A = 0%, B = 21%, C = 21% and D = 42%. For experiment B, the device was turned upside down to have particles migrate in the opposite direction compared to C. Data suggest not only an amplitude enhancement, but also an expected M-shaped feature present in D. (b) Normalised histograms representing a total of 1084 events demonstrating a near 3.5 times enhancement in signal from A to D.

aperture,[5] where multiple nonconductive sheaths are used to direct flow of microtargets in conductive media next to a pair of coplanar electrodes in a µ-Coulter counter. Another uses a tunable pneumatic valve to mechanically direct microtargets next to the electrodes.[16] These approaches allow for increased sensitivities by reducing sensing volumes, but there

remains some uncertainty related to variability in particle trajectories above the electrodes. While we demonstrate a simple device that simultaneously enhanced sensitivity and accuracy, we submit that combining buoyancy-based settling (focusing) with these other schemes would further improve on measurement accuracy by confining particles to trajectories that are as close to the coplanar sensing electrodes as possible.

3.5 Conclusions

As shown both through FEM modelling and experimental work, focusing microtargets next to the electrodes allows for heightened accuracy and up to a 3.5-fold signal enhancement. The introduced buoyancy-based method is simple to implement and readily combined with current volume sensing technologies. Future work will explore using the M-shaped current pulse to automatically compensate for target height effect on volume measurement, and thus increase the sensitivity of volume sensors using coplanar electrodes. To increase throughput in future devices, a lengthened meandering channel will allow for beads to flow longer, allowing them to settle more efficiently in rapid flow systems.

3.6 Acknowledgements

The authors thank Dylan Stone for assisting in electrode fabrication and Radin Tahvildari for help in sample preparation. This work is supported by the National Sciences and Engineering Research Council of Canada and the Canadian Foundation for Innovation.

Manuscript: Using active microfluidic flow focusing to sort particles and cells based on high-resolution volume measurements

- This work was submitted to Microelectronic Engineering on September 3rd 2013, accepted February 3rd 2014 and was available online February 13th 2014.
- I, Jason Riordon, contributed the large majority of the work presented in this scientific article: this includes all computer modelling, device design, microfabrication (photolithography, lift-off, PDMS moulding), electrical setup, software design, pressure control, cell culturing, data acquisition and all analysis presented herein. I wrote the first draft, and completed revisions thereafter.
- Mike Nash, an undergraduate student, assisted with some of the coding algorithms.
- Matias Calderini, an undergraduate student, helped with electrode fabrication.
- Hilary Phenix, doctoral student, and Dr. Mads Kaern provided the initial yeast samples used for this work.
- Lukasz Andrzejewski, research technologist, assisted with detection and sorting algorithms and video capture software.
- This manuscript has been modified from the original, in order to match the formatting style of this thesis. Section titles were added to guide the reader through the work. References are consolidated at the end of the thesis.
- The supplementary material presented in section 4.7 was published with this work.

4 Using active microfluidic flow focusing to sort particles and cells based on high-resolution volume measurements

Reproduced with permission by Elsevier from:

Riordon, J., Nash, M., Calderini, M. & Godin, M. Using active microfluidic flow focusing to sort particles and cells based on high-resolution volume measurements. *Microelectronic Engineering* **118,** 35–40 (2014). doi:10.1016/j.mee.2014.02.003.

4.1 Abstract

We demonstrate a microfluidic device that integrates high-sensitivity volume sensing with active pressure-driven flow sorting. Label-free size-based sorting of microparticles and cells is achieved using hydrodynamic flow focusing combined with a resistive pulse sensor with tunable sensitivity that utilizes the Coulter principle. Measurements are performed in real time, and pressure-driven flows are automatically adjusted in feedback to direct microparticles into one of multiple outlet sorting channels at 97.3% efficiency and with a resolution of ~3 μm^3. In a subsequent test, cells were sorted by volume from a single culture of Saccharomyces cerevisiae (yeast) at 100% efficiency. Next, we demonstrate the device's ability to size a population of cells at high-throughput and identify features of interest prior to sorting. Subpopulations of arrested G1 and M-phase cells were successfully resolved from a single yeast culture. This integrated on-chip sizing and sorting method is ideal for sorting small numbers of particles/cells at very high resolution.

4.2 Introduction

Fluorescence-activated cell sorting (FACS) has long since been the method of choice for high-throughput sorting of cells, critical to applications such as medical diagnostics,[78] cell therapy[80] and purification.[79] Herein, light scattering and fluorescence signals are used to quickly identify cells and sort them downstream through electrostatic

deflection. Attempts to miniaturize this technology have produced lab-on-chip, low-cost, disposable devices suitable for point of care diagnostics.[81–84] Fluorescence-based techniques require cell-specific markers, which exist for many cell types but can be unsuitable in some applications such as stem cell isolation.[123] Many alternative microfluidic label-free sorting techniques have been proposed: these include passive methods, such as pinched flow fractionation,[92,93] lateral displacement,[91] hydrophoretic[94] or diffusive filtering,[95] and active sorting mechanisms, such as optical tweezers,[124,125] magnets,[126] acoustics[88,89] and dielectrophoresis (DEP).[6,100,127] For example, Song and Choi demonstrated a hydrophoretic system capable of sorting particles of diameter 12 µm, 15 µm and 20 µm.[98] Takagi *et al.* demonstrated sorting of particles of 1.0, 2.1, 3.0 and 5.0 µm in diameter using an asymmetric pinched flow fractionation technique.[93] External commercial Coulter-based systems are often used to characterize sorting efficiency.[99] On-chip Coulter-based systems, microfluidic volume sensors,[3–5,17,112] monitor the change in ionic current as cells/microparticles traverse a sensing volume. The displaced ions cause a resistive pulse proportional to the object's volume, thus enabling the real-time volume sizing of individual cells. Volume sensors have been shown effective at sizing a variety of biological targets, including Madin-Darby Canine Kidney (MDCK) cells[8], red blood cells[18] and Escherichia coli.[28] These sensors exhibit very high resolution:[128] Saleh and Sohn. demonstrated the volume measurement of ~500 nm diameter colloidal particles at a resolution of ±5 nm.[129] In order to achieve sorting at high resolution, combining on-chip sorting methods in feedback with these high-sensitivity microfluidic volume sensors becomes attractive. Recently, Song *et al.* reported such a sorting device where cells were sorted one at a time through electrokinetic flow manipulation, redirecting each cell based on individual volume sensor measurements.[104] In such combinatory systems, a user benefits from the high-resolution

offered by volume sensors, combined with the sorting capabilities of DEP or electrokinetics.

In this paper, we report a microfluidic system that combines high-resolution volume sensing with hydrodynamic flow sorting, where output into one of several collection ports is achieved through pressure-driven flow focusing and redirection (Fig. 4-1a). The sorting device is fabricated using multilayered polydimethylsiloxane (PDMS), so as to integrate on-chip valves.[63] In pressurizing a separate control layer, adjacent flow channels can be compressed to achieve useful geometric features. Here, these valves serve two distinct purposes: sensor tuning and particle sieving. As reported in an earlier work,[16] a tuning valve can be used to adjust the height of the sensing channel itself, above the electrodes. Since sensitivity scales with sensing volume, this technology allows a user to optimally size the sensor for a chosen range of target particles. A sieve valve is used to compress a channel to a height sufficient to obstruct and collect particles, without blocking fluid flow.[130] This application is useful to collect and concentrate sorted samples, and optically verify sorting efficiency and purity. Sorting by hydrodynamic focusing is achieved by squeezing a central stream of liquid flowing from the sensing channel between two side streams. In finely adjusting pressures, the sample stream can be reduced in width, and actively manipulated into a selected output channel by altering pressure conditions in these two side channels. This is accomplished through two computer-controlled regulators operating in feedback. This technology allows the isolation of a subpopulation of microtargets satisfying pre-set volume thresholds from a highly heterogeneous sample, while providing immediate population volume statistics. We demonstrate device functionality by extracting 5.6 μm diameter polystyrene microspheres from a solution also

containing both larger 8.3 µm and smaller 3.9 µm particles. Sorting efficiency is quantified using complementary video microscopy. Optionally, on-chip sieve valves are integrated to collect and concentrate the extracted sample, permitting on-chip observation. To demonstrate the sorting device's ability to sort cells, *Saccharomyces cerevisiae* (yeast) satisfying a preset volume range were extracted from a continuous population distribution. Further, a high-throughput detection-only mode of operation can be used to rapidly size a population, and identify sub-populations of interest prior to sorting. This capability was demonstrated by sizing a heterogeneous population of arrested yeast cells at high-throughput, which through cell arrest were induced to display subpopulation modes. These modes are easily resolvable, allowing subsequent sorting. The use of localised, internal electrodes practically eliminates Joule heating, and limits electric field sample exposure to <100 ms, which are often cited as concerns relative to biological cell viability.[61] To our knowledge, this work is the first to combine pressure-driven flow with resistive pulse sensing, and we believe this chip ideal for applications where a small quantity of cells are to be extracted at high resolution and high efficiency.

4.3 Material and methods

4.3.1 Microfabrication

The sorting device is fabricated using multilayered soft lithography[16,63] with SU-8 10 (MicroChem), SU-8 2050 (MicroChem) and P4620 (AZ Electronic Materials) photoresists through PDMS moulding (Sylgard 184 Silicone Elastomer Kit). The valve mould was created through photolithographic patterning of 50 µm thick SU-8 2050 on a silicon wafer. The mould was then silanized with (tridecafluoro-1,1,2,2-tetrahydrooctyl)trichlorosilane (Sigma Aldrich), and 7:1 base:curing agent ratio PDMS was poured to a thickness of 4 mm.

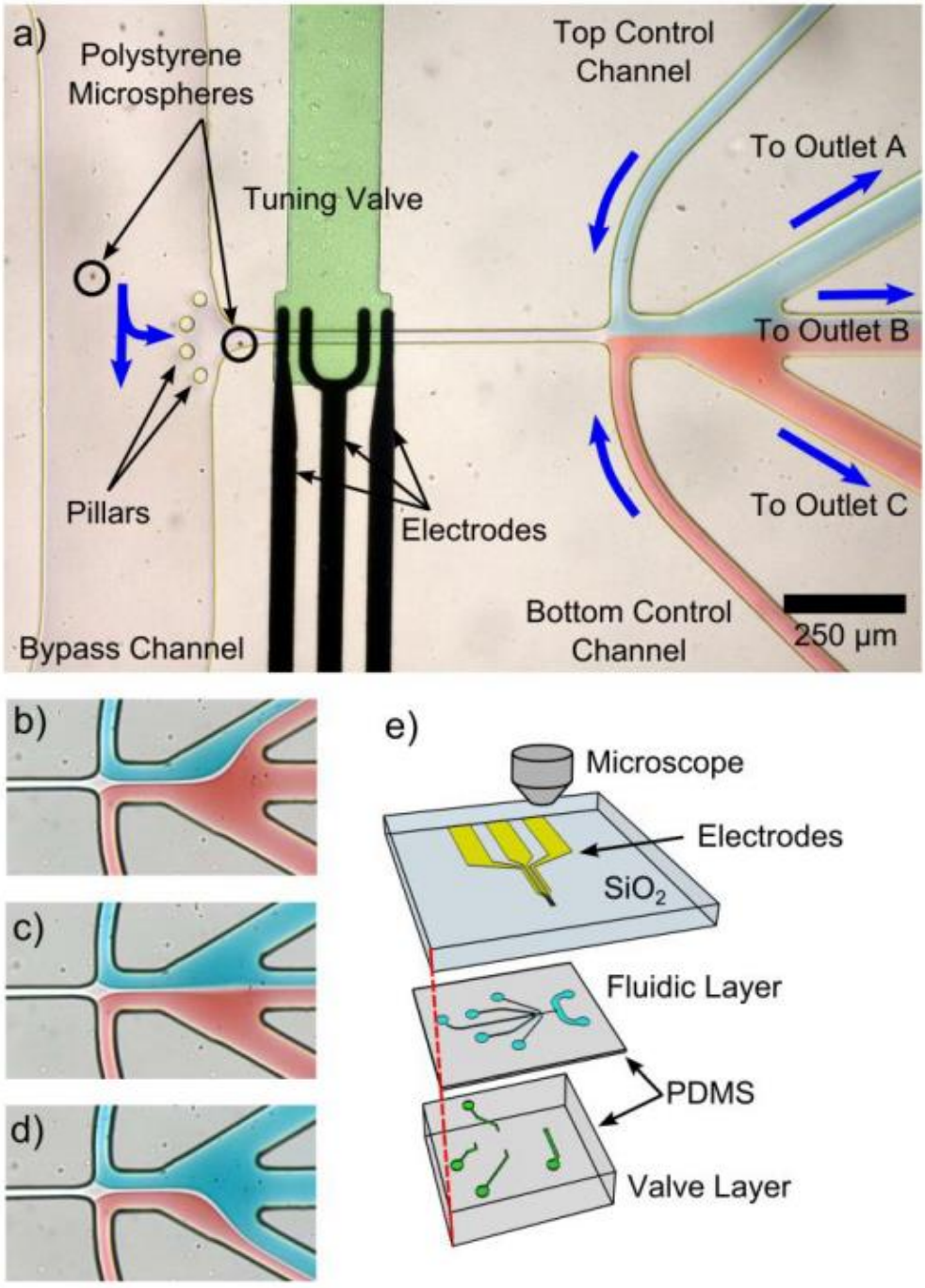

Figure 4-1 (a) Resistive pulse sensor (Coulter counter) with pressure-based flow sorting. Microspheres or cells are pressure-driven through the bypass channel (left), and drawn through the sensor where electrical pulse amplitude is acquired. Custom LabView® software analyzes the signal and automatically redirects the central flow stream into one of three outlets (b-d) through pressure adjustment in the Top and Bottom control channels. Blue arrows denote flow direction. Food colouring is used to highlight flow direction and PDMS layers. e) Schematic view of each layer of the device.

The fluidic layer mould is created by first preparing a 10 µm SU-8 10 adhesion layer on a silicon wafer; a 24 µm thick P4620 layer is then prepared and reflowed at 200 ºC to permit the moulding of rounded microchannels. After silanization, 20:1 PDMS was spin-coated on the fluidic layer mould to a thickness of 40 µm. Gold electrodes were micro-patterned onto a glass microscope slide by e-beam evaporation to a thickness of 70 nm (with 5 nm Ti adhesion layer) using a lift-off process described elsewhere.[16] The fluidic and valves layers were then bonded together using an oxygen plasma treatment, followed by a 1 hour oven bake. The composite PDMS structure and the electrode layer are then bonded to one another following another plasma treatment. Device layers are shown in Fig.4-1e. Detailed device specifications are presented as supplementary material, section 4.8.1.

4.3.2 Signal acquisition and setup

The volume sensor operates on the Coulter principle, whereby cells/microparticles are sized by monitoring the change in ionic current between the two planar electrodes. A 50 kHz, 220 mV RMS potential is applied by a function generator (Stanford Research Systems DS345) and sent to a low-noise preamplifier operating at unity gain (Stanford Research Systems SR560), which serves to isolate the function generator from the rest of the circuit. This frequency was chosen so as to be sufficiently high to avoid electrical double layer effects,[44] but low enough so pulse amplitude becomes purely a function of target volume (<100kHz).[117] The preamplifier connects to a first electrode; the second electrode is grounded. Only two electrodes are utilised in this detection scheme. A current amplifier (Keithley 428) measures the current in series, and outputs 10^5 V/A to a lock-in amplifier (Stanford Research Systems SR830 DSP). A data acquisition (DAQ) card (NI USB-6353; National Instruments) acquires the lock-in signal, which is then monitored in real-time

using custom LabView® software. A pulse detector algorithm scans through the data, and extracts the amplitude and peak width of measured particle detection events. The DAQ card operates in feedback, outputting a voltage to two digital precision pressure regulators (ITV-1011 SMC), which control pressure-driven flow along the top and bottom control microchannels, visible in Fig.4-1a. All other pressures, including the tuning and sieve valves, are kept constant using manual precision pressure regulators (SMC IR2000-N02-R and SMC IR2010-N02-R). These regulators apply pressure to glass vials, which are connected to tubing that lead into the PDMS chip, as described elsewhere.[16] The device is housed in a temperature-controlled aluminium enclosure under an upright microscope (pictured in supplementary material, section 4.8.2). It should be noted that the electronic equipment described in this section was used at the prototype state and may not be suitable for most point-of-care technologies due to bulk and cost. However, electronic chip-based alternatives that perform these basic functions exist, and can be substituted to reduce size and cost.[131]

4.3.3 Device operation

Fig. 4-1a shows a bird's eye view of the device, where aqueous food colouring (Club House) is used to highlight flows and channels. Cells/particles flow through the bypass channel (top to bottom), and are drawn through the central sensing channel via a pressure gradient. PDMS pillars fence the channel entrance, preventing agglomerations of particles/cells from obstructing the sensor. Individual cells/particles sequentially flow over a pair of planar electrodes, where volume is measured. A tuning valve, housed on a separate, adjacent PDMS layer is used to adjust the channel height locally over the electrodes to maximise sensitivity for a given experiment.[16] Care was taken to minimise

sensing channel volume, while maintaining sufficient height so as to prevent particles/cells from becoming obstructed at the entrance. Immediately after measurement, flow along the Top and Bottom control channels is adjusted, enabling redirection of the focalised central flow containing particles/cells into any of the three outlet channels. This process is visible in Fig. 4-1b-d. A low Reynolds number $Re \leq 0.1$ maintains laminar flows throughout the microchannels, permitting reliable control of the sorting outlet. Sieve valves[132] are positioned downstream (not visible in Fig. 4-1a) along the output channels and allow the collection and concentration of the extracted sample.

4.4 Results and discussion

4.4.1 Polystyrene microspheres

Polystyrene microspheres (Bangs Labs) were used to evaluate the system's performance. A sample solution was prepared so as to have ~10^6 particles mL^{-1} in an aqueous solution of 0.08 % bovine serum albumin (BSA), 16 % glycerol, and 0.015 % Tween 20, while maintaining a 0.08 M concentration of KCl. Glycerol is used to minimize microsphere sedimentation, whereas the detergent and BSA prevent potential bead agglomeration and wall adhesion. Deionised water was used in the Top and Bottom control channels. Data was acquired over 5 hours, allowing the detection and sorting of a total of 1818 microspheres. Pressure settings are discussed in supplementary material, section 4.8.3. Temperature was maintained at 20ºC. Fig. 4-2a shows typical current change pulses detected for each of the three microspheres in solution. The bypass channel was filled with a sample containing polystyrene particles (size standards) of three different diameters: 3.9 ± 0.3 µm, 5.6 ± 0.2 µm and 8.3 ± 0.7 µm. The concentrations of all three particle sizes were kept similar as to permit the acquisition of a sufficient number of data points for each size to produce quality

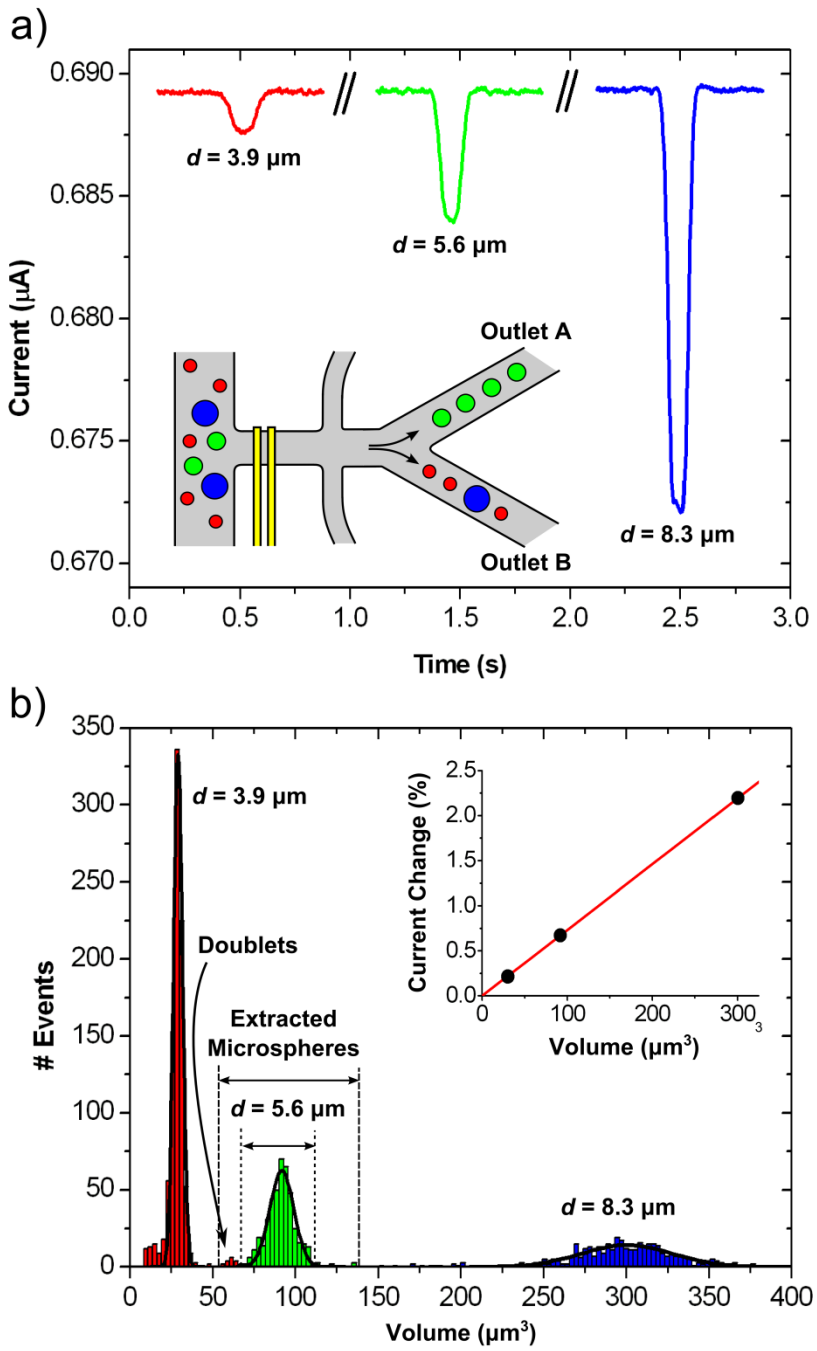

Figure 4-2 (a) Typical current pulses observed for polystyrene microspheres measuring 3.9 µm, 5.6 µm and 8.3 µm in diameter. Inset schema shows the feedback-based flow redirection scheme. Two of the three channels shown in Fig. 4-1 were used. (b) Histogram of 1818 events, with Gaussian fits. Coloration was added to highlight these subpopulations, as confirmed by optical microscopy. Vertical dashed lines indicate how volume thresholds can be adjusted to extract a subpopulation of particles. Extracted 5.6 µm particles were sent to Outlet A. Inset graphic shows the expected linear relationship between mean current change amplitude from each microsphere and manufacturer-supplied microsphere volume. Error bars are too small to be visible.

histograms. In addition to demonstrating sorting, these histograms can then be used to ascertain subpopulation statistics, and verify the linearity of the sensor. The inset graphic describes the flow redirection scheme used for this experiment. Microspheres were sent by default to Outlet B, while those that satisfied a current change condition $\Delta I/I_0 \geq 0.4$ % and $\Delta I/I_0 < 1.0$ % were redirected to Outlet A. The goal being the extraction of the medium sized particles from the heterogeneous sample, microspheres satisfying this condition were only redirected if separated from non-triggering events by a sufficient time interval.

4.4.2 Sorting sensitivity

Fig. 4-2b depicts a histogram for the entire dataset. Events belonging to each of the three microsphere sizes were independently fitted to Gaussian functions. Events that registered between 55 μm^3 and 68 μm^3 were in fact doublet events, pairs of smaller 3.9 µm diameter microspheres, and were not considered in the fit. Neither were events below 0.15 %, which were flagged as noise fluctuations. From curve fitting each Gaussian distribution, we obtain standard deviations of 0.1 µm, 0.2 µm and 0.3 µm (relative standard deviations of 8%, 11% and 11%) for the 3.9 µm, 5.6 µm and 8.3 µm diameter microsphere subpopulations, respectively. For each microsphere size, standard deviations on subpopulations were similar or significantly less than polydispersity information provided by the manufacturer through Coulter counter/sizing measurement. This result is consistent with other findings.[16,128] Evidently, these inherent sample polydispersities overshadow potential variations caused by other factors, such as variable sample trajectories through the sensor[46] or pressure instabilities. In another work,[17] it was found that trajectories could be finely controlled by adjusting buoyancy: in maintaining stable flow conditions and constant buoyancy, targets travel through the sensor following similar flow trajectories,

guaranteeing strong signal reproducibility. Pressure variations are also a concern, as these will cause the flexible PDMS walls to contract/expand, and thus affect the resistive pulse calibration. For this reason, flow and pressure conditions were kept constant throughout the sorting experiment. The inset in Fig. 4-2b highlights the linearity of the current changes as a function of microsphere volume, and provides a current change – to – volume calibration of 0.00717 ± 0.00002 %/μm^3 (*R* squared of 0.99941). In our separation scheme, sorting resolution is intrinsically linked to detection sensitivity, and can be estimated by measuring peak to peak baseline noise: ~ 150 pA, or 3 μm^3. This means individual pulses are said to be accurate to within 3 μm^3. It should be notes that this estimate does not account for variability between pulses due to sample polydispersity or trajectory changes, for example.

4.4.3 Sorting purity and throughput

Sorting purity was analysed by complementing the electrical signal measurements with video microscopy. In this experiment, 97.3 % of the extracted particles were properly sorted based on the desired selection volume thresholds, with 0.5 % of events corresponding to improperly sorted 8.3 µm particles and 2.2 % being smaller 3.9 µm ones. The improperly sorted particles were redirected in error, either because two particles of different sizes went through the sensing volume in quick succession, or due to a poor signal. In such cases, our peak detection algorithm occasionally failed to identify the target particle. These events were rare, but these undetected particles were sometimes binned incorrectly. However, these detection algorithm challenges required operating at a particle density that was relatively low, and that higher concentrations would likely lead to lower purity.

Fig. 4-2b also shows that the sample contained doublets of the smaller 3.9 μm particles that have similar but slightly smaller volumes than the single medium sized particles. Fortunately, the system has enough resolution to mitigate these issues by allowing tighter thresholds if desired. Fig. 4-2b shows two sets of thresholds, where the doublets can be discarded as well. This ability to tighten the extraction threshold makes this device equally well suited to isolate rare events corresponding to a narrow size range. While the device is capable of high-resolution volume measurement, sorting speed is limited by actuation and stabilization time. The time interval between event detection, pressure actuation, and achieving stable flow conditions is about 400 ms. This delay is due to the response time of the SMC ITV1011 regulators, as well as the volume over which pressure is applied, including the vial, tubing and microchannels. This delay, combined with the distance between electrodes and outlet channel trifurcation (~800 μm), limits throughput to ~30 cells/min with this current configuration, or a cell density of ~5 x 10^6 cells/ml. This throughput is comparable to other automatic electrokinetic feedback-based systems,[104] but is much lower than typical passive sorting techniques [90] and conventional FACS (10,000-20,000 cells s^{-1} [77]) that does not measure volume.

4.4.4 Sieve valve

Sieve valves were positioned along each of the outlet channels to optionally collect and concentrate sorted microspheres, as shown in Fig. 4-3b. These valves were kept partially closed, so as to collect microspheres in transit without interrupting flow. In the microsphere separation experiment, ~180 microspheres of diameter 5.6 μm were concentrated from a volume of ~100 μL (sample volume processed during the experiment) down to ~100 fL.

This also helped confirm extracted sample purity. Sieve valves provide a useful means of verifying sorting purity at a glance and to concentrate diluted samples.

4.4.5 Application: sorting cells

To demonstrate live cell sorting capabilities, a population of Saccharomyces cerevisiae (yeast) was sorted according to preset volume conditions. Yeast provides an excellent opportunity to test device functionality for a continuous population of non-spherical, often oddly shaped budding cells. Cells were prepared following a procedure described in

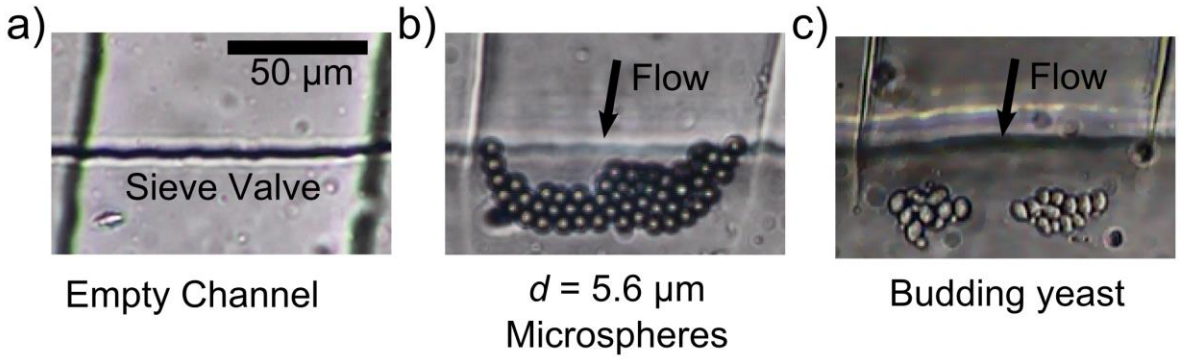

Figure 4-3 (a) Microfluidic sieve valve positioned along Outlet A. Microspheres 5.6 µm in diameter (b) or *Saccharomyces cerevisiae* cells (c) can be captured during sorting. The sieve valve presses down on the microchannel, enabling the immobilization of microspheres in transit without interrupting flow. Trapped particles or cells are released by deactivating the valve.

supplementary material, section 4.8.4, and introduced into the sorting chip. Sensor calibration was performed using polystyrene size standards prior to processing cells. The validity of using spherical microparticles to calibrate microfluidic volume sensors used to size non-spherical cells has been discussed elsewhere,[103] where estimates predict an added 3 % uncertainty in volume measurement. The sorting process was just as effective for live cells as it was for microspheres, and a similar sizing resolution was achieved (3 μm^3). The hydrodynamic flow redirection mechanism behaves identically, irrespective of the sample to be sorted. Fig. 4-4a shows the result of a 45 minute sorting experiment, where 42 cells of

volume satisfying 100 $\mu m^3 \leq V < 140\ \mu m^3$ were extracted from a bulk population (176 cells). In this experiment, video microscopy was used to confirm that the sorting device performed perfectly with a sorting purity of 100 %.

Unlike other dedicated sorting chips that require prior knowledge of a sample size distribution, our chip can also be operated in a high-speed mode to rapidly analyse a population prior to sorting. This is particularly useful for previously uncharacterized and heterogeneous biological samples. This analysis of a sample's volume distribution can afterward be used to set proper sorting thresholds to extract a subpopulation of interest, albeit at lower speed. To demonstrate this ability, we rapidly analysed a population of live but arrested yeast cells. In this experiment, a single yeast culture was prepared in such a way so as to force the emergence of subpopulations within a volume distribution histogram. A kinase inhibitor (1-NM-PP1, Cedarlane) was added to the yeast culture to arrest the cells in the G1 and M cell stages.[133] following a procedure similar to that of Bryan *et al.*[7] and summarized in supplementary material, section 4.8.4. The arrested culture reveals distinct subpopulations after 4 hours of incubation at 30 ºC, corresponding to different stages in the cell cycle. The device was operated in a high-throughput (900 cells/min) non-sorting mode of operation to rapidly size 43,000 cells, as shown in Fig. 4.4b. To accommodate larger cells, the tuning valve had to be released to a greater extent, reducing sensitivity. A separate calibration was performed. Our noise level was about 0.2 % of baseline, granting a 40 μm^3 resolution. Although this is larger than what was achieved during sorting, this is largely sufficient to rapidly analyze a population. Events below 100 μm^3 lie below our confidence level (S/N <2), whereas peaks located >600 μm^3 are the result of multiple cells passing at once. Figure 4-4b clearly shows the emerging sub-populations and modes corresponding to

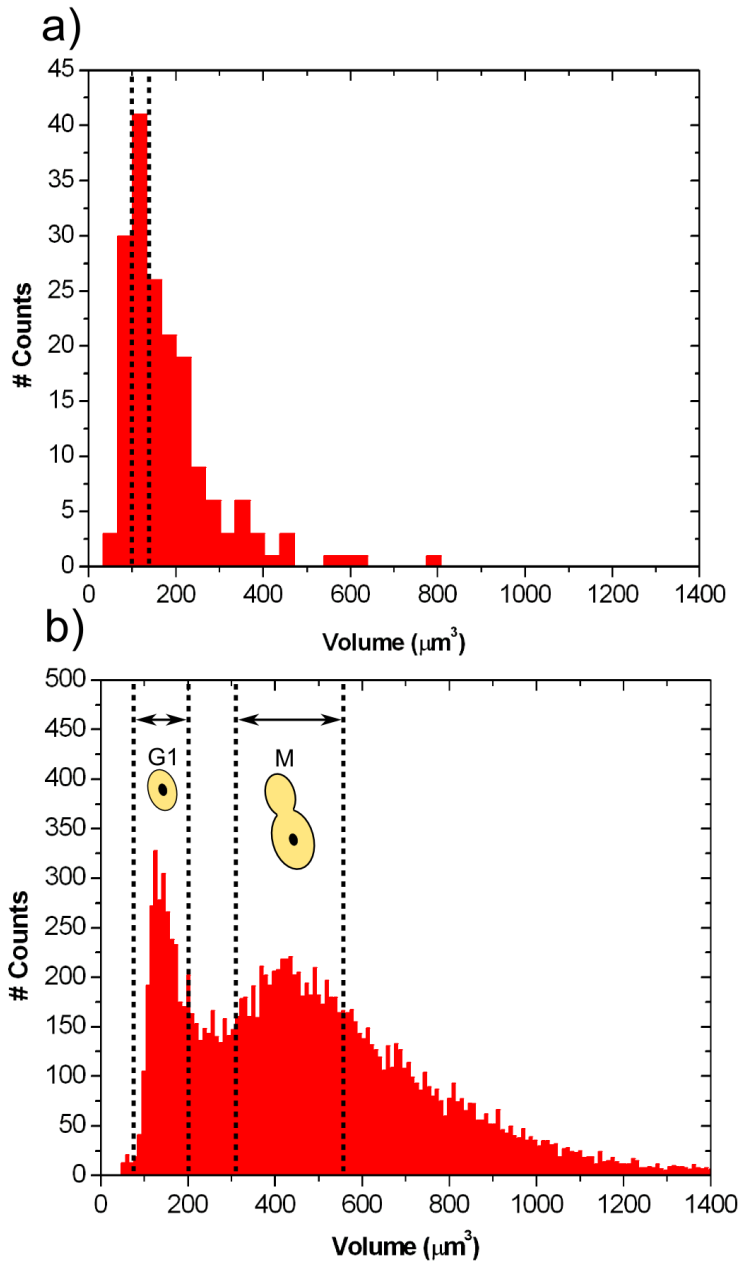

Figure 4-4 (a) Individual cells satisfying pre-set volume conditions are extracted into a separate outlet. Dotted lines represent subsample that was extracted, confirmed through video microscopy. (b) Histogram showing the volume distribution of a single culture of arrested *Saccharomyces cerevisiae*. The growth of G1-arrested and M-arrested cells causes volume subpopulation modes to emerge. By setting appropriate thresholds, cells belonging to specific subpopulations can later be extracted at high-resolution.

G1 and M phase cells are easily distinguished. The dotted lines highlight the thresholds to be used for sorting/extracting these sub-populations.

Fig. 4-3c highlights the capture and subsequent release of sorted yeast cells using on-chip sieve valves. While cell growth studies are not the focus of this work, sizing/extracting such samples demonstrates our ability to extract a (i) heterogeneous, (ii) oddly shaped population of cells from a single cell culture.

4.5 Conclusions

In this work, we demonstrated the high-efficiency sorting of microparticles and cells based on high-resolution volume measurements using hydrodynamic flow focusing. Microspheres and cells were collected and observed on-chip using sieve valves. Sorting purities of 97.3 % and 100 % were achieved for sorting particles and cells, respectively. A sizing resolution of 3 μm^3 was demonstrated, a value exceeding that of passive cell sorting devices for this range of sizes. Biological cells exhibit continuous size distributions, requiring sorting systems that can resolve volume at high-resolution. Future work will examine sorting mammalian cells based on volume.

4.6 Acknowledgements

The authors thank Hilary Phenix and Mads Kaern for providing initial yeast cell cultures and Lukasz Andrzejewski for scripting assistance. This work is supported by the Natural Sciences and Engineering Research Council of Canada (NSERC) and the Canadian Foundation for Innovation (CFI).

4.7 Supplementary Material

4.7.1 Device specifications

Fig. 4-5 shows a schematic view of the device used for all data presented in this work. Multiple devices were used for preliminary experiments, such as the one pictured in Fig.4-1a, and used different electrode configurations. Only the two rightmost electrodes are used for the resistive pulse measurement.

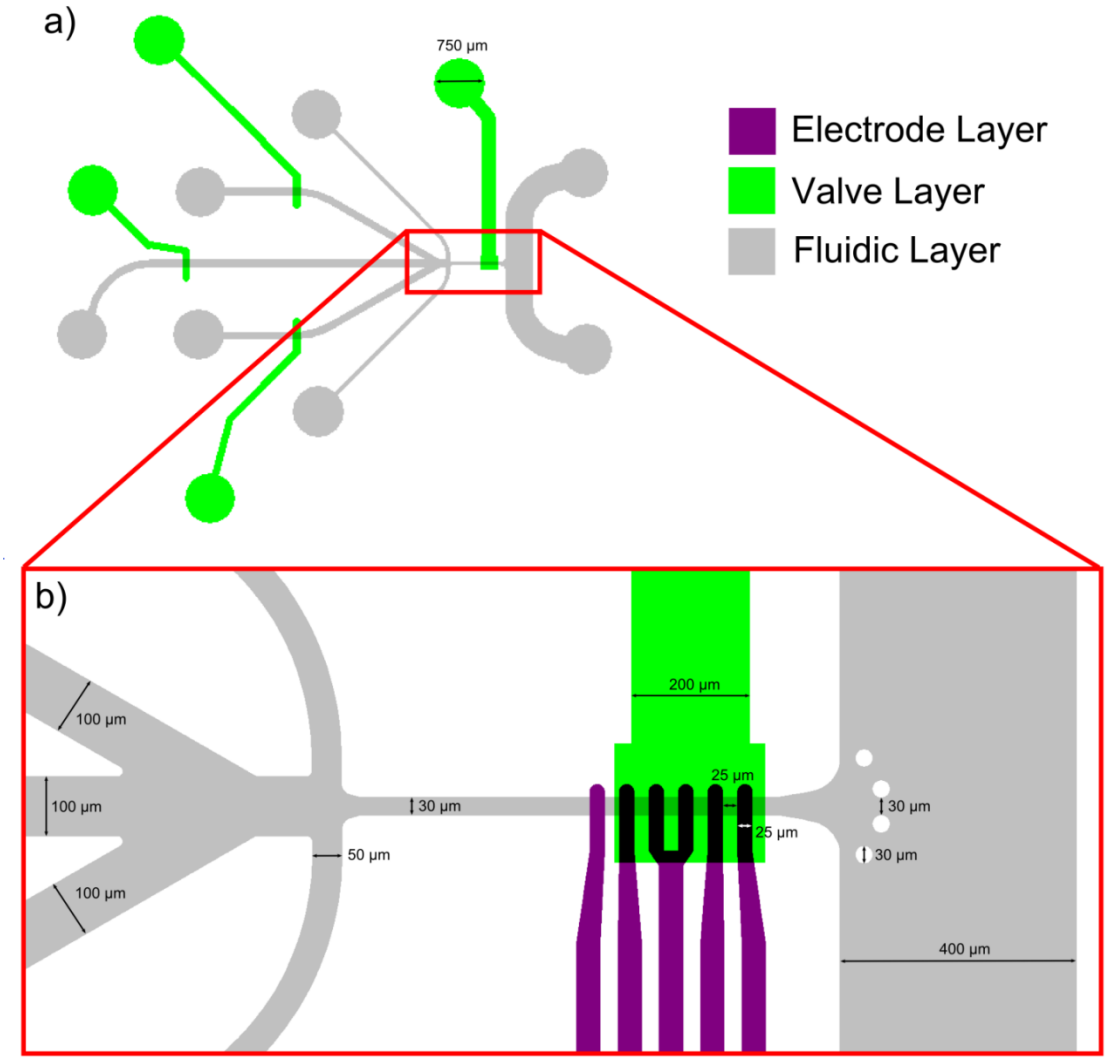

Figure 4-5 Schematic view of the microfluidic cell sorter with fluidic layer (grey), valve layer (green) and electrode layer (purple). The view in (a) is presented without electrodes for clarity. (b) Enlarged view of the center of the device.

4.7.2 Temperature-controlled aluminum enclosure

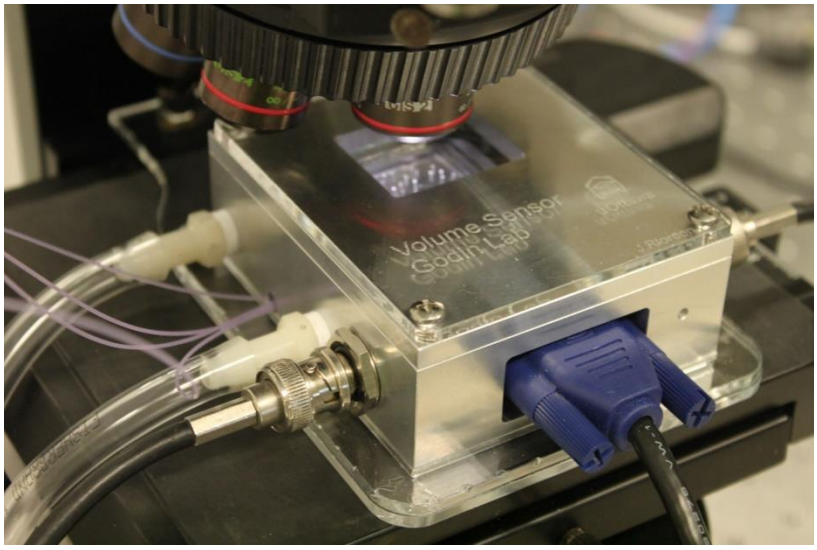

Figure 4-6 Custom aluminum enclosure that houses the cell sorting chip. The enclosure is temperature-controlled using a recirculating water bath.

4.7.3 Pressure considerations

Each pressure was precisely adjusted to maximise device efficiency. The pressure controlling the sensing channel height was set to reduce the sensing volume as much as possible without obstructing the flow of microspheres (0.2 MPa), and to render the volume sensor as sensitive as possible. Sieve valves were set to reduce the channel cross-section as little as possible (0.18 MPa), so as to not limit flow, while keeping the channels narrow enough to trap the smallest microspheres. Pressures at each end of the bypass channel were set to create a top-down particle velocity of ~50 µm/s (0.015 MPa, 0.010 MPa). Outlet pressures were identical (0.03 MPa), and chosen to draw microspheres through the sensing channel at ~1 mm/s. Top/Bottom control channel pressures were set sufficiently high to focus the particle stream, and alternated between values meant to steer the stream into each of the three outlets. For the experiments detailed in this work where a single sub-population

is extracted, only two settings were used (redirect to Outlet A: Top = 0.040 MPa, Bottom = 0.020 MPa; redirect to Outlet B: Top = 0.032 MPa, Bottom = 0.021 MPa).

4.7.4 *Saccharomyces cerevisiae* sample preparation

4.7.4.1 Sorting Experiment

Saccharomyces cerevisiae (MATa, Cdc28-as1) was cultured overnight, (30º C, 300 RPM) in yeast bacto-peptone (YPD) with 2% w/v glucose and 1X adenine. Cells were resuspended in 1X PBS through centrifugation, then added to a solution containing Percoll (Sigma Aldrich), Final concentrations were 73% Percoll, 0.01% BSA, 0.25X PBS and ~1E7 cells/ml.

4.7.4.2 Arrest Experiment

Saccharomyces cerevisiae (MATa, Cdc28-as1) was cultured in an incubating shaker to $OD_{600} < 0.7$ (30º C, 300 RPM) in yeast bacto-peptone (YPD) with 2% w/v glucose. Cells were then arrested via Cdc-28 inactivation[133] through addition of a kinase inhibitor: 40 µM of 1-NM-PP1 (Cedarlane) in DMSO. The culture was incubated at 30º C for 4 hours. A cell suspension was washed with 1X PBS through centrifugation, then added to a solution containing 73% Percoll (Sigma Aldrich), 0.1% BSA and 0.25X PBS (~10^6 particles mL^{-1}). Percoll was used to make the cells neutrally buoyant, thus preventing sedimentation. The suspension was then cooled to 5º C to halt growth, and introduced into the microfluidic sorting chip. For sorting, a 1X PBS solution was used for top/bottom control channels, instead of deionised water.

4.8 Additional notes

It is worth mentioning that the sorting method used in this article was the last in a long line of less successful sorting attempts, using various other microfluidic schemes. The first attempt consisted of utilizing simple valve actuation to redirect flow into one of multiple channels. In this method, flow control was completely controlled by valves, so computer controlled regulators were not necessary. While this method lead to cell-by-cell sorting, it was deemed too slow to be of practical use. In addition, in systems with multiple such valves, obtaining a strong seal in closed valves became an issue. Measures were taken to reduce this, such as using a photocurable epoxy to "patch" areas where leaks occurred,[134] but to no avail. Another redirection scheme involved a "continuous" flow method, whereby valves would simply redirect flow into different channels without requiring a full seal. This method also suffered from high-actuation times, and was rejected in favor of the work published in this Chapter.

It should also be noted that the temperature control system pictured in Section 4.7.2 was fully customized for this particular application. The control chamber was built to fit easily under an upright microscope, guaranteeing proper focal distance to the sample and sufficient illumination. A thermistor was calibrated, and installed to monitor the temperature at the chip. A temperature control system (Isotemp 3016, Fisher Scientific) was used to circulate water through the aluminum enclosure. A PCB chip was designed to fit within the chamber, and attach to a second PCB located on individual microfluidic chips, which are wire-bonded to the electrodes. External electronics are connected via BNC connectors on the side of the enclosure, or a D-Sub connector at the front (Figure 4-7).

Finally, the cells used in this study were carefully cultured to exponential phase by first performing a number of control tests with an OD measurement system (GeneQuant III). Prior to performing an experiment, cell cultures were diluted to sufficient concentration that morning, or the previous evening (generally 1E6 cells/ml.

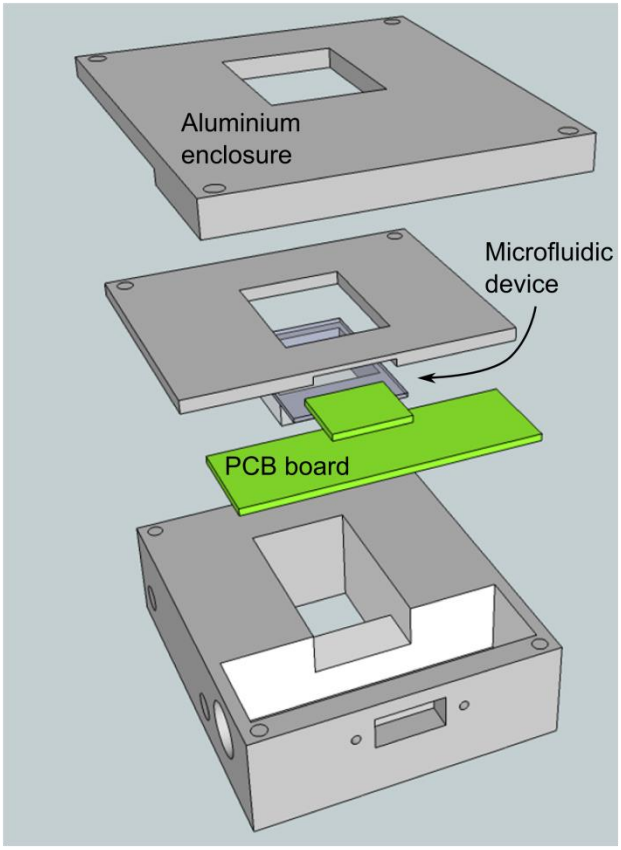

Figure 4-7: Customized temperature-controlled enclosure.

Manuscript: Quantifying the volume of single cells continuously using a microfluidic pressure-driven trap with media exchange

- This work was submitted to Biomicrofluidics on January 31st 2014, accepted February 15th 2014 and published online February 28th 2014.
- I, Jason Riordon, contributed the large majority of the work presented in this scientific article: this includes all computer modelling, device design, microfabrication (photolithography, lift-off, PDMS moulding), electrical setup, software design, pressure control, cell culturing, data acquisition and all analysis presented herein. I wrote the first draft.
- Mike Nash, an undergraduate student, assisted with some of the coding algorithms, and helped perform initial trapping experiments.
- Wenyang Jing, a masters student, helped fabricate the devices used in this work.
- Dr. Benjamin Watts, a postdoctoral researcher, helped fabricate the electrodes.
- Hilary Phenix, doctoral student, and Dr. Mads Kaern provided the initial yeast samples used for this work.
- Lukasz Andrzejewski, research technologist, assisted with detection and sorting algorithms and video capture software.
- This manuscript has been modified from the original, in order to match the formatting style of this thesis. Section titles were added to guide the reader through the work. References are consolidated at the end of the thesis.
- The supplementary material presented in section 5.7 was published with this work.

5 Quantifying the volume of single cells continuously using a microfluidic pressure-driven trap with media exchange

Reproduced with permission from:

Riordon, J., Nash, M., Jing, W. & Godin, M. Quantifying the volume of single cells continuously using a microfluidic pressure-driven trap with media exchange. *Biomicrofluidics* **8,** 011101 (2014). doi: 10.1063/1.4867035.

5.1 Abstract

We demonstrate a microfluidic device capable of tracking the volume of individual cells by integrating an on-chip volume sensor with pressure-activated cell trapping capabilities. The device creates a dynamic trap by operating in feedback; a cell is periodically redirected back and forth through a resistive pulse sensor (Coulter principle). Sieve valves are positioned on both ends of the sensing channel, creating a physical barrier which enables media to be quickly exchanged while keeping a cell firmly in place. The volume of individual *Saccharomyces cerevisiae* cells was tracked over entire growth cycles, and the ability to quickly exchange media was demonstrated.

5.2 Introduction

Measuring cell growth is of primary interest to researchers who seek to study the effects of drugs, nutrients, disease, and environmental stress. This has traditionally been accomplished by monitoring the optical transmittance of large ensembles of cells and applying the Beer-Lambert Law.[21,22] Such population-scale measurements provide important culture statistics, but averaging obscures the behaviour of individual cells. In addition, these techniques often require cell synchronicity in order to correlate growth with specific points in the cell cycle, but synchronicity typically decays rapidly in many cell lines including *Saccharomyces cerevisiae* (yeast) cultures.[23] Researchers have thus adopted methods that study the growth of individual cells. Quantifying cellular growth is especially

challenging since proliferating cells such as yeast or *E. coli* are irregularly shaped, and will only increase in size by a factor of two.[13] Growth will affect the mass, volume and density of the cell; having access to each of these characteristics is important in obtaining a complete picture of this process. Time-lapse fluorescence microscopy can provide valuable information as to the cell cycle progression of individual cells,[135] but 2D optics requires geometric assumptions, and thus provide an incomplete picture of growth.[10,14]

Microfluidic lab-on-chip devices with integrated sensors can provide high-resolution growth tracking of individual cells, either through mass, volume or density monitoring.[13,14,110] Recently, a microfluidic mass sensor was used to track the buoyant mass of individual cells using a suspended microchannel resonator (SMR).[13,111] Monitoring growth can also be accomplished by tracking volume using microfluidic volume sensors,[14] or resistive pulse sensors (RPS) operating on the Coulter principle.[3] Trapping can be achieved by either (1) cycling the target back and forth through the sensor (pressure-driven[13], electrokinetic[14]) or (2) holding a cell in place (posts[136], chevron structure[8], E-Field[137]). The former, dynamic approach, allows a single cell to be sampled periodically by reversing flow directions after a cell is detected. Simple in its implementation, this technique also has the ability to compensate for a drifting baseline current resulting from parasitic ionic changes within the sensing channel or other sources of noise. On the other hand, static traps allow cells to be held in place while the buffer is rapidly exchanged.[8] The ability to dynamically change cellular growth conditions during an experiment can lead to significant insight into the behaviour of cells in environments of varying salinity, oxidative or osmotic conditions, as well as the effect of nutrients and drugs.

In this work, we propose a device capable of tracking growth using high-resolution volume measurements, combining the best attributes of both types of measurement systems; continuous baseline correction and the ability to rapidly exchange cell media. This is accomplished by using a pressure-driven, feedback-based dynamic trap, whereby a cell is cycled back and forth through the sensor within a microfluidic channel. On-chip sieve valves positioned at both ends of the sensing channel are able to selectively capture a cell while the solution is being replaced. As proof of principle, the volume of several individual yeast cells was monitored over the course of their respective growth cycles, and the ability to quantify growth response to media exchange was demonstrated.

5.3 Experimental details

Devices were fabricated using multilayered soft lithography with polydimethylsiloxane (PDMS) moulding.[63] The completed device is pictured in Figure 5-1a; full fabrication protocols are presented as supplementary material. Resistive pulses were acquired by applying a 50 kHz, 220 mV AC voltage between a pair of electrodes, and measuring the drawn current. This frequency is sufficiently elevated to avoid the electrical double layer capacitance at the electrode-electrolyte interface,[44] but low enough to avoid sensitivity to cell impedance.[117] The electrical setup used for these experiments has been described previously.[16] A temperature controller maintains the device at 30 ºC. Inlet pressures *I1* and *I2*, and valve pressures *V1* and *V2* are controlled with manual regulators (SMC IR2000-N02-R and SMC IR2010-N02-R); outlet pressures are computer-controlled (SMC ITV-1011). A cell suspension is loaded into the bypass channel, and made to flow through the central channel through a pressure gradient. Once a cell of interest is detected, valves are sealed (*V1*=*V2*=35 psi), and bypasses are flushed and replaced with fresh media. After 2

min, valves are pressurized to 24 psi where they compress the channel to a sufficient height to restrict the passage of yeast cells, while allowing the media to flow through the central channel. In trapping mode, when a pulse is detected, the pressure settings at *O1* and *O2* are adjusted to redirect the cell back and forth through the sensor. Through custom LabView® software, these outlet pressure settings are feedback-adjusted to maintain a speed of 250 μm/s in both directions at a detection frequency of 30 cells/min (Figure 5-1d). To minimize the effects of channel stretching/shrinking, the sum of pressures at *O1* and *O2* is held constant. This precaution was taken since the sensing channel structured within the flexible PDMS polymer will alter its geometry based on internal pressure.[138] The short central channel ensures steady nutrient replenishment from the bypasses. For example, a glucose molecule takes ~4 min to diffuse from the bypass to the electrodes. In practice, Taylor-Aris dispersion will reduce this replenishment time considerably. Based on video analysis, 25% of the central channel's media is replenished every pressure reversal (video presented as supplementary material on publisher website). Polystyrene microspheres of 3.9 ± 0.3 μm, 5.6 ± 0.2 μm and 8.3 ± 0.7 μm (NIST size standards) were used to calibrate the sensor, and obtain the current pulse-to-volume calibration for every solution (supplementary material). The validity of this calibration method is discussed elsewhere.[103] Care was taken to limit trajectory-based variations in signal: the device is positioned with electrodes at the top of the sensing channel, and with the negatively buoyant cells/particles flowing along the bottom.

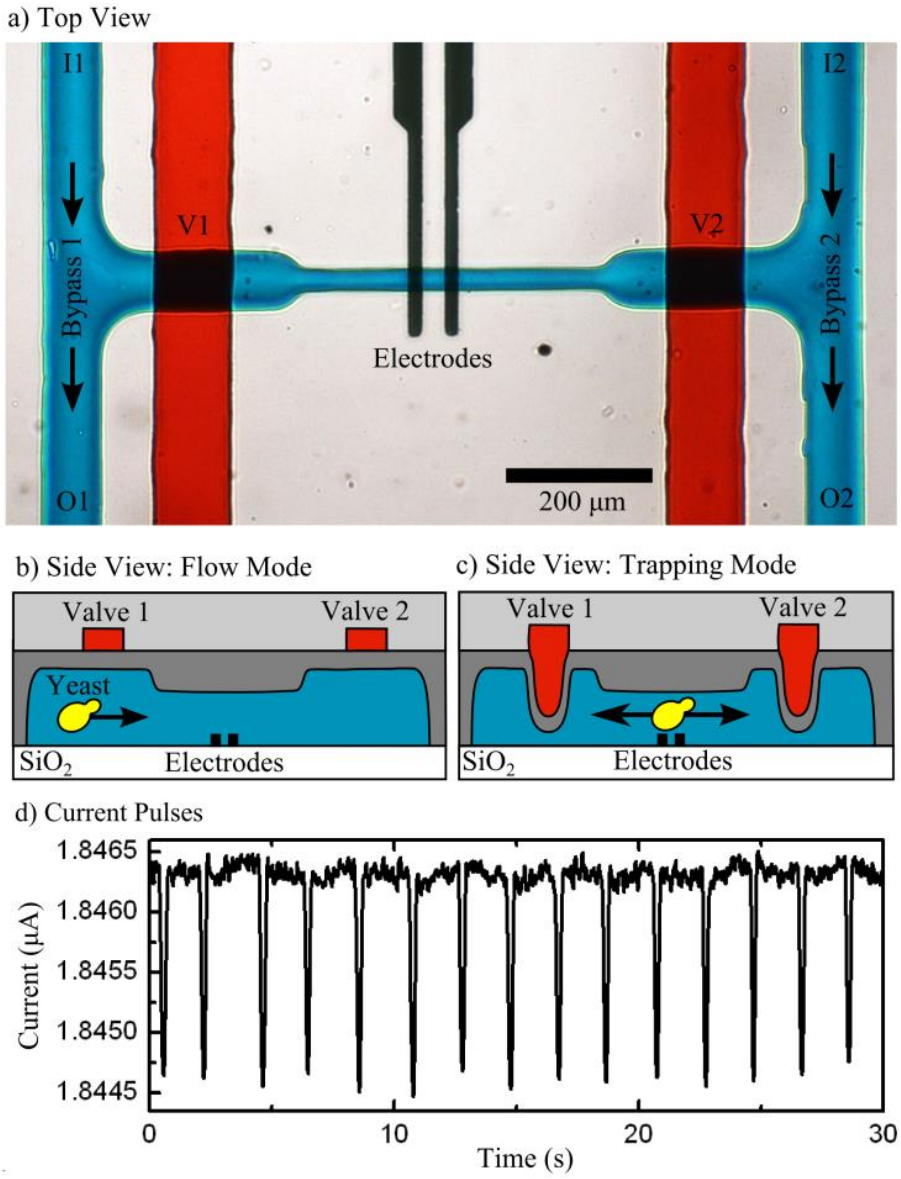

Figure 5-1 (a) Micrograph of the microfluidic device. Two parallel bypass channels are connected by a sensing channel with sensing electrodes. Pressure is applied at inlets (I1, I2) and outlets (O1, O2) to control flow conditions. Valves (V1, V2) are positioned over each end of the sensing channel. Food coloring is used to highlight the valve (red) and fluidic layers (blue). (b) Flow mode: valves are unpressurized, and cells flow freely through the device. (c) Trapping mode: valves are pressurized to capture a cell within the central channel. Pressure-driven flow cycles the cell back and forth across the sensor. (d) Typical current pulses measured for a yeast cell.

5.4 Results and discussion

5.4.1 Cell growth

Saccharomyces cerevisiae[a] was cultured to exponential phase at 30°C in an incubator/shaker in yeast bacto-peptone (YPD) with 2% w/v glucose, supplemented with 0.2M NaCl, 0.05% bovine serum albumin (BSA) and 42 mg/L adenine. Sodium chloride was added to enable the resistive pulse measurement, at a concentration where cells are viable;[139] BSA was used to prevent cell agglomeration; adenine was supplemented since this particular yeast mutant does not produce its own supply. A cell suspension was introduced into the device, from which a cell at the early stages of its cell cycle was captured, and dynamically trapped for 100 min. Three typical cell growth results are shown in Figure 5-2a. Since the culture was not synchronized, this leads to variability between 'initial' cell volumes: there is a 27% difference in initial volume between the cells identified by red squares and green triangles. This is caused by (1) optical limits, whereby cells chosen for study are not all at the exact same cell cycle stage and (2) differences in the age of the mother cell: the more buds a mother cell has produced, the larger it becomes.[140] On average, captured yeast cell demonstrated a doubling time consistent with growth rates under ideal incubator/shaker conditions; nutrient depletion, electric field and shear stresses are not affecting growth. Optical inspection of budding cells confirms that most growth is occurring at the daughter cell, as expected.[140] A strong signal-to-noise allows for high resolution volumetric measurements (4 μm^3); cell asymmetry[14] and trajectory

[a] Full name: BY4743 Mat a/alpha, genotype: his3Δ1/his3Δ1 leu2Δ0/leu2Δ0 LYS2/lys2Δ0 met15Δ0/MET15 ura3Δ0/ura3Δ0 ade2::LEU2/ade2::URA3

variability[17,18,46] lead to a relative standard deviation of 6% for cells and 4% for microspheres of similar size. While mass or protein synthesis methods have indicated linear[9] or exponential[10–13] growth curves, volume-based methods have suggested sigmoidal patterns.[14,141] Prior to daughter cell emergence, and later in the cycle as the daughter cell emerges, volumetric growth rate declines.[108] In this work, it is difficult to ascertain with mathematical rigor the shape of the growth profile; however, for each cell, volume increases steadily throughout the growth cycle before declining near the end of the cycle.

5.4.2 Media exchange

To demonstrate our ability to easily exchange media while maintaining a trap, the solution was exchanged 40 mins into a yeast growth cycle; culture media was replaced with a pure saline solution 0.2M NaCl + 0.05% BSA, and then replaced again with culture media at 80 mins (Figure 5-2b). Cell growth is halted temporarily while in saline solution, before resuming normal growth thereafter. The cell cycle time is extended by this period. The cell volume drifts downward after the initial solution change at 40 mins. Though this drift lies within our uncertainty bounds, cellular responses to osmotic shock on similar timescales have been documented elsewhere.[142] This result demonstrates an ability to quickly exchange cell media, and observe cellular response.

5.5 Conclusions

In conclusion, we have demonstrated a microfluidic device capable of maintaining a dynamic, pressure-driven cell trap, which can monitor cellular volume over the cell cycle. Concurrent optical microscopy allows for real-time visual inspection of the cells. In addition, sieve valve integration provides for the exchange of media or the addition of

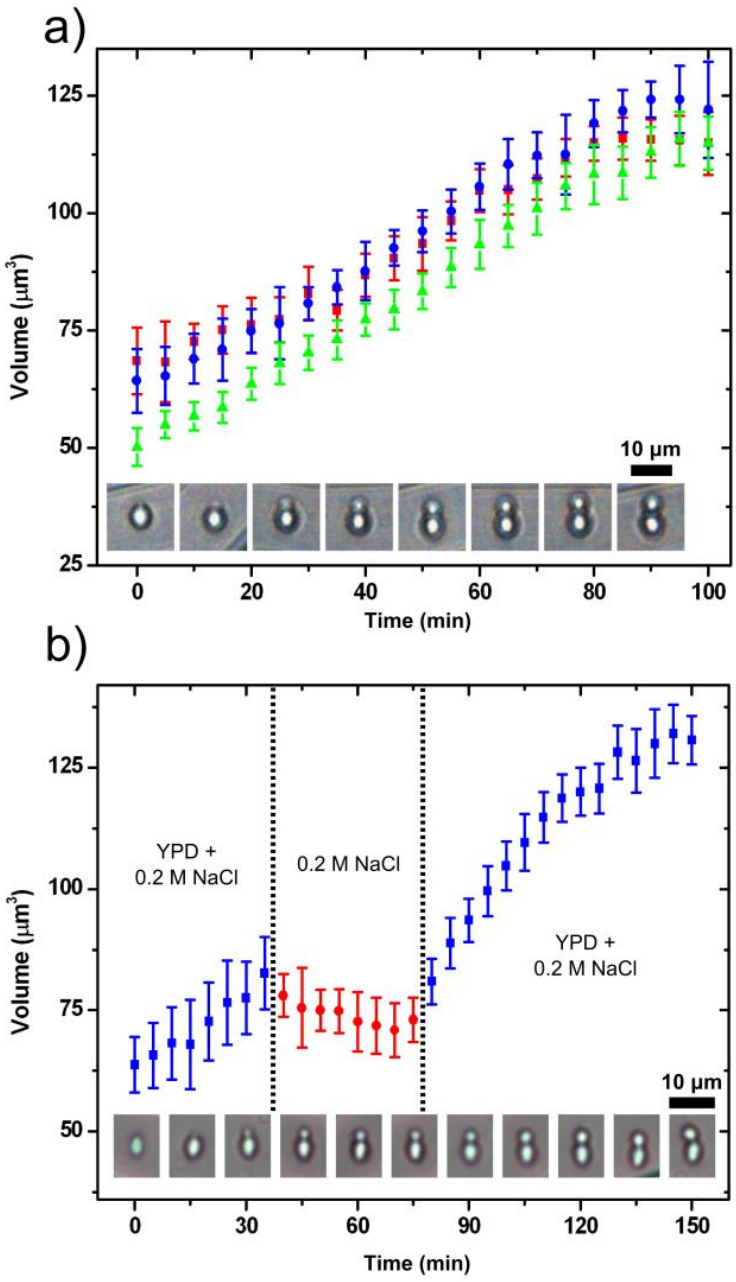

Figure 5-2 (a) Growth curves for 3 cells trapped in succession. Simultaneous optical and electrical measurements allow cell cycle stage to be correlated with volume. Pictures of cell corresponding to the red squares are presented in 15 minute increments. A cell is cycled through the sensor every 2 s. For clarity, each data point for yeast volume represents the average of data points over a period of 5 min, with standard deviation. (b) Demonstration of an interrupted growth cycle, where YPD+0.2M NaCl was replaced with 0.2M NaCl at 40 min, and then again returned to YPD+0.2M NaCl at 80 min. The media exchange process takes 4 min.

drugs. Such a platform could also be key in cancer cell cytotoxicity assays,[143] where growth response to anticancer drugs could be monitored.

5.6 Acknowledgements

The authors thank Hilary Phenix and Mads Kaern for useful discussions and for supplying initial yeast cultures, Lukasz Andrzejewski for assistance in scripting, and Benjamin Watts for microfabrication help. This work is supported by the Natural Sciences and Engineering Research Council of Canada (NSERC) and the Canadian Foundation for Innovation (CFI).

5.7 Supplementary Material

5.7.1 Fabrication

A fluidic flow layer mold was constructed through photolithographic patterning of P4620 photoresist (AZ Electronic Materials) on a silicon wafer. This layer was reflowed at 200 ºC to create rounded channels, 20 µm thick at the narrow part of the central channel and 28 µm thick at the bypass/wider part of the central channel. A 10 µm SU8-10 (Microchem) layer was used to enhance adhesion to the substrate. Silanization treatment with (tridecafluoro-1,1,2,2-tetrahydrooctyl)trichlorosilane (Sigma Aldrich) was performed to facilitate the removal of the moulded polydimethylsiloxane (PDMS) (Sylgard 184). PDMS of 20:1 base:curing agent ratio was spin-coated to a thickness of 35 µm. The control channel mould was fabricated using 50 µm thick SU-8 2050 (Microchem), followed by a similar silanization treatment. The PDMS control layer (sieve valves) was moulded to a thickness of 4 mm. Gold electrodes were deposited on glass microscope slides by E-beam deposition to a thickness of 50 nm (5 nm Ti adhesion layer), and patterned using a lift-off technique described elsewhere.[16] The fluidic layer and the valve layer were aligned with a mask

aligner, bonded with an oxygen plasma treatment, and cured in an oven at 80ºC. These combined layers were then bonded to the electrode layer following the same procedure.

5.7.2 Video

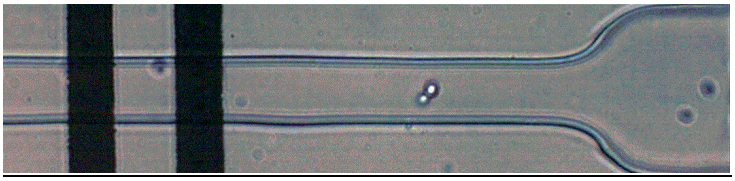

Figure 5-3: Screen capture of a yeast cell caught in a dynamic trap.

Caption: Demonstration of a yeast cell caught in a dynamic, pressure-driven trap.

5.7.3 Calibration curves

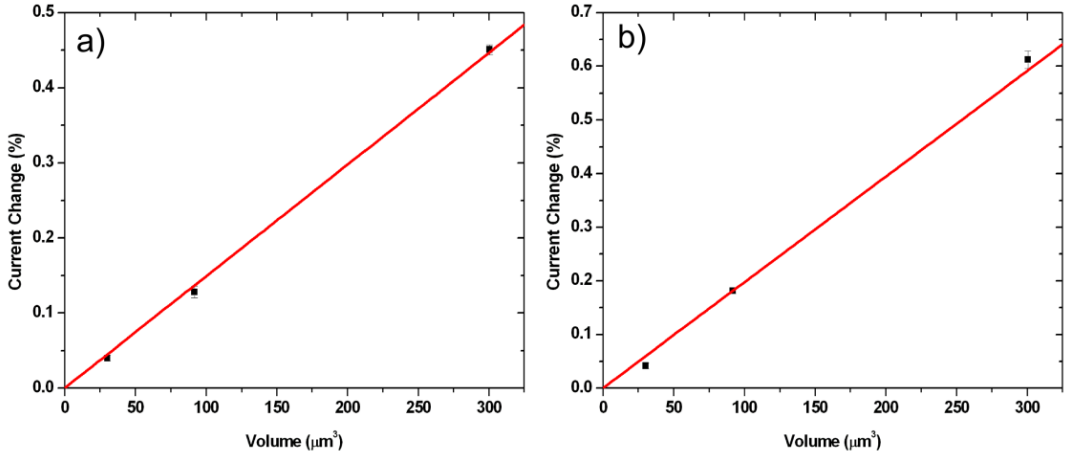

Figure 5-4: Calibration curves for both solutions. Polystyrene microspheres of diameter 3.9 ± 0.3 µm, 5.6 ± 0.2 µm and 8.3 ± 0.7 µm (NIST size standards) were used. (a) Solution of yeast bacto-peptone (YPD) with 2% w/v glucose, supplemented with 0.2M NaCl, 0.05% bovine serum albumin (BSA) and 42 mg/L adenine. (b) Solution of 0.2M NaCl, 0.05% bovine serum albumin (BSA). Slope calibrations of 1.49E-3 ± 2E-5 %/µm3 and 1.97E-3 ± 4E-5 %/µm3 were measured from linear fits for (a) and (b), respectively.

These curves represent current pulse-to-volume calibration curves for the two solutions discussed in this work (Figure 5-4). The calibration slope changes by 32 % between solutions, and could be an indication that particle trajectory is solution-dependant. The

baseline conductivity was identical for each solution (1.8 μA), indicating that the geometry of the channel does not change due to swelling or small pressure changes. Relative standard deviation (RSD) was found to be approximately 6% for cells, but varied considerably for microspheres based on volume. As mentioned in the main text, similarly-sized microspheres (d = 5.6 μm) have a 4% RSD. Larger microspheres have a stronger signal-to-noise, leading to better fitting accuracy (2% RSD for d = 8.3 μm microspheres).

5.8 Additional notes

It is worth mentioning that other trapping designs were explored before achieving this finalized design. These generally featured longer sensing channels, similar to the design used for the buoyancy experiments in Chapter 3 (Figure 3-2). Trapping in these long channels was much easier, since there was plenty time to catch cells in the trap, without risk of losing them in the bypass channels. However, the fear was that these cells were suffering from nutrient depletion. Thus, once the trapping algorithm was improved and valves used consistently, this long channel design was put aside in favor of a short sensing channel. In terms of channel dimensions, preliminary testing suggested that channels of lower height lead to a stronger signal-to-noise (sensitivity increase), but at the cost of an increased dependence on yeast orientation during transit. A 20 μm height for channels was chosen as a compromise. Also, particles were made to sink through negative buoyancy away from the sensor. This helped ensure high accuracy and reproducibility, without exposing the cells to higher electric fields at electrode edges.

The trapping algorithm itself has a number of parameters that can be tuned/adjusted to trap in different ways. For example, the delay between switching in either direction can be extended, to change the number of measurements per minute. Pulse width was set to 200 μs, but for certain applications higher/lower pulses might be preferable. These parameters and many more can be easily configured to suit trapping requirements.

6 Other Contributions

In addition to the primary work listed in Chapters 2-5, I have also contributed to other projects over the course of this work. In 2013, I co-authored a paper "Hollow core photonic crystal fiber as a reusable Raman biosensor" with collaborators from Dr. Hanan Anis' engineering group at the University of Ottawa.[144] In this project, I worked closely with Ph.D. student Altaf Khetani in developing a system for rapid microfluidic exchange within hollow core photonic crystal fibers (HC-PCF). A reliable, reproducible method to reuse HC-PCF biosensors was developed, paving the way towards point-of-care applications. Preliminary work was also presented and published at the 2013 SPIE BiOS conference.[145]

- Khetani, **J. Riordon**, V. Tiwari, A. Momenpour, M. Godin, and H. Anis, "Hollow core photonic crystal fiber as a reusable Raman biosensor," *Opt. Express*, vol. 21, no. 10, pp. 12340–12350, May 2013.
- A. Khetani, A. Momenpour T. Monfared, V. S. Tiwari, H. Anis, **J. Riordon**, and M. Godin, "Hollow core photonic crystal fiber as a robust Raman biosensor," 2013, Optical Fibers & Sensors for Medical Diagnostics & Treatment App. XIII, vol. 8576, p. 85760F–85760F–6.

I have also contributed to other projects currently in development, in particular work on a cell concentrator for water and food safety applications.

7 Conclusion

In conclusion, this work successfully demonstrated systematic improvements in microfluidic volume sensor accuracy, sensitivity and detection range, using tunable sensing channels and novel use of buoyancy-based trajectory control. In compressing the sensing volume, increased sensitivity was achieved, and ~1 μm^3 *E.coli* cells that would have been undetected by larger channels were successfully measured. FEM modelling was used to validate experimental data. Microfluidic volume sensors functionality was then combined with feedback-based pressure driven flow controls to achieve (a) volume-based label-free cell separation and (b) long-term growth measurements of budding yeast. For cell-sorting, near 100% sorting efficiency was demonstrated for both a mix of polystyrene microspheres and live yeast cells. Further, sufficient resolution to identify subpopulations of yeast cells based on cell cycle stage was demonstrated. In cell growth experiments, a dynamic cell trap was maintained for extended periods, successfully mapping the growth of individual cells. Sieve valves enabled cell media to be quickly and easily exchanged while keeping the target cell firmly in place. Fast flowing bypass channels supplied a fresh supply of cell culture media to the trapped cell, while a temperature control system maintained temperature at constant and optimal 30 ºC.

In designing and fabricating these volume sensing devices, care has been taken to use materials and equipment readily available in many biochemistry labs. This is a major advantage of soft lithography. Simple to implement techniques, such as buoyancy or pressure-driven flow control, also make this work of general interest to the field. The hope is that the technological innovations presented herein will inspire researchers to integrate some of these in their own work. To some extent, this has already started to occur,

particularly with respect to the tunable volume sensor *Lab on a Chip* article. In just over a year, this work has garnered 8 citations, in varied fields.

In the Godin Biosensing lab, the work presented herein will continue with an eye towards (1) studying more biologically relevant targets, and (2) expanding on technological applications. This work has established microfluidic technological tools, which can now be applied towards a variety of exciting projects. For cell sorting, the goal will be to demonstrate the isolation of proliferating chondrocytes for applications in regenerative medicine. The low-electric field, PDMS biocompatibility and overall cell-friendly nature of the developed hydrodynamic cell sorting mechanism is compatible with mammalian cells. For the growth sensor, there is interest in studying the effect of drugs on cellular growth cycles and on using fluorescent tags as cell stage indicators. The fact that drugs can easily be infused into the sensing region, and direct cellular growth response observed, opens the door to new and exciting cell assays. This extends not only to yeast, but also to other cell types, such as cancer cells. The volumetric response of cancer cells to various anticancer drugs such as cytarabine or carboplatin could be studied. Technological innovations are also being pursued. One avenue of research is multiplexing of growth measurements. In using a longer sensing channel, similar to the one used in Chapter 3 (Figure 3-2), multiple targets could be monitored at once. The periodic, serialized measurement of multiple targets could allow the volume sensing chip to process volume changes in a large number of targets at once. As mentioned in Chapter 6, the development of multilayered PDMS sieve valves lead to ongoing research on an *E.coli* concentrator chip, for applications in food and water safety. These are but a few of the promising research veins that will be explored in years to come, each directly stemming from this work.

8 References

1. Feynman, R. P. There's Plenty of Room at the Bottom: An Invitation to Enter a New Field of Physics. (1959). at <www.its.caltech.edu/ ~ feynman/plenty.html>
2. Whitesides, G. M. The origins and the future of microfluidics. *Nature* **442,** 368–373 (2006).
3. Coulter, W. H. High-speed automatic blood-cell counter and cell-size analyzer. *Proc Natn Electron Conf* **12,** 1034 (1956).
4. Scott, R., Sethu, P. & Harnett, C. K. Three-dimensional hydrodynamic focusing in a microfluidic Coulter counter. *Rev. Sci. Instrum.* **79,** 046104 (2008).
5. Rodriguez-Trujillo, R. *et al.* High-speed particle detection in a micro-Coulter counter with two-dimensional adjustable aperture. *Biosens. Bioelectron.* **24,** 290–296 (2008).
6. Kang, Y., Li, D., Kalams, S. A. & Eid, J. E. DC-Dielectrophoretic separation of biological cells by size. *Biomed. Microdevices* **10,** 243–249 (2008).
7. Bryan, A. K., Engler, A., Gulati, A. & Manalis, S. R. Continuous and Long-Term Volume Measurements with a Commercial Coulter Counter. *PLoS ONE* **7,** e29866 (2012).
8. Hua, S. Z. & Pennell, T. A microfluidic chip for real-time studies of the volume of single cells. *Lab. Chip* **9,** 251 (2009).
9. Mitchison, J. M. The growth of single cells: II. Saccharomyces cerevisiae. *Exp. Cell Res.* **15,** 214–221 (1958).
10. Woldringh, C. L., Huls, P. G. & Vischer, N. O. Volume growth of daughter and parent cells during the cell cycle of Saccharomyces cerevisiae a/alpha as determined by image cytometry. *J. Bacteriol.* **175,** 3174–3181 (1993).
11. Elliott, S. G. & McLaughlin, C. S. Rate of macromolecular synthesis through the cell cycle of the yeast Saccharomyces cerevisiae. *Proc. Natl. Acad. Sci.* **75,** 4384–4388 (1978).
12. Talia, S. D., Skotheim, J. M., Bean, J. M., Siggia, E. D. & Cross, F. R. The effects of molecular noise and size control on variability in the budding yeast cell cycle. *Nature* **448,** 947–951 (2007).
13. Godin, M. *et al.* Using buoyant mass to measure the growth of single cells. *Nat. Methods* **7,** 387–390 (2010).
14. Sun, J., Stowers, C. C., Boczko, E. M. & Li, D. Measurement of the volume growth rate of single budding yeast with the MOSFET-based microfluidic Coulter counter. *Lab. Chip* **10,** 2986 (2010).
15. Johnson, B. F. Autoradiographic analysis of regional cell wall growth of yeasts: Schizosaccharomyces pombe. *Exp. Cell Res.* **39,** 613–624 (1965).
16. Riordon, J., Mirzaei, M. & Godin, M. Microfluidic cell volume sensor with tunable sensitivity. *Lab. Chip* **12,** 3016 (2012).
17. Riordon, J., M. -Catafard, N. & Godin, M. Using the fringing electric field in microfluidic volume sensors to enhance sensitivity and accuracy. *Appl. Phys. Lett.* **101,** 154105–154105–4 (2012).
18. Gawad, S., Schild, L. & Renaud, P. Micromachined impedance spectroscopy flow cytometer for cell analysis and particle sizing. *Lab. Chip* **1,** 76–82 (2001).

19. Riordon, J., Nash, M., Calderini, M. & Godin, M. Using active microfluidic flow focusing to sort particles and cells based on high-resolution volume measurements. *Microelectron. Eng.* **118,** 35–40 (2014).
20. Riordon, J., Nash, M., Jing, W. & Godin, M. Quantifying the volume of single cells continuously using a microfluidic pressure-driven trap with media exchange. *Biomicrofluidics* **8,** 011101 (2014).
21. Svanberg, S. *Atomic and Molecular Spectroscopy: Basic Aspects and Practical Applications ; with 14 Tables*. (Springer, 2004).
22. Myers, F. B. & Lee, L. P. Innovations in optical microfluidic technologies for point-of-care diagnostics. *Lab. Chip* **8,** 2015 (2008).
23. Walker, G. M. Synchronization of yeast cell populations. *Methods Cell Sci. Off. J. Soc. Vitro Biol.* **21,** 87–93 (1999).
24. Ghallab, Y. H. & Badawy, W. *Lab-on-a-chip: Techniques, Circuits, and Biomedical Applications*. (Artech House, 2010).
25. Squires, T. M. & Quake, S. R. Microfluidics: Fluid physics at the nanoliter scale. *Rev. Mod. Phys.* **77,** 977–1026 (2005).
26. Tabeling, P. *Introduction to Microfluidics*. (Oxford University Press, 2006).
27. Cheung, K., Gawad, S. & Renaud, P. Impedance spectroscopy flow cytometry: On-chip label-free cell differentiation. *Cytometry A* **65,** 124–132 (2005).
28. Bernabini, C., Holmes, D. & Morgan, H. Micro-impedance cytometry for detection and analysis of micron-sized particles and bacteria. *Lab. Chip* **11,** 407 (2011).
29. Velve-Casquillas, G., Le Berre, M., Piel, M. & Tran, P. T. Microfluidic tools for cell biological research. *Nano Today* **5,** 28–47 (2010).
30. Paguirigan, A. L. & Beebe, D. J. Microfluidics meet cell biology: bridging the gap by validation and application of microscale techniques for cell biological assays. *BioEssays News Rev. Mol. Cell. Dev. Biol.* **30,** 811–821 (2008).
31. Young, E. W. K. & Beebe, D. J. Fundamentals of microfluidic cell culture in controlled microenvironments. *Chem. Soc. Rev.* **39,** 1036–1048 (2010).
32. Lee, J. N., Jiang, X., Ryan, D. & Whitesides, G. M. Compatibility of Mammalian Cells on Surfaces of Poly(dimethylsiloxane). *Langmuir* **20,** 11684–11691 (2004).
33. Arneborg, N. *et al.* Interactive optical trapping shows that confinement is a determinant of growth in a mixed yeast culture. *FEMS Microbiol. Lett.* **245,** 155–159 (2005).
34. Huang, G., Mei, Y., Thurmer, D. J., Coric, E. & Schmidt, O. G. Rolled-up transparent microtubes as two-dimensionally confined culture scaffolds of individual yeast cells. *Lab. Chip* **9,** 263–268 (2009).
35. Minc, N., Bratman, S. V., Basu, R. & Chang, F. Establishing new sites of polarization by microtubules. *Curr. Biol. CB* **19,** 83–94 (2009).
36. Leclerc, E., Sakai, Y. & Fujii, T. Cell Culture in 3-Dimensional Microfluidic Structure of PDMS (polydimethylsiloxane). *Biomed. Microdevices* **5,** 109–114 (2003).
37. Cesaro-Tadic, S. *et al.* High-sensitivity miniaturized immunoassays for tumor necrosis factor alpha using microfluidic systems. *Lab. Chip* **4,** 563–569 (2004).
38. Du Roure, O. *et al.* Force mapping in epithelial cell migration. *Proc. Natl. Acad. Sci. U. S. A.* **102,** 2390–2395 (2005).
39. Toepke, M. W. & Beebe, D. J. PDMS absorption of small molecules and consequences in microfluidic applications. *Lab. Chip* **6,** 1484–1486 (2006).

40. Paszkowiak, J. J. & Dardik, A. Arterial Wall Shear Stress: Observations from the Bench to the Bedside. *Vasc. Endovascular Surg.* **37,** 47–57 (2003).
41. Flickinger, M. C. *Downstream Industrial Biotechnology: Recovery and Purification*. (John Wiley & Sons, 2013).
42. Robinson, J. P. Wallace H. Coulter: Decades of invention and discovery. *Cytometry A* **83A,** 424–438 (2013).
43. Sun, J., Stowers, C. C., Boczko, E. M. & Li, D. Measurement of the volume growth rate of single budding yeast with the MOSFET-based microfluidic Coulter counter. *Lab. Chip* **10,** 2986 (2010).
44. Nieuwenhuis, J. H., Kohl, F., Bastemeijer, J., Sarro, P. M. & Vellekoop, M. J. Integrated Coulter counter based on 2-dimensional liquid aperture control. *Sens. Actuators B Chem.* **102,** 44–50 (2004).
45. Cheung, K. C. *et al.* Microfluidic impedance-based flow cytometry. *Cytom. Part J. Int. Soc. Anal. Cytol.* **77A,** 648–666 (2010).
46. Sun, T., Green, N. G., Gawad, S. & Morgan, H. Analytical electric field and sensitivity analysis for two microfluidic impedance cytometer designs. *Nanobiotechnology IET* **1,** 69–79 (2007).
47. Hoffman, R. A. & Britt, W. B. Flow-system measurement of cell impedance properties. *J. Histochem. Cytochem.* **27,** 234–240 (1979).
48. Rodriguez-Trujillo, R., Mills, C. A., Samitier, J. & Gomila, G. Low cost micro-Coulter counter with hydrodynamic focusing. *Microfluid. Nanofluidics* **3,** 171–176 (2006).
49. Schoch, R. B., Han, J. & Renaud, P. Transport phenomena in nanofluidics. *Rev. Mod. Phys.* **80,** 839 (2008).
50. Sparreboom, W., Berg, A. van den & Eijkel, J. C. T. Transport in nanofluidic systems: a review of theory and applications. *New J. Phys.* **12,** 015004 (2010).
51. Madou, M. J. *Solid-State Physics, Fluidics, and Analytical Techniques in Micro- and Nanotechnology*. (CRC Press, 2011).
52. Wang, P. & Liu, Q. *Cell-Based Biosensors*. (Artech House, 2009).
53. Voldman, J. Electrical Forces for Microscale Cell Manipulation. *Annu. Rev. Biomed. Eng.* **8,** 425–454 (2006).
54. Foster, K. R. & Schwan, H. P. Dielectric properties of tissues and biological materials: a critical review. *Crit. Rev. Biomed. Eng.* **17,** 25–104 (1989).
55. Holzel, R. Electrorotation of single yeast cells at frequencies between 100 Hz and 1.6 GHz. *Biophys. J.* **73,** 1103–1109 (1997).
56. Hölzel, R. & Lamprecht, I. Dielectric properties of yeast cells as determined by electrorotation. *Biochim. Biophys. Acta* **1104,** 195–200 (1992).
57. Asami, K., Hanai, T. & Koizumi, N. Dielectric properties of yeast cells. *J. Membr. Biol.* **28,** 169–180 (1976).
58. Glasser, H. & Fuhr, G. Cultivation of cells under strong ac-electric field—differentiation between heating and trans-membrane potential effects. *Bioelectrochem. Bioenerg.* **47,** 301–310 (1998).
59. Anderson, J. A., Huprikar, S. S., Kochian, L. V., Lucas, W. J. & Gaber, R. F. Functional expression of a probable Arabidopsis thaliana potassium channel in Saccharomyces cerevisiae. *Proc. Natl. Acad. Sci.* **89,** 3736–3740 (1992).
60. Cui, X. *et al.* Lensless high-resolution on-chip optofluidic microscopes for Caenorhabditis elegans and cell imaging. *Proc. Natl. Acad. Sci.* **105,** 10670 (2008).

61. Cetin, B. & Li, D. Dielectrophoresis in microfluidics technology. *Electrophoresis* **32,** 2410–2427 (2011).
62. Tang, G. Y. *et al.* Joule heating and its effects on electroosmotic flow in microfluidic channels. *J. Phys. Conf. Ser.* **34,** 925 (2006).
63. Unger, M. A. Monolithic Microfabricated Valves and Pumps by Multilayer Soft Lithography. *Science* **288,** 113–116 (2000).
64. Xia, Y. & Whitesides, G. M. Soft Lithography. *Angew. Chem. Int. Ed.* **37,** 550–575 (1998).
65. Hillborg, H. *et al.* Crosslinked polydimethylsiloxane exposed to oxygen plasma studied by neutron reflectometry and other surface specific techniques. *Polymer* **41,** 6851–6863 (2000).
66. Tan, S. H., Nguyen, N.-T., Chua, Y. C. & Kang, T. G. Oxygen plasma treatment for reducing hydrophobicity of a sealed polydimethylsiloxane microchannel. *Biomicrofluidics* **4,** (2010).
67. Eddings, M. A., Johnson, M. A. & Gale, B. K. Determining the optimal PDMS–PDMS bonding technique for microfluidic devices. *J. Micromechanics Microengineering* **18,** 067001 (2008).
68. Bhattacharya, S., Datta, A., Berg, J. M. & Gangopadhyay, S. Studies on surface wettability of poly(dimethyl) siloxane (PDMS) and glass under oxygen-plasma treatment and correlation with bond strength. *J. Microelectromechanical Syst.* **14,** 590–597 (2005).
69. Huh, D., Gu, W., Kamotani, Y., Grotberg, J. B. & Takayama, S. Microfluidics for flow cytometric analysis of cells and particles. *Physiol. Meas.* **26,** R73 (2005).
70. Keller, H. U., Fedier, A. & Rohner, R. Relationship between light scattering in flow cytometry and changes in shape, volume, and actin polymerization in human polymorphonuclear leukocytes. *J. Leukoc. Biol.* **58,** 519–525 (1995).
71. Robinson, J. P. Wallace H. Coulter: Decades of invention and discovery. *Cytometry A* **83A,** 424–438 (2013).
72. Zhu, J., Tzeng, T.-R., Hu, G. & Xuan, X. DC dielectrophoretic focusing of particles in a serpentine microchannel. *Microfluid. Nanofluidics* **7,** 751–756 (2009).
73. Lagally, E. T., Lee, S.-H. & Soh, H. T. Integrated microsystem for dielectrophoretic cell concentration and genetic detection. *Lab. Chip* **5,** 1053 (2005).
74. Lee, M. G., Choi, S. & Park, J.-K. Three-dimensional hydrodynamic focusing with a single sheath flow in a single-layer microfluidic device. *Lab. Chip* **9,** 3155–3160 (2009).
75. Golden, J. P. *et al.* Multi-wavelength microflow cytometer using groove-generated sheath flow. *Lab. Chip* **9,** 1942–1950 (2009).
76. Herzenberg, L. A. *et al.* The History and Future of the Fluorescence Activated Cell Sorter and Flow Cytometry: A View from Stanford. *Clin. Chem.* **48,** 1819–1827 (2002).
77. Wolff, A. *et al.* Integrating advanced functionality in a microfabricated high-throughput fluorescent-activated cell sorter. *Lab. Chip* **3,** 22–27 (2003).
78. Battistini, L. *et al.* CD8+ T cells from patients with acute multiple sclerosis display selective increase of adhesiveness in brain venules: a critical role for P-selectin glycoprotein ligand-1. *Blood* **101,** 4775–4782 (2003).
79. Sugiyama, T. & Kim, S. K. Fluorescence-activated cell sorting purification of pancreatic progenitor cells. *Diabetes Obes. Metab.* **10,** 179–185 (2008).

80. Zhou, X. *et al.* Isolation of Purified and Live Foxp3+ Regulatory T Cells using FACS Sorting on Scatter Plot. *J. Mol. Cell Biol.* **2,** 164–169 (2010).
81. Cho, S. H., Chen, C. H., Tsai, F. S., Godin, J. M. & Lo, Y.-H. Human mammalian cell sorting using a highly integrated micro-fabricated fluorescence-activated cell sorter (?FACS). *Lab. Chip* **10,** 1567–1573 (2010).
82. Krüger, J. *et al.* Development of a microfluidic device for fluorescence activated cell sorting. *J. Micromechanics Microengineering* **12,** 486 (2002).
83. Fu, A. Y., Chou, H.-P., Spence, C., Arnold, F. H. & Quake, S. R. An Integrated Microfabricated Cell Sorter. *Anal. Chem.* **74,** 2451–2457 (2002).
84. Studer, V., Jameson, R., Pellereau, E., Pépin, A. & Chen, Y. A microfluidic mammalian cell sorter based on fluorescence detection. *Microelectron. Eng.* **73–74,** 852–857 (2004).
85. Wang, M. D., Yin, H., Landick, R., Gelles, J. & Block, S. M. Stretching DNA with optical tweezers. *Biophys. J.* **72,** 1335–1346 (1997).
86. Whyte, G. *et al.* An optical trapped microhand for manipulating micron-sized objects. *Opt. Express* **14,** 12497–12502 (2006).
87. Applegate, J., Squier, J., Vestad, T., Oakey, J. & Marr, D. Optical trapping, manipulation, and sorting of cells and colloids in microfluidic systems with diode laser bars. *Opt. Express* **12,** 4390–4398 (2004).
88. Shi, J., Huang, H., Stratton, Z., Huang, Y. & Huang, T. J. Continuous particle separation in a microfluidic channel via standing surface acoustic waves (SSAW). *Lab. Chip* **9,** 3354–3359 (2009).
89. Petersson, F., Åberg, L., Swärd-Nilsson, A.-M. & Laurell, T. Free Flow Acoustophoresis: Microfluidic-Based Mode of Particle and Cell Separation. *Anal. Chem.* **79,** 5117–5123 (2007).
90. Pamme, N. Continuous flow separations in microfluidic devices. *Lab. Chip* **7,** 1644–1659 (2007).
91. Huang, L. R., Cox, E. C., Austin, R. H. & Sturm, J. C. Continuous Particle Separation Through Deterministic Lateral Displacement. *Science* **304,** 987–990 (2004).
92. Yamada, M., Nakashima, M. & Seki, M. Pinched Flow Fractionation: Continuous Size Separation of Particles Utilizing a Laminar Flow Profile in a Pinched Microchannel. *Anal. Chem.* **76,** 5465–5471 (2004).
93. Takagi, J., Yamada, M., Yasuda, M. & Seki, M. Continuous particle separation in a microchannel having asymmetrically arranged multiple branches. *Lab. Chip* **5,** 778–784 (2005).
94. Choi, S., Song, S., Choi, C. & Park, J.-K. Continuous blood cell separation by hydrophoretic filtration. *Lab. Chip* **7,** 1532–1538 (2007).
95. Sethu, P., Sin, A. & Toner, M. Microfluidic diffusive filter for apheresis (leukapheresis). *Lab. Chip* **6,** 83–89 (2006).
96. Shendruk, T. N. *et al.* Field-flow fractionation and hydrodynamic chromatography on a microfluidic chip. *Anal. Chem.* **85,** 5981–5988 (2013).
97. Choi, S. & Park, J.-K. Hydrophoresis: A New -Phoretic Method for High-Resolution Particle Separation. in *Solid-State Sens. Actuators Microsyst. Conf. 2007 TRANSDUCERS 2007 Int.* 1769–1772 (2007). doi:10.1109/SENSOR.2007.4300496
98. Song, S. & Choi, S. Design rules for size-based cell sorting and sheathless cell focusing by hydrophoresis. *J. Chromatogr. A* **1302,** 191–196 (2013).

99. Alvankarian, J., Bahadorimehr, A. & Yeop Majlis, B. A pillar-based microfilter for isolation of white blood cells on elastomeric substrate. *Biomicrofluidics* **7,** 014102–014102–16 (2013).
100. Song, Y. *et al.* DC dielectrophoresis separation of marine algae and particles in a microfluidic chip. *Sci. China Chem.* **55,** 524–530 (2012).
101. Mernier, G. Label-free Sorting and Counting of Yeast Cells for Viability Studies. *Procedia Chem.* **1,** 385–388 (2009).
102. Yunus, N. A. M., Nili, H. & Green, N. G. Continuous separation of colloidal particles using dielectrophoresis. *Electrophoresis* **34,** 969–978 (2013).
103. Sun, J. *et al.* Simultaneous On-Chip DC Dielectrophoretic Cell Separation and Quantitative Separation Performance Characterization. *Anal Chem* **84,** 2017–2024 (2012).
104. Song, Y. *et al.* Automatic particle detection and sorting in an electrokinetic microfluidic chip. *Electrophoresis* **34,** 684–690 (2013).
105. Joshua I. Molho, A. E. H. Fluid transport mechanisms in microfluidic devices.
106. Monod, J. The Growth of Bacterial Cultures. *Annu. Rev. Microbiol.* **3,** 371–394 (1949).
107. Sevick, E. M., Chance, B., Leigh, J., Nioka, S. & Maris, M. Quantitation of time- and frequency-resolved optical spectra for the determination of tissue oxygenation. *Anal. Biochem.* **195,** 330–351 (1991).
108. Mitchison, J. M. in *Int. Rev. Cytol.* **Volume 226,** 165–258 (Academic Press, 2003).
109. Woldringh, C. L., Huls, P. G. & Vischer, N. O. Volume growth of daughter and parent cells during the cell cycle of Saccharomyces cerevisiae a/alpha as determined by image cytometry. *J. Bacteriol.* **175,** 3174–3181 (1993).
110. Burg, T. P. *et al.* Weighing of biomolecules, single cells and single nanoparticles in fluid. *Nature* **446,** 1066–1069 (2007).
111. Bryan, A. K., Goranov, A., Amon, A. & Manalis, S. R. Measurement of mass, density, and volume during the cell cycle of yeast. *Proc. Natl. Acad. Sci. U. S. A.* **107,** 999–1004 (2010).
112. Sridhar, M. *et al.* Experimental characterization of a metal-oxide-semiconductor field-effect transistor-based Coulter counter. *J. Appl. Phys.* **103,** 104701 (2008).
113. Mansoor Nasir, D. A. A. Hydrodynamic focusing of conducting fluids for conductivity-based biosensors. *Biosens. Bioelectron.* (2009). doi:10.1016/j.bios.2009.10.033
114. Chen, H. *et al.* Electromechanical Properties of Pressure-Actuated Poly(dimethylsiloxane) Microfluidic Push-Down Valves. *Anal Chem* **80,** 6110–6113 (2008).
115. Galas, J.-C., Studer, V. & Chen, Y. Characterization of pneumatically activated microvalves by measuring electrical conductance. *Microelectron. Eng.* **78-79,** 112–117 (2005).
116. Schafer, R. W. What Is a Savitzky-Golay Filter? [Lecture Notes]. *IEEE Signal Process. Mag.* **28,** 111–117 (2011).
117. Gawad, S., Cheung, K., Seger, U., Bertsch, A. & Renaud, P. Dielectric spectroscopy in a micromachined flow cytometer: theoretical and practical considerations. *Lab. Chip* **4,** 241 (2004).

118. Sun, T., Green, N. G., Gawad, S. & Morgan, H. Analytical electric field and sensitivity analysis for two microfluidic impedance cytometer designs. *Nanobiotechnology IET* **1,** 69–79 (2007).
119. Ferrer, J., Prats, C. & López, D. Individual-based Modelling: An Essential Tool for Microbiology. *J. Biol. Phys.* **34,** 19–37 (2008).
120. Allen, T. *Particle Size Measurement Volume 1*. (Springer, 1996).
121. Fu, L.-M., Tsai, C.-H. & Lin, C.-H. A high-discernment microflow cytometer with microweir structure. *ELECTROPHORESIS* **29,** 1874–1880 (2008).
122. Choi, S. & Park, J.-K. Sheathless Hydrophoretic Particle Focusing in a Microchannel with Exponentially Increasing Obstacle Arrays. *Anal Chem* **80,** 3035–3039 (2008).
123. Radisic, M., Iyer, R. K. & Murthy, S. K. Micro- and nanotechnology in cell separation. *Int. J. Nanomedicine* **1,** 3–14 (2006).
124. Enger, J., Goksör, M., Ramser, K., Hagberg, P. & Hanstorp, D. Optical tweezers applied to a microfluidic system. *Lab. Chip* **4,** 196–200 (2004).
125. Ozkan, M., Wang, M., Ozkan, C., Flynn, R. & Esener, S. Optical Manipulation of Objects and Biological Cells in Microfluidic Devices. *Biomed. Microdevices* **5,** 61–67 (2003).
126. Adams, J. D., Kim, U. & Soh, H. T. Multitarget magnetic activated cell sorter. *Proc. Natl. Acad. Sci.* **105,** 18165–18170 (2008).
127. Valero, A., Braschler, T., Demierre, N. & Renaud, P. A miniaturized continuous dielectrophoretic cell sorter and its applications. *Biomicrofluidics* **4,** (2010).
128. Sridhar, M. *et al.* Experimental characterization of a metal-oxide-semiconductor field-effect transistor-based Coulter counter. *J. Appl. Phys.* **103,** 104701 (2008).
129. Saleh, O. A. & Sohn, L. L. Quantitative sensing of nanoscale colloids using a microchip Coulter counter. *Rev. Sci. Instrum.* **72,** 4449–4451 (2001).
130. Melin, J. & Quake, S. R. Microfluidic large-scale integration: the evolution of design rules for biological automation. *Annu. Rev. Biophys. Biomol. Struct.* **36,** 213–231 (2007).
131. Castillo-Fernandez, O., Rodriguez-Trujillo, R., Gomila, G. & Samitier, J. High-speed counting and sizing of cells in an impedance flow microcytometer with compact electronic instrumentation. *Microfluid. Nanofluidics* 1–9 doi:10.1007/s10404-013-1225-6
132. Marcus, J. S., Anderson, W. F. & Quake, S. R. Microfluidic Single-Cell mRNA Isolation and Analysis. *Anal. Chem.* **78,** 3084–3089 (2006).
133. Bishop, A. C. *et al.* A chemical switch for inhibitor-sensitive alleles of any protein kinase. *Nature* **407,** 395–401 (2000).
134. Park, W., Han, S. & Kwon, S. Fabrication of membrane-type microvalves in rectangular microfluidic channels via seal photopolymerization. *Lab. Chip* **10,** 2814–2817 (2010).
135. Hahn, A. T., Jones, J. T. & Meyer, T. Quantitative analysis of cell cycle phase durations and PC12 differentiation using fluorescent biosensors. *Cell Cycle Georget. Tex* **8,** 1044–1052 (2009).
136. Luongo, K. *et al.* Microfluidic device for trapping and monitoring three dimensional multicell spheroids using electrical impedance spectroscopy. *Biomicrofluidics* **7,** 034108 (2013).
137. Park, H. Single-cell manipulation on microfluidic chip by dielectrophoretic actuation and impedance detection. *Sens. Actuators B Chem.* **150,** 167–173 (2010).

138. Hardy, B. S., Uechi, K., Zhen, J. & Pirouz Kavehpour, H. The deformation of flexible PDMS microchannels under a pressure driven flow. *Lab. Chip* **9,** 935 (2009).
139. Logothetis, S., Walker, G. M. & Nerantzis, E. T. Effect of salt hyperosmotic stress on yeast cell viability. (2007). at <http://kmi-web23.open.ac.uk:8081/display/1154722>
140. Hartwell, L. H. & Unger, M. W. Unequal division in Saccharomyces cerevisiae and its implications for the control of cell division. *J. Cell Biol.* **75,** 422–435 (1977).
141. Scopes, A. W. & Williamson, D. H. The growth and oxygen uptake of synchronously dividing cultures of saccharomyces cerevisiae. *Exp. Cell Res.* **35,** 361–371 (1964).
142. Knudsen, S. M., von Muhlen, M. G., Schauer, D. B. & Manalis, S. R. Determination of Bacterial Antibiotic Resistance Based on Osmotic Shock Response. *Anal. Chem.* **81,** 7087–7090 (2009).
143. Sugiura, S., Edahiro, J., Kikuchi, K., Sumaru, K. & Kanamori, T. Pressure-driven perfusion culture microchamber array for a parallel drug cytotoxicity assay. *Biotechnol. Bioeng.* **100,** 1156–1165 (2008).
144. Khetani, A. *et al.* Hollow core photonic crystal fiber as a reusable Raman biosensor. *Opt. Express* **21,** 12340–12350 (2013).
145. Khetani, A. *et al.* Hollow core photonic crystal fiber as a robust Raman biosensor. 85760F–85760F (2013). doi:10.1117/12.2004692
146. Ugolini, S. & Bruschi, C. V. The red/white colony color assay in the yeast Saccharomyces cerevisiae: epistatic growth advantage of white ade8-18, ade2 cells over red ade2 cells. *Curr. Genet.* **30,** 485–492 (1996).
147. Guthrie, C. & Fink, G. R. *Guide to Yeast Genetics and Molecular and Cell Biology*. (Gulf Professional Publishing, 2004).
148. Goldberg, D. T. *Barron's AP Biology*. (Barron's Educational Series, 2010).

9 Appendix

9.1 List of Photomasks

9.1.1 Electrodes

Designation/Date/ Project/Notes	Full View	Close View
E1/Aug 2009 (Jeff Salvail)	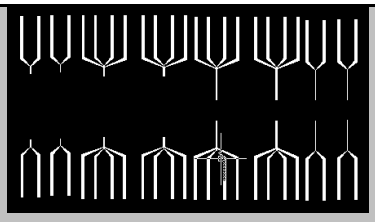	
E2/May 2011 Project: Tunable volume sensor Polarity: Positive** PR: S1813	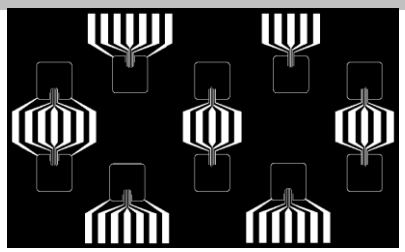	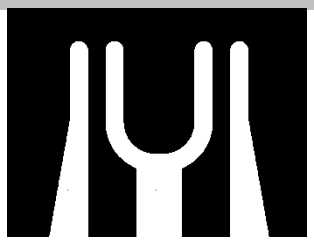
E3/Dec 2011 Project: Cell Sorting Polarity: Positive* PR: S1813	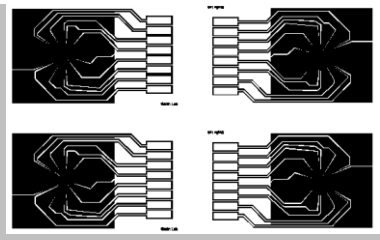	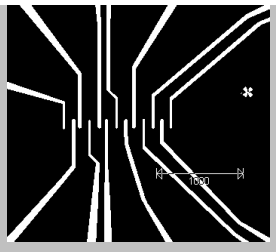
E4/Jan 2013 Project: Cell Sorting Polarity: Negative PR: S1813	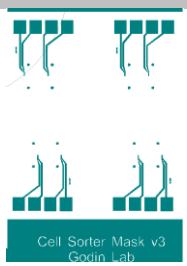	
E5/Nov 2013 Project: Cell Trapping Polarity: Negative PR: S1813		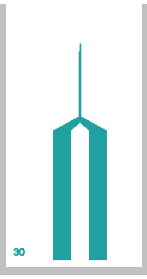

**Emulsion down

9.1.2 Channels

C2/Sep 2010
(Maryam Mirzaei)
Project: Tunable volume sensor
Polarity: Positive
PR: AZ P4620

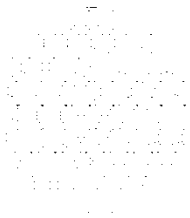

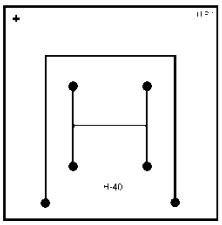

C3/May 2011
Project: Fringing E-Field
Polarity: Negative*
PR: SU-8 10

C4/Aug 2011
Project: Tunable volume sensor
Polarity: Positive
PR: AZ P4620

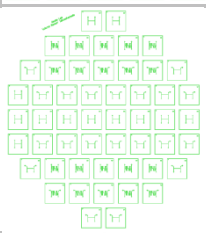

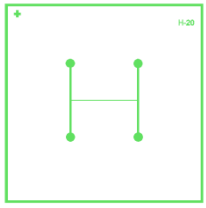

C5/Dec 2011
Project: Cell Sorter
Polarity: Positive
PR: AZ P4620

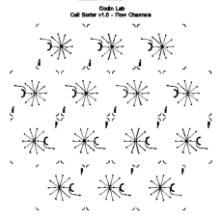

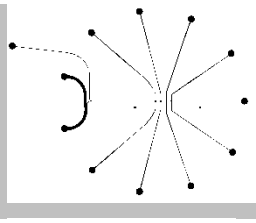

C6/June 2012
Project: Cell Sorter
Polarity: Positive
PR: AZ P4620

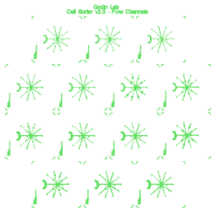

C7/June 2012
Project: Cell trapping
Polarity: Positive
PR: AZ 50XT

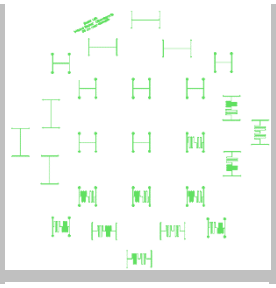

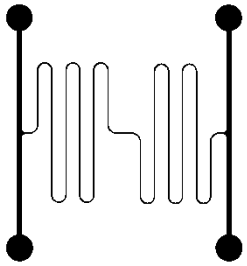

C8/June 2012
Project: Cell Sorter
Polarity: Negative*
PR: SU-8 10

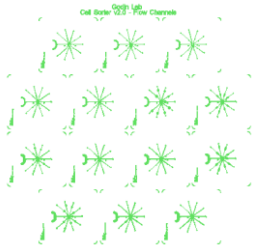

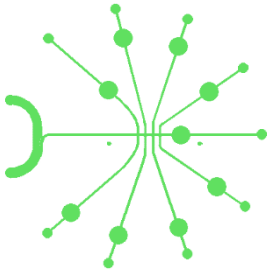

C9 Jan 2013 Project: Cell Sorter Polarity: Negative* PR: SU-8 2050	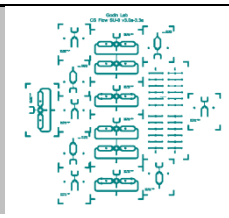		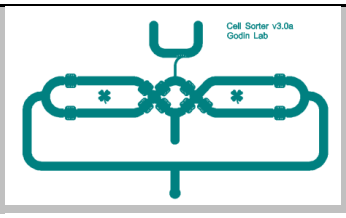
C10 Project: Cell Sorter Polarity: Positive PR: AZ 50X	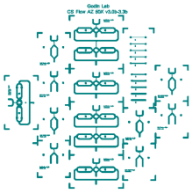		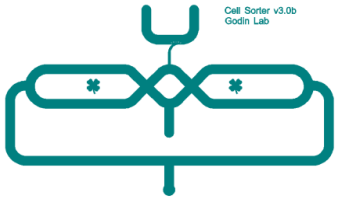
C11 Project: Cell Sorter Polarity: Positive PR: AZ P4620	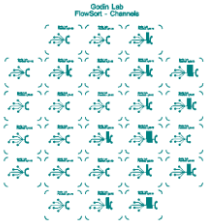		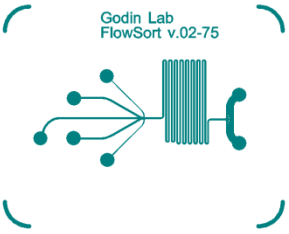
C12 Project: Concentrator Polarity: Positive PR: AZ P4620	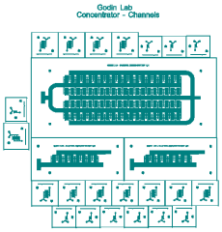		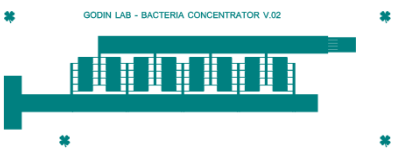
C13 October 2013 Project: Cell trapping Polarity: Positive PR: AZ P4620	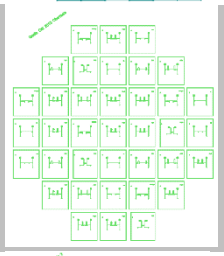		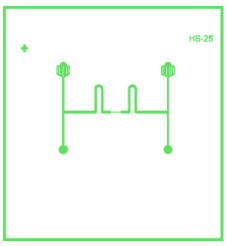
C14/October 2013 Polarity: Positive PR: AZ P4620	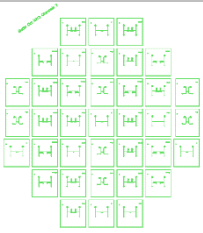		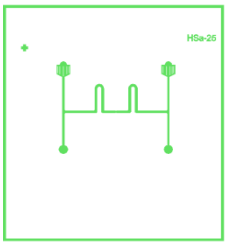
C15/October 2013 Polarity: Positive PR: AZ P4620	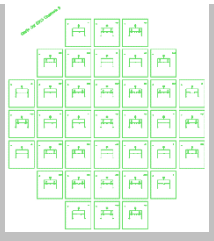		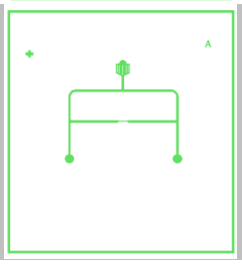

*Inverted

9.1.3 Valves

V1/Sep 2010 (Maryam Mirzaei) Project: Tunable volume sensor Polarity: Negative* PR: SU-8 10		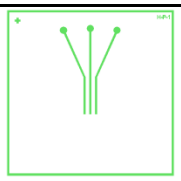
V2/May 2011 Project: Tunable volume sensor Polarity: Negative* PR: SU-8 10	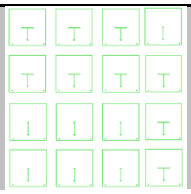	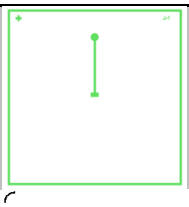
V3 Dec 2011 Project: Cell sorter Polarity: Negative* PR: SU-8 10	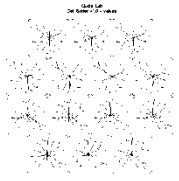	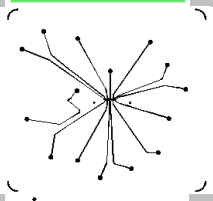
V4 June 2012 Project: Cell Sorter Polarity: Negative* PR: AZ P4620	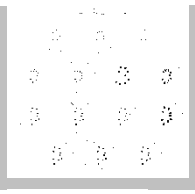	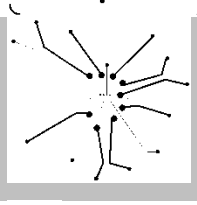
V5 June 2012 Project: Cell Trapping Polarity: Negative* PR: SU-8 10		
V6 Jan 2013 Project: Cell Sorting Polarity: Negative* PR: SU-8 2050		
V7 March 2013 Project: Cell Sorting Polarity: Negative* PR: SU-8 2050		
V8 March 2013 Project: Concentrator Polarity: Negative* PR: SU-8 2050	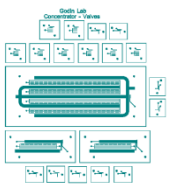	
V9 October 2013 Project: Cell trapping Polarity: Negative* PR: SU-8 10	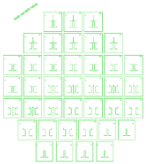	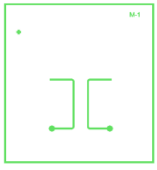

*** Inverted**

9.2 Detailed Protocols

9.2.1 Fabrication

9.2.1.1 Piranha Clean

9.2.1.1.1 Summary

Piranha is a powerful mix of sulfuric acid and hydrogen peroxide, used to clean microfluidic channels and render surfaces highly hydrophilic. Since it acts as an oxidizer, it is particularly useful against organics. The idea is to mix 1 part hydrogen peroxide into 3 parts sulfuric acid. For cleaning wafers or glass slides, mix 10 ml of hydrogen peroxide with 30 ml sulfuric acid.

9.2.1.1.2 Safety

- Safety goggles
- Nitrile gloves and rubber gloves
- Face shield
- Lab coat
- Lab apron
- Fume hood

9.2.1.1.3 Materials

- Sulfuric acid
- Hydrogen peroxide
- Glass spill dish
- Small beaker
- Flat-end tweezers
- Graduated cylinder
- *Bluesorb* wipes
- Two glass dishes

9.2.1.1.4 Protocol

1. Lay out a few *Bluesorb* wipes around your work area in the fume hood, especially in areas prone to spillage. Place your distilled water beaker, glass dishes and in the spill dish. Fill one of the dishes with deionised water; the other will be the main reaction dish.
2. Take out the small sulfuric acid bottle from the acid safety cupboard, and place inside the spill dish. Using the graduated cylinder, carefully transfer 30 ml into the reaction dish. For added safety, do so with body behind the fume hood's window.
3. Clean up any drops and replace sulfuric acid bottle in the acid safety cupboard.
4. Take out the hydrogen peroxide from the refrigerator, and place inside the spill dish. Using the (rinsed out) graduated cylinder, carefully transfer 10 ml into the reaction vial.
5. Shuffle the dish, allowing the solution to mix well. Add a wafer or glass slides, depending on what is to be cleaned. Be sure to blow off any dust with nitrogen prior to immersion.
6. Clean up any drops and replace hydrogen peroxide in the refrigerator.
7. Let the piranha solution sit for 30 min.
8. Transfer the wafer/slides to the second dish with deionised water; dump the acid into a waste beaker with water (dilute). Be sure to label this waste, and dispose of it in acid waste once it has finished reacting.
9. Let the wafer/slides stay immersed in water for 5 min, then transfer to another glass dish with deionised water for another 5 min. Replace the water twice more, then transfer to the clean room. Blow dry with nitrogen.

9.2.1.2 Electrodes

9.2.1.2.1 Summary

Lift-off is a technique used to pattern metallic films using photolithography. In this procedure, *Shipley* S1813 photoresist is used in conjunction with toluene to create micro-sized features on glass slides. A negative mask is used, so as to expose the glass where electrodes are to be placed. These steps are prior to depositing a metallic layer. This procedure in particular has seen many changes and optimizations over the last 4 years; this protocol represents the current up-to-date iteration. This protocol should be followed once the glass slides are thoroughly cleaned using piranha. Thank you to Benjamin Watts and Matias Calderini for helping perfect the protocol.

9.2.1.2.2 Safety

- Safety goggles
- Nitrile Gloves
- Lab coat
- Fume hood

9.2.1.2.3 Materials

- Cleaned microscope slides
- 2 glass dishes
- Flat tweezers
- Tetramethylammonium hydroxide (TMAH)
- Toluene
- *Shipley* S1813 Photoresist
- Hot plate
- Magnetic stirrer, 2 cm
- Aluminum foil
- Positive photomask
- Spin coater
- Mask aligner
- Pasteur pipette + bulb
- N-Methyl-2-pyrrolidone (NMP)
- Isopropanol (IPA)

9.2.1.2.4 Protocol

1. **Setup** Wrap a hot plate with aluminum foil. Program the spin coater:

    a. 10s @ 500 RPM, ACL = 015
    b. 30s @ 4000 RPM, ACL = 010
    c. 20s @ 200 RPM, ACL = 005

    Set the mask aligner timer to 10 seconds, and position your mask.

2. **10 min @ 200ºC** Place slides on hot plate at 200°C for 10 minutes, then let cool 2 min. This step removes any adsorbed humidity from the surface of the slides.
3. **Spin coat** Place a slide on the spin coater (slide attachment) and vacuum in place. Use the Pasteur pipette to dispense ~1 mL of S1813 photoresist. Running the program will create a film of about 1.4 micron thickness.
4. **Prebake 60s @ 90ºC** Place slide on hot plate for 60s at 90ºC.
5. **UV Expose 10s** Place slide on silicon wafer using tape alignment previously determined. Close lid, make final positioning adjustments, then slide into the light. Make sure you have eyewear protection.
6. **Toluene soak 60s + N_2 dry** Place slide in toluene dish for 1 minute. In this step, the top of the PR is being chemically modified to develop slower than resist underneath (top is less soluble). This leads to undercut features favorable to lift-off. Dry with high-purity nitrogen.
7. **Postbake 15s @ 115ºC** Place slide on hot plate, and bake for 15s. Remove with tweezers, place on aluminum foil for 1 min cooling.
8. **Develop in diluted TMAH + N_2 dry** Create a solution of diluted TMAH: 8 mL TMAH in 76 mL of deionized water in the glass dish, and place above a (cool) hot plate with the spinning tool. Set to spin at 400 RPM. Note that this solution behaves differently for

the first slide compared to later slides. The first slide that is immersed will likely be wasted, as the solution is initially aggressive. As more and more slides are exposed, the solution slowly loses its potency. TMAH should be partially replenished every few slides, so as to have a development time of 20-30s. It is *very* important not to overdevelop. After development, use the tweezers to transfer a slide to a second glass dish with deionized water. N_2 dry.

9. **Microscope verification** Use the microscope to verify slide quality, and adjust procedure as necessary.
10. **Metal deposition** Once 12-20 slides are complete, deposit a thin, 40 nm Au layer with 5 nm Ti adhesion layer. This can be performed at the Carleton University MicroFabrication Facility, either by thermal deposition or e-beam evaporation.
11. **Lift-off with NMP** Use NMP to etch the photoresist, leaving only the metal-on-glass electrodes. The etchant should be heated to 70ºC to accelerate the process. This process will take longer than development times, generally between 5-2 20 mins.

9.2.1.3 SU8 / AZ P4620 Mould

9.2.1.3.1 Summary

A master (mould) is used in soft lithography to create PDMS microchannels. A number of photoresists exist; this section will describe the procedure for the three most popular types used in this work. A wafer is first cleaned using a piranha etch, then, in a cleanroom environment, photoresist is spin-coated to the desired thickness. SU8 10 is used primarily for thin films up to 10 µm thick, whereas SU8 2050 is generally for samples requiring a 10-50 µm thickness. Both are negative photoresists, and so are used in conjunction with a negative photomask. AZ P4620 is a positive photoresist, used to make layers 10-25 µm in thickness. AZ P4620 does not bond well to bare silicon wafers, and as such requires a primary layer of SU8 10. AZ P4620 can be reflowed via an additional heating step, allowing channels to assume a rounded shape. The fabrication parameters will vary according to the type of photoresist chosen, as well as desired thickness. Optimized parameters can be found in *manufacturer documentation*. As an example, the procedure to fabricate a mould for rounded AZ P4620 with narrow sensing channels ~20 µm thick will be described. It will be prepared with an SU-8 10 adehsion layer, followed by two thin AZ P4620 layers. Here, it is understood that the narrowest features assume a height of 20 µm, while wider features will reflow to a taller height (reflow is uneven).

9.2.1.3.2 Safety

- Safety goggles
- Nitrile Gloves
- Lab coat
- Fume hood

9.2.1.3.3 Materials

- Aluminum foil

- Glass dish
- Photoresist: SU-8 10 / SU-8 2050 / AZ P4620
- 2 glass dishes
- Developer: SU-8 / AZ 400K
- Flat tweezers
- Photomask
- 2 hot plates
- Spin coater
- Mask aligner

9.2.1.3.4 Protocol

- **Setup** Wrap a hot plate with aluminum foil. Turn on the mask aligner and lamp.
- **10 min @ 200ºC** Place the wafer on the hot plate for 10 mins at 200 ºC. This steps removes any adsorbed humidity from the wafer surface. Let cool 2 min.
- **Spin coat** Program the spin coater:

    a. 10s @ 500 RPM, ACL = 100
    b. 60s @ 3000 RPM, ACL = 500
    c. 10s @ 0 RPM, ACL = 300

    Pour SU-8 10 so as to cover most of the wafer. Use the wafer alignment tool to center the wafer.
- **Prebake 2 min @ 75 ºC + 5 min @ 105 ºC** Bake at selected settings, then let the wafer cool for 2 min.
- **UV Expose 20s** Expose the wafer without any mask.
- **Postbake 1 min @ 75 ºC + 2 min @ 105 ºC** Bake at these settings, then let the wafer cool for 2 min.
- **Develop 2 min** Develop the wafer for 2 min, then rinse in IPA and dry with N_2.
- **Spin coat** Program the spin coater:

    a. 3s @ 300 RPM, ACL = 100
    b. 60s @ 2100 RPM, ACL = 600
    c. 10s @ 500 RPM, ACL = 400

d. 10s @ 10000 RPM, ACL = 250
e. 5s @ 0 RPM, ACL = 200

Pour on the AZ P4620, and run the program.

- **Prebake 85s @ 110 ºC** Bake at selected settings, then let the wafer cool for 2 min.
- **Spin coat** Program the spin coater:

    a. 3s @ 300 RPM, ACL = 100
    b. 60s @ 1600 RPM, ACL = 600
    c. 10s @ 500 RPM, ACL = 400
    d. 10s @ 10000 RPM, ACL = 250
    e. 5s @ 0 RPM, ACL = 200

    Pour on the AZ P4620, and run the program.

- **Prebake 165s @ 110 ºC** Bake at selected settings, then let the wafer cool for 2 min.
- **2 hr wait** Wait at least an hour before exposure. It is *very* important that the film be allowed to reabsorb moisture prior to UV exposure. Thicker layers require longer wait times.
- **UV expose 80s** UV expose the wafer for 80s. If this exposure leaves parts of the film looking "crispy", shorten exposure time for the next wafer.
- **Develop** Submerge the film in AZ 400K (diluted 4:1 in water) for about 5 min, or until all the features appear fully developed. Rinse in deionized water and N_2 dry.
- **Reflow 5 min @ 75°C + 5 min @ 95°C + 5 min @ 150°C + 5 min @ 200°C** Bake as described. It is important that the ramping of temperature be as slow/smooth as possible. Use the dektak to measure heights before and after reflow.

9.2.1.4 Multilayered PDMS

9.2.1.4.1 Summary

This protocol details the fabrication of a 2 layer PDMS device, consisting of a valve layer (top) and channel layer (below). It is assumed that masters for respective layers have already been fabricated. The idea is to modify the silicone elastomer base to curing agent ratio, thereby modifying PDMS elasticity. This allows the fabrication of a multilayered device with a soft channel layer, and stiff valve layer. This is consistent with "push-down" style valves. As an example, a 30 µm channel will be created with a 5 mm valve layer.

9.2.1.4.2 Safety

- Safety goggles
- Nitrile Gloves
- Lab coat
- Fume hood

9.2.1.4.3 Materials

- Valve and microchannel moulds
- Tape
- Stereo microscope
- Tweezers
- Scale
- Spin coater
- Mask aligner
- Sonicator
- Oxygen Plasma
- Ethanol
- Isopropanol (IPA)

9.2.1.4.4 Protocol

- **Aminosilane treatment** Place the dish in the vacuum chamber, along a 1µL drop of trichlorosilane a petri dish. Vacuum for 5 min, then wait 1 hour for it to coat the master. Full name: (tridecafluoro-1,1,2,2-tetrahydrooctyl)trichlorosilane This

treatment is required every few times the wafer is used as a mould. It acts as a non-adhesion layer, allowing for easy removal of the cured PDMS.

- **Mix PDMS 7:1** Mix enough PDMS so as to have a thickness of about 5 mm throughout the dish. Make sure to maintain the 7:1 ratio; if too much is added, add more base as required. Use a pipette tip to mix the solution for over 5 min under the fume hood. Dry the valve master with nitrogen, and place in a polystyrene dish. Use Scotch tape to fix the wafer at the center of the dish by taping all sides. We want to prevent the wafer from floating up, or PDMS from getting under the wafer once the liquid PDMS is poured in.
- **Mix PDMS 20:1** Prepare the PDMS as before, but with 10 g of base and 0.5 g of curing agent.
- **30 min degass** Place both PDMS mixtures in the vacuum chamber, both covered. Let it degass until bubbles are removed (~20 min). Note that sometimes residual surface bubbles remain; use N_2 to break these, or at least blow these away from crucial areas.
- **Spin coat** Spin coat the PDMS on the channel master mould, with the following settings:
- **10 min @ 200ºC** Place the wafer on the hot plate for 10 mins at 200 ºC. This step removes any adsorbed humidity from the wafer surface. Let cool 2 min.
- **Spin coat** Program the spin coater:

    a. 10s @ 500 RPM, ACL = 100
    b. 60s @ 2000 RPM, ACL = 300
    c. 10s @ 0 RPM, ACL = 200

and coat the 20:1 PDMS.

- **Bake** Bake the valve layer for 24 mins; bake the channel layer for 20 mins. Let cool 5 mins.
- **Cut out devices** Cut out the valves, and punch holes using the 750 µm hole-punch. Punched holes should be straight and smooth. Faulty punches have caused leaks in the past, so be sure holes are being punched correctly. When punching, position a secondary PDMS under the main one so as to not damage the puncher, and improve punching quality. Use the tape to clean the devices, paying close attention to picking up the small PDMS pieces leftover from the punching process.
- **PDMS:PDMS Alignment and bonding** Use the mask aligner to carefully align the channels to the valves. This step involves exposing both PDMS layers with a 30 W oxygen plasma for 30s prior to bonding. Since the oxygen treatment does not last very long (<5 min), it is important to quickly align the layers after this treatment, and press them together. To perform the alignment, place the wafer and turn on vacuum in soft contact mode. Place a blank clean slide on the slide holder accessory, and vacuum it in place. Place your first device channels facing down beneath the glass slide. It should still be sticky enough to stay in place. Close the aligner lid, and adjust the channel position to correspond to the valve. You may do so first by eye, then by using the microscope. When all is in place, turn the elevation knob to lift the channels into the valves. This may require multiple XY adjustments to get it just right. When there is contact, turn the knob a bit further so as to make contact over the viewing area. Next, remove the sample vacuum to release the slide, and lift the lid. The slide should stay in place during plate lift. Peel off the glass slide, and put it back in position with vacuum. Continue as such until all valve

PDMS pieces are positioned on the wafer. Be careful to lower the Z stage between devices, so as to not damage anything. Also note that the lid lifts in an arc, so move your wafer out of the way as necessary to prevent contact between PDMS devices.

- **1 hr Bake** Bake the bonded devices for an hour in the oven. This treatment should be at least 30 min in duration. Let cool 5 min.
- **PDMS:Electrode Alignment and bonding** First, prepare the electrodes by cleaning them with consecutive 5 min long sonication treatments, with soap water, deionised water, ethanol and IPA. Dry with N_2. Cut out the PDMS devices, which now contain both the valve and flow channel layers. Punch them as before, and again use the tape to clean the surface. Alignment and bonding can be performed as before. However, it is simplest to attach the electrode slide to a glass slide with tape, and vaccum-fix that slide to the top of the aligner. The PDMS part is positioned at the bottom.
- **1 hr Bake** Bake the bonded devices for an hour in the oven. This treatment should be at least 30 min in duration. Let cool 5 min.

9.2.2 Yeast cultures and YPD Broth

9.2.2.1 Summary

Yeast strains used in these studies were acquired from the Kaern lab, with the assistance of Hilary Phenix. Strain (b) was used in the trapping experiments described in Chapter 5, while strain (c) was used in the sorting experiments in Chapter 4.

9.2.2.2 Strain descriptions

Yeast strains used in these studies were acquired from the Kaern lab, with the assistance of Hilary Phenix.

a) BY4742 Mat alpha, genotype: *his3Δ1 leu2Δ0 lys2Δ0 MET15 ura3Δ0* (haploid, smaller)
b) BY4743 Mat a/alpha, genotype: *his3Δ1/his3Δ1 leu2Δ0/leu2Δ0 LYS2/lys2Δ0 met15Δ0/MET15 ura3Δ0/ura3Δ0 ade2::LEU2/ade3::URA3* (diploid, larger)
c) cdc28::cdc28::CDC28(F88G)-HIS6 (haploid)

BY4742 and BY4743 mutant strains do not produce their own supply of adenine. Adenine serves a variety of purposes within the cell, in particular respiration[146]. For example, it forms adenosine triphosphate (ATP) and adenosine diphosphate (ADP) and is a basic building block of RNA and DNA. There is evidence that adenine deprivation may impede growth.[147,148] Thus, in the experiments described in Chapters 4 and 5, adenine was supplemented.

9.2.2.3 Recipe for YPD-based culture media

This recipe is modified from standard YPD (yeast bacto-peptone). Salt was added to permit volume sensing, and BSA was added to minimize cell adhesion to channel walls. To make 100 mL of solution:

a. 2 g bacto peptone
b. 1 g yeast extract
c. 8 mL of concentrated (25%) glucose
d. 1.17 g NaCl
e. 91 mL deionised water
f. 1 mL of 100X adenine

Final concentrations are 2% glucose, 0.05% BSA, 42.2 mg/L adenine and 0.2 M NaCl. To make standard YPD, simply remove the NACl and BSA. Be sure to prepare the solution under sterile conditions (use ethanol to sterilize all glassware). As a final sterilization step, use either the autoclave or a filter.

9.2.2.4 Culturing cells

Yeast cells multiply every 1:45-2:00 hours. To have a culture of cells of optical density (OD) < 0.7 ready by 10 am the following morning, a saturated culture would be serially diluted by a factor of 5E6 at 6 pm. Usually, a few cultures would be made at higher and lower concentrations, so as to guarantee a concentration in the correct range the following morning. Incubation is at 30 ºC at 300 RPM. Use the 100 mL vials so as encourage the solution to fully aerate, and use the parafilm to seal the cover.

The following morning, place a drop of the culture on a glass slide, and observe under the microscope. Budding cells should be clearly visible.

9.2.3 *E.coli* cultures and LB broth

9.2.3.1.1 Summary

E.coli was used to demonstrate biodetection in the tunable volume sensor work described in Chapter 2.

9.2.3.1.2 Strain descriptions

A single wild-type *E.coli* strain was used in this study:

9.2.3.1.3 Recipe for LB culture media

Lysogeny borth (LB) is prepared according to manufacturer specifications. 25 g of powder is added to 1 L of deionised water, and autoclaved.

9.3 LabVIEW

9.3.1 Summary

A large numbers of LabVIEW© programs were created specifically for this work. These programs perform a variety of functions, from sorting or trapping cells to analysing large data files for peak events. The main programs developed for this work are here summarized. Thank you to Lukasz Andrzejewski and Mike Nash for assistance in developing these programs.

9.3.2 Peak detection (*Peak_detector_window.vi*)

A single peak detection algorithm is used as a SubVI to analyse short segments of data, and return information with respect to peak width, amplitude and baseline. This piece of software makes use of *Peak Detector VI*, a LabVIEW VI designed to output the amplitude and position of multiple peaks or valleys within an array, with respect to a given expected width and threshold. In the *Peak_detector_window.vi* SubVI, this functionality is combined with a baseline calculation.

9.3.3 Detecting peaks in .DAT files (*Cell_detection_manual.vi* and *Cell_detection_auto.vi*)

The Cell_detection_manual.vi and Cell_detection_auto.vi programs are used to read through a binary file, and extract peaks according to chosen filtering, width and threshold settings. These programs are used to analyse files after they have been recorded, and check for peaks with alternate settings. An identical *Peak_detector_window.vi* SubVI is used. This program can also be used to troubleshoot detection settings (optimization) prior to attempting to trap or sort cells and particles. The manual version of this program allows a

user to select whether or not individual peaks are to be recorded. Althoug time-consuming, this functionality can be useful for smaller files where accuracy is of increased importance.

9.3.4 Filtering .DAT files (*Signal_analyzer.vi*)

This program allows a user to quickly filter segments of data from a binary file. The effect of this filtering can be examined in real-time. Once filtering parameters are set, the *Save* button enables the entire file to be converted to a second filtered .DAT file. If a simple graph in .CSV format is desired, the *Export graph* button serves this purpose.

9.3.5 Real-time cell trapping (*Cell_trapping.vi*)

Cell_trapping.vi is a trapping program aimed at keeping cell within a dynamic, pressure-driven trap (Fig. 9-1). A number of parameters are used to adjust a trap to a user's specifications. *Target Width (ms)* is used to have pressures increment so as to maintain a selected peak width, generally around 200 ms. *P Inc* is the increment by which pressures will adjust after every detection cycle (default = 0.005 psi). The software operates by first defining starting pressures for the outputs of the left and right bypasses, *Mid Left* and *Mid Right*. *Left Inc* and *Right Inc* are pressure increments by which the pressures will change around the starting pressures to initiate flow in either the left or right direction (in units of 0.004 psi). For example, in setting *Mid Left* and *Mid Right* to 3.0001 psi, *Left Inc* to 36 and *Right Inc* to -6, we have the following settings: pressures at *O1* and *O2* will be at *PL*=2.9761 (pressure at *O1*) and *PR=3.0241* (pressure at *O2*) for right flow or *PL=2.8561* and *PR=3.1441* for left flow. Either way, pressure average is maintained at 3.0001 psi, reducing PDMS pressure-based swelling. In the above example, the pressure gradient is in the same direction, but changes in magnitude. In most devices, there exists a pressure bias already driving cells in a given direction, so pressure requirements to drive flow in either

direction will vary accordingly. To facilitate the trapping process, these key functions have been keyboard mapped to the *Insert*, *Home*, *Page Up*, *Delete*, *End* and *Page Down* keys. Once the Adjust key has been pressed, this functionality allows a user to station himself at the microscope with the keyboard, and adjust these settings while observing cell/microparticles movements. Once settings have been set to drive cells in either direction, hitting the *F12* key initiates the automatic trap. The software takes over, and will increment pressures to obtain and maintain the peak width that was selected. Other parameters of note are the *Reverse-Time(s)* and *Rev Kick-Threshold(s)*. The former acts as a delay, and prevents a single event from triggering twice. The latter is a time-based pressure reversal, whereby if a peak is not detected in a certain interval, pressures will automatically reverse. This serves to restart the trap in the event that a peak goes undetected.

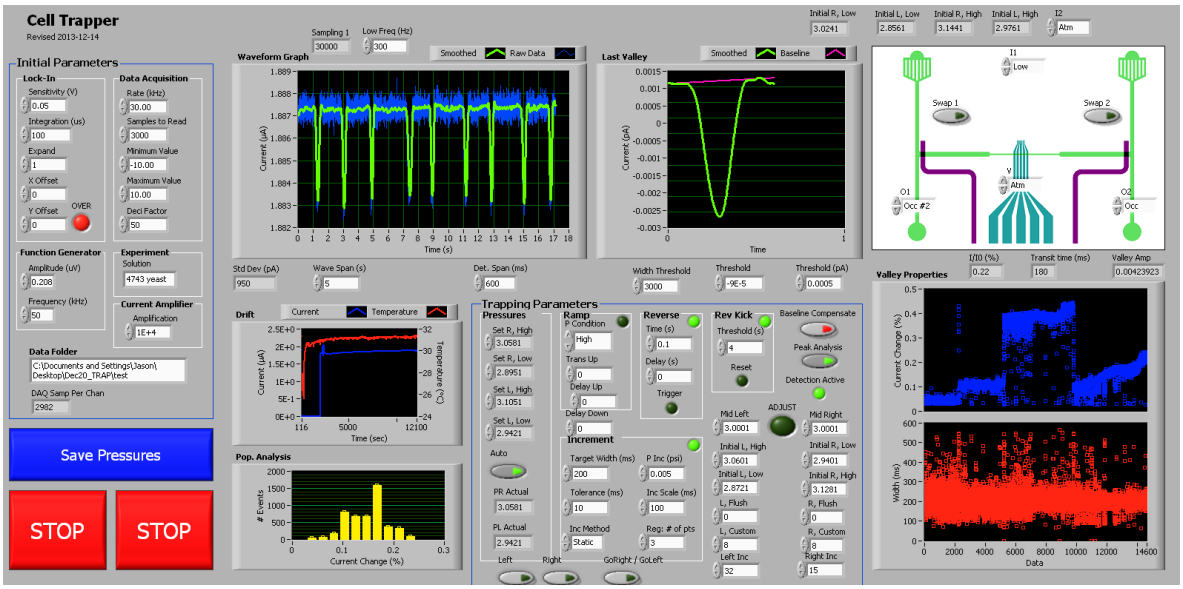

Figure 9-1 Screenshot of the *Cell_trapping.vi* cell trapping program.

9.3.6 Real-time cell sorting (*CellSorter_TwoChannels.vi* and *CellSorter_ThreeChannels.vi*)

CellSorter_TwoChannels.vi and *CellSorter_ThreeChannels.vi* are programs designed to sort cells into 2 or 3 channels, respectively. A user selects a certain pulse amplitude range (*Lower (%)* and *Upper (%)*), and cells satisfying this condition are selectively isolated from the main stream. *Redirect time (s)* (default = 8s) controls for how long flow is redirected, before defaulting back to the original setting.